Christian v. Sperber

The Exchange of the Stable Isotopes of Oxygen between Carbon Dioxide and Soil Water

Masterarbeit unter der Leitung von:

Prof. Dr. Nicolas Brüggemann und Prof. Dr. Markus Weiler

Garmisch-Partenkirchen 26. Oktober 2010

Acknowledgements:

First I would like to thank Prof. Dr. Nicolas Brüggemann and Prof. Markus Weiler for giving me such an exciting research topic and guiding me through any kinds of difficulties during this study. Because of the detailed and precise explanations whenever a question occurred and the motivating support during all time I was enthused with my research from the beginning until the end.

Rudy Meier helped me during the whole course of my experiments with his knowledge and expertise in the laboratory. Without him I would have lost the fight with the pressure regulator. Dr. Benjamin Wolf was at every time ready to help when I had trouble with my R-Code and always knew advice with all other sorts of questions. Carola Blessing was a fantastic team player. The discussions with her deepened the understanding of the subject and always raised further questions.

One cannot start a master's thesis without the successful completion of the preceding courses. I want to thank all my class mates for their help and the discussions we had during the first three semesters of our master's program. In particular Kadti Huber who took a lot of time and patience to explain me fundamental questions during the first term.

Also I would like to thank Emil Blattmann who gave me a patient and extensive introduction into the technical course of action of the Bruggatour and was helpful whenever a question arose. The excellent lectures of Dr. Christoph Külls and Dr. Helmer Schack-Kirchner sparked my enthusiasm with stable isotopes in environmental research and soils science respectively.

I. Content

II. List of Figures

III. List of Tables

Extended Summary:

This study established a new method, which allowed the simultaneous and continuous measurement of concentration and isotopic composition of CO_2 and water vapor above a soil column under laboratory conditions by combining a Tunable Diode Laser Absorption Spectroscopy (TDLAS) and Wavelength-Scanned Cavity Ring Down Spectroscopy (WS-CRDS). Two gas-tight cuvettes were filled with two different types of quartz sand (fine and medium grain size). A gas mixture of dry synthetic air and CO_2 was introduced from the top of the cuvettes to simulate the atmosphere while pure CO_2 was released from the bottom of the cuvettes through a perforated PTFE tube to simulate soil/root respiration. Several experiments were conducted in order to explore the influence of soil moisture, organic litter layer and the presence of the enzyme carbonic anhydrase on the isotopic composition of soil-released CO_2 and water vapor above a soil column.

The results of the experiments showed that the isotopic composition of the water vapor above the soil column depended on both the isotopic composition of the soil water and on the evaporation rate. The presence of an organic litter layer had a significant influence on the evaporation rate and hence on the isotopic composition of the water vapor above the soil column.

The isotopic composition of soil-released CO_2 is controlled by several processes which lead to either kinetic or thermodynamic fractionation. During the first 24 h of the experiment, before the soil columns were irrigated, a kinetic fractionation effect on the oxygen isotopic composition of CO_2 could be observed, which was attributed to diffusion. This kinetic fractionation was dependent on the type of sand in the cuvette and the presence of organic litter layer on top of the soil column. After each irrigation event, thermodynamic fractionation could be observed, which was due to the equilibrium reaction between soil water and CO_2. The effect of soil moisture was strongest after the first irrigation and diminished during the subsequent irrigations.

The presence of carbonic anhydrase had a significant effect on the oxygen isotopic composition of the CO_2 because the enzyme accelerated the equilibrium reaction between soil water and CO_2. However, unrealistically high $\delta^{18}O\text{-}CO_2$ values indicated that a significant part of the CO_2, which entered the cuvettes from the top, invaded the soil column where it also equilibrated with the soil water. Under the assumption that all CO_2, which entered the soil column from the top, equilibrated with the soil water due to the accelerated reaction by carbonic anhydrase, the proportional amount of the CO_2, which invaded the soil column from above, could be calculated.

Key Words: Tunable Diode Laser Spectroscopy, Wavelength-Scanned Cavity Ring Down Spectroscopy, CO_2, soil water, isotopic composition, evaporation, organic litter layer, carbonic anhydrase

1. Introduction

1.1 Motivation

During the past decades global warming has led to an increased interest in the origin and destination of atmospheric CO_2. The temporal and spatial quantification of CO_2 fluxes between the atmosphere, the oceans and the biosphere remains a difficult task, especially at large scales. The burning of fossil fuels is the main contributor to the increased concentration of atmospheric CO_2, whereas oceans and terrestrial ecosystems act as net sinks (IPCC 2007). Because the burning of fossil fuels is still at the center of the global energy economy, it is very likely that global warming will proceed in the coming decades. It is thus of uttermost importance to obtain a detailed understanding of how ecosystems will react to this global change. Whilst the acidification of oceans due to rising atmospheric CO_2 concentrations is well documented (Doney et al. 2009) the response of terrestrial ecosystems is not yet well understood. The terrestrial biosphere acts both as a sink and a source of atmospheric CO_2. On the one hand it absorbs carbon dioxide during photosynthesis, on the other hand it produces carbon dioxide because of autotrophic and heterotrophic respiration. It is expected that with rising global temperatures the photosynthetic CO_2 uptake by plants will decrease in regions which are warm and dry and increase in regions which are colder and humid. Simultaneously, microbial activity in the soils will increase with warmer temperatures, provided that water is not a limiting factor. This will lead to higher respiration rates in the soils and thus larger CO_2 fluxes from the soils into the atmosphere. But to which extent photosynthetic and respiratory CO_2 fluxes will change at large scales remains uncertain (Friedlingstein et al. 2006).

One possible tool to gain more detailed knowledge is the use of the stable isotopic composition of atmospheric CO_2 as a tracer. The isotopic composition of atmospheric CO_2 is influenced by a number of processes. While the stable carbon isotope composition of atmospheric CO_2 can help to differentiate between the relative contribution of oceanic and terrestrial processes and biomass burning to the atmospheric CO_2 concentration (Tans and White, 1988; Flanagan et al., 2005), the oxygen isotopic composition of CO_2 can serve as a useful tool to separate between different terrestrial isotope fluxes. In terrestrial ecosystems photosynthesis and soil respiration have a different effect on the $\delta^{18}O$ values of CO_2. This is mainly due to the hydration reaction which transfers the different oxygen isotopic compositions of leaf or soil water to CO_2 (Farquhar et al. 1993). Despite the recognition of the predominant influence of terrestrial processes on the $\delta^{18}O$ values of atmospheric CO_2, there are still many uncertainties. A more detailed knowledge about temporal and spatial variations of the different effects of photosynthesis and soil respiration on the oxygen isotopic composition of CO_2 is necessary to be able to draw precise conclusions. To date only few studies have analyzed the oxygen isotopic composition of CO_2 at the ecosystem scale, mostly so

in forested ecosystems (Flanagan et al. 1997, 1999; Sternberg et al. 1998; Harwood et al. 1998, 1999, Bowling et al. 2003; Mortazavi et al, 2004; Seibt et al. 2006; Welp et al. 2006; Wingate et al. 2008, 2010) in grasslands (Hesterbreg and Siegenthaler, 1991; Ehleringer et al. 2002; Riley et al. 2003) and in agroecosystems (Yakir and Wang, 1996; Buchmann and Ehleringer, 1998, Griffis et al. 2005, Lee et al. 2009). Even fewer studies exist on the oxygen isotopic composition of CO_2 from soil respiration at smaller scales (Ammundson et al. 1996; Miller et al., 1999).

1.2 Literature Review

1.2.1 Atmosphere

Francey and Tans (1987) discovered a latitudinal pattern of the oxygen isotope composition of atmospheric CO_2 and introduced the potential of the oxygen isotope composition of CO_2 as an atmospheric tracer. Their measurements revealed that the $\delta^{18}O$ values of atmospheric CO_2 are fairly constant at southern latitudes, whereas they become steadily lower going north from about 40° S latitude. The authors concluded that there had to be a very big isotopic exchange flux in order to produce such an isotopic gradient (Francey and Tans, 1987). This could not be explained by the isotopic exchange of CO_2 with ocean water because on the one hand the total air-sea flux of CO_2 is too small, and on the other hand the isotope signatures of CO_2 equilibrated with cold ocean water at the pole and warm ocean water at the equator differ from the observed $\delta^{18}O$ values of atmospheric CO_2 (Pearman et al. 1983). The gradient could not be explained by isotopic exchange of CO_2 with cloud droplets either because the average total residence time of a CO_2 molecule in a cloud droplet is too short to permit complete hydration (Mills and Urey, 1940; Bottinga and Craig 1968). Laboratory experiments excluded a possible exchange of CO_2 with other atmospheric sources like oxygen or water vapor as well. The isotopic effect of the combustion of fossil fuels could only account for about one fourth of the observed gradient. The authors thus assumed that the exchange of oxygen isotopes between water and CO_2 during photosynthesis and respiration might be the main reason for the observed gradient. This assumption was supported by the fact that the land mass of the northern hemisphere is much larger than on the southern hemisphere, and that there is a latitudinal and continental effect on the isotopic composition of precipitation (Francey and Tans, 1987).

Airplane sampling of air over Switzerland during the course of one year gave more information about annual means and seasonal variations of the oxygen isotopic composition of tropospheric CO_2. The results showed a clear annual cycle with maximums in the summer and minimums in the winter which could only be explained by the exchange of CO_2 with the vegetation and the soils (Friedli et al. 1987). These findings supported the hypothesis of Francey and Tans (1987).

Nakazawa et al. (1997) conducted a study where airplane samples were taken in the troposphere over Russia. The measurements of the oxygen isotopic composition of the air samples indicated that ecosystem-respired CO_2 at northern latitude is depleted in ^{18}O, reflecting the low $\delta^{18}O$ values of precipitation as source water due to the continental and latitudinal fractionation effect (Nakazawa et al., 1997).

1.2.2 Soil Effects

Another study in Switzerland measured the isotopic composition of CO_2 in a grass-covered soil at different depths during one year (Hesterberg and Siegenthaler, 1991). The measured $\delta^{18}O$-CO_2 values agreed well with those from calculations using the equilibrium fractionation factors between H_2O and CO_2. This confirmed the hypothesis of oxygen isotopic equilibrium between CO_2 and soil water. The authors developed a diffusion-reaction model which also suggested a kinetic fractionation due to the diffusional transport of CO_2 through the soil column, as lighter isotopologues of CO_2 diffuse faster through the soil to the atmosphere. Thus, the oxygen isotopic composition of the CO_2, which reaches the atmosphere, depends on the rate of equilibration with soil water. If the CO_2 production is concentrated in the top layers of the soil, the $\delta^{18}O$-CO_2 values are determined by a competition between production, isotopic equilibrium with soil water and the diffusional transport of CO_2 (Hesterberg and Siegenthaler, 1991).

In a detailed review, Ammundson et al. (1998) described the different processes and their effects on the oxygen isotopic composition of soil-respired CO_2. The diffusion-reaction model of Hesterberg and Siegenthaler (1991) was further developed and solved analytically by the application of commercial mathematics software. The authors emphasize the importance of the reaction rate of isotopic exchange between CO_2 and soil water and draw the conclusion that for reaction rates $k > 0.001s^{-1}$ in soils with CO_2 production in the top 30 cm, full equilibration between CO_2 and H_2O occurs (Ammundson et al., 1998). A previous study in the Sierra Nevada showed that there is a good agreement between measured $\delta^{18}O$ values of CO_2 and calculated $\delta^{18}O$ values of CO_2 in equilibrium with measured soil water. Assuming that the $\delta^{18}O$ value of biologically produced CO_2 is in isotopic equilibrium with the water in microorganisms, no diffusional enrichment of soil CO_2 compared to the CO_2 from biological production could be seen. This confirms the hypothesis of a competition of the effects of CO_2 production, diffusion and isotopic equilibrium on the oxygen isotopic composition of soil CO_2 (Wang et al., 1996; Ammundson et al., 1998). The study by Ammundson et al. (1998) also introduced the effect of invasion. During this process atmospheric CO_2 diffuses into the soil where it equilibrates with soil water and then diffuses back again to the atmosphere. Hence it is important to

account for the gross CO_2 fluxes from the atmosphere into the soil and from the soil to the atmosphere. Considering these gross fluxes, the influence of desert soils on the oxygen isotopic composition of atmospheric CO_2 might increase greatly. Though respiration rates in deserts are low, they cover a huge land area where atmospheric CO_2 may invade and equilibrate with soil water. This soil water is most likely highly enriched due to evaporation (Ammundson et al., 1998). Another review by Flanagan and Ehleringer (1998) examined the potential use of oxygen isotopes to interpret changes in magnitude and timing of seasonal fluctuations of atmospheric CO_2. As a reduction in CO_2 concentration can be caused by either an increase of photosynthetic uptake or a decrease in respiration, concentration measurements alone are not sufficient to differentiate between the effects of both processes on the change (Flanagan and Ehleringer, 1998). A review by Ehleringer et al. (2002) synthesized theory and field studies to characterize isotopic scaling of CO_2 fluxes. The study examined how stable isotopes can be used to separate net ecosystem exchange fluxes to be able to calculate changes in the balance of respiration and photosynthesis. In addition, the differences between the $\delta^{18}O$-CO_2 values from forests and grasslands were explored as well as their use to further partition terrestrial CO_2 fluxes (Ehleringer et al., 2002).

Tans (1998) developed exact analytical solutions of differential equations that described the isotopic signature of soil-respired CO_2 and the effect of atmospheric CO_2 which invades into the soils on the oxygen isotopic composition of atmospheric CO_2. The analytical solutions were developed under certain simplified assumptions for the case that CO_2 production in the soil decreases exponentially with depth, for the case that CO_2 production in the soil as a function of depth is constant and for the case of a zone of constant production underneath an inert surface layer, as for example in snow-covered soils or deserts which have a completely dry upper layer. As a result, in most cases only the upper 5-10 cm of the soils are important for the oxygen isotopic composition of the CO_2 which diffuses from the soil to the atmosphere. The study argued that the use of the Keeling plot approach (the plotting of the isotope ratios against the inverse of the CO_2 concentration in order to derive the isotopic composition of one source) can lead to significant mistakes, if applied to ^{18}O, because isotopic exchange with the soil water is independent of any sources (Tans, 1998).

Miller et al. (1999) conducted direct measurements of natural soils under various conditions in order to examine the relationship between the depth profiles of $\delta^{18}O$ values of soil water and the $\delta^{18}O$ values of soil-respired CO_2 and the effect of diffusion and invasion on the oxygen isotopic composition of soil-respired CO_2. The drying of soils as well as the input of new water to the soil had a very strong influence on the $\delta^{18}O$ values of soil-respired CO_2, indicating the importance of the hydrological cycle on the oxygen isotopic composition of atmospheric CO_2. In the first 5 cm of the soil, the CO_2 diffusion to the atmosphere was too fast for the hydration reaction to occur. The zone

between 5 and 15 cm below the surface appeared to have the biggest influence on the $\delta^{18}O$ values of soil-respired CO_2. Below 15 cm the oxygen isotopic composition of CO_2 was readjusted during the diffusion process towards the surface. This indicated that a steep gradient of the $\delta^{18}O$ values of soil water in the upper layer of the soil does not have a major effect on the oxygen isotopic composition of soil-respired CO_2 (Miller et al., 1999).

1.2.3 Vegetation Effects

Farquhar et al. (1993) examined the effect of vegetation on the isotopic composition of atmospheric CO_2. Their study confirmed the conclusions drawn by Francey and Tans (1987) and Friedli et al. (1987) about the importance of terrestrial processes in determining the $\delta^{18}O$ values of atmospheric CO_2. Plants take up soil water with their roots and transport it through the xylem into the leaves where it experiences a pronounced evaporative enrichment. During photosynthesis, CO_2 diffuses through the stomata into the leaves, where it dissolves and exchanges its oxygen with water either in the chloroplasts, in the case of C3 plants, or mesophyll, in the case of C4 plants. The process is catalyzed by the enzyme carbonic anhydrase. This very fast enzymatic reaction guarantees a full equilibration between the CO_2 and leaf water. While only about one third of the CO_2, which enters the leaves, is actually fixed, two thirds diffuse back into the atmosphere (Yakir and Sternberg, 2000). Thus, the CO_2, which diffuses back out of the leaves, is enriched in $\delta^{18}O$ relative to the background CO_2. Similar to soil a diffusional fractionation occurs when CO_2 molecules enter and leave the leaves through the stomata. The authors developed equations which describe the interactions of leaf fluxes with the $\delta^{18}O$ values of CO_2 and highlighted the importance of the effect of different biomes on the isotopic composition of atmospheric CO_2 (Farquhar et al, 1993).

Yakir and Wang (1996) and Yakir and Sternberg (2000) introduced the combined measurements of stable oxygen isotopes as well as concentration and flux measurements of CO_2 and H_2O above crop fields and grasslands. This method allowed the separation of net CO_2 exchange into photosynthetic and soil respiration components, as well as the evapotranspiration flux into soil evaporation and leaf transpiration, by using the Keeling plot approach, in which a linear regression of $\delta^{18}O$ values plotted versus the inverse of the CO_2 concentration along a height gradient yields the isotopic composition of the source. Prerequisite for this application is the knowledge of the isotopic composition of CO_2, organic matter, soil water and water vapor. Hence a high precision in isotopic sampling and analysis is necessary. For the application of Keeling plots it is also critical that the $\delta^{18}O$ values between the exchange fluxes from photosynthesis and respiration are different and that the $\delta^{18}O$ values of the atmospheric background are different to the ones from the biological system. However, the Keeling

plot approach is not suited for applications on longer timescales because it requires steady state conditions (Yakir and Wang, 1996; Yakir and Sternberg, 2000). Buchmann and Ehleringer (1998) applied the Keeling plot approach and measured the CO_2 concentrations and the $\delta^{18}O$ values of CO_2 within alfalfa (C3 plant) and corn (C4 plant) canopies. While strong temporal and spatial variations within the crop fields could be observed, there were no significant differences between the two crops. Highest CO_2 concentrations and lowest $\delta^{18}O$ values were found close to the soil surface, indicating the influence of soil respiration and isotopic exchange of soil-respired CO_2 with more depleted soil water. In contrast, the CO_2 concentrations in the canopy were significantly lower while the $\delta^{18}O$ values were higher, indicating the photosynthetic uptake of CO_2 and the isotopic exchange of CO_2 with enriched leaf water. During the course of a day, $\delta^{18}O$ values of the total ecosystem respiration increased steadily from about 29‰ vs. V-SMOW at nighttime to about 36‰ vs. V-SMOW at daytime. These values are in good agreement with those calculated by Yakir and Wang (1996) for similar crops in Israel. However the application of the Keeling plot approach revealed only weak relationships between the inverse of the CO_2 concentration and the $\delta^{18}O$ values of CO_2 (Buchmann and Ehleringer, 1998).

1.2.4 Modelling

In addition to field studies, several mathematical models have been developed over the years in order to simulate the ecosystem CO_2 exchange and its effects on the oxygen isotopic composition of atmospheric CO_2 on the regional or global scale. Ciais et al. (1997) calculated the global oxygen isotope fluxes of CO_2 by merging multiple different models. For the calculation of the terrestrial CO_2 fluxes the authors coupled the SiB2 photosynthesis model with the Colorade State University General Circulation Model (GSU GCM). The isotopic composition of meteoric water was derived from the NASA GISS climate model, and the air-sea $\delta^{18}O$ exchange was based on the HAMOC ocean model. The $\delta^{18}O$ values of CO_2 from fossil fuel burning and biomass burning were assumed to be the same as atmospheric O_2 (-23‰ vs. V-SMOW). The study concluded that the overall oceanic and anthropogenic contributions are small compared to the isotopic exchange between the atmosphere and the terrestrial ecosystems. While leaf exchange globally enriches the oxygen isotopic composition of atmospheric CO_2, soil exchange has the opposite effect. In a companion paper the influence of each reservoir in different geographical areas was examined with a three-dimensional atmospheric transport model (TM2). These calculations showed that the seasonal cycle of $\delta^{18}O$-CO_2 is controlled by variations in photosynthesis and respiration (Ciais et al., 1997 a+b). Another atmospheric three-dimensional transport model explored the influence of specific land regions on the seasonal and latitudinal variations in $\delta^{18}O$-CO_2. The calculated values agreed well with the

measurements from 22 different stations and showed that the Siberian taiga has the major influence on the seasonality of the $\delta^{18}O$-CO_2 values in the northern hemisphere. This is mainly due to the continental climate which results in low $\delta^{18}O$ of meteoric water and a stronger seasonality of the CO_2 fluxes. The study also confirmed the relatively low effect of the air-sea exchange, the burning of fossil fuel and deforestation on the $\delta^{18}O$-CO_2 values (Peylin et al., 1999).

Stern et al. (1999) tested the sensitivity of the $\delta^{18}O$-CO_2 values from the soil to variations of parameters of the diffusion–production–reaction model of Hesterberg and Siegenthaler (1991). The analysis found that the most important parameter, which controls the isotope ratio of soil CO_2, is the oxygen isotope composition of soil water. The second most important parameter is the rate of oxygen isotope exchange between CO_2 and soil water. The authors suggest that this rate may be two orders of magnitude lower than the exchange rate between aqueous CO_2 and water. The third most important influence on the oxygen isotopic composition of soil CO_2 consists of several parameters, which each have about the same importance: the rate of soil respiration, the distribution of respiration in the soil, the effective diffusivities, the air-filled pore space and, in extreme cases, advection. Fourth, the transient effects which may be caused by variations in the respiration rates have only a very small influence on the isotopic composition of soil CO_2 (Stern et al., 1999). In another study, Stern et al. (2001) argued that the relevant soil CO_2 flux is much larger than previously modeled. In their simulation they highlight the significance of the atmospheric CO_2 exchange with soils that are biologically inactive on the $\delta^{18}O$ values of atmospheric CO_2 because soils with low respiration rates tend to have the most extreme soil water $\delta^{18}O$ values. This may be in particular the case in desert soils (Stern et al., 2001).

Riley et al. (2003) developed a detailed model (ISOLSM) that simulates the $\delta^{18}O$ values of canopy water vapour, leaf water, soil water, the isotopic fluxes (isofluxes) of photosynthetic CO_2, the exchange reaction of CO_2 with soil water and leaf water, and the diffusive fluxes of soil CO_2, including nonbiotic CO_2 exchange. The model is able to simulate seasonal and diurnal variations in the isofluxes of CO_2 from soils and also demonstrates the impact of rooting depths, carbonic anhydrase activity in soils and leaves, and the $\delta^{18}O$ values of atmospheric water vapor on the isotopic composition of CO_2 from ecosystems (Riley et al., 2003).

Between 1993 and 1997, the NOAA-CU measurements of atmospheric $\delta^{18}O$-CO_2 showed a decrease of about 0.5‰. While Gillon and Yakir (2001) attributed this observation mainly to a land-use change, namely the conversion of C3 forests to C4 grasslands, Ishizawa et al. (2002) proposed another explanation suggesting that land-use change would only account for a decrease of about 0.02‰ yr^{-1}. They developed a multi-box model of the global carbon cycle to study the role of

biospheric metabolism in the observed decline of $\delta^{18}O$ in atmospheric CO_2. The model simulates a decrease of the amount of CO_2, which diffuses back out of the plant to the atmosphere during photosynthesis due to higher photosynthetic uptake. Hence the proportion of CO_2, which is enriched in $\delta^{18}O$ relative to the atmosphere, decreases. This results in a total decline of the $\delta^{18}O$ values of atmospheric CO_2, suggesting that an increase in photosynthetic activity in the northern hemisphere is the main reason for the observed downward trend of $\delta^{18}O$-CO_2 (Ishizawa et al., 2002).

Another model within the framework of the European project EUROSIBERIAN CARBONFLUX examined the processes, which effect the oxygen isotopic composition of atmospheric CO_2 and CO_2 fluxes on the continent of Eurasia north of 40°N, by integrating a simulation of the $\delta^{18}O$ values of water cycle pools. The calculations were validated with data from direct net ecosystem exchange measurements from eddy-flux towers and atmospheric measurements of CO_2 and $\delta^{18}O$-CO_2 at 3000 m a.s.l. The model simulations showed realistic results for the spatial and temporal variations of the water isotopic compositions and the CO_2 fluxes, but underestimated the amplitude of $\delta^{18}O$ of atmospheric CO_2. A large gradient in leaf discrimination from west to east is explained by the water isotope gradient but mostly by an increase in relative humidity in the canopy east from 60° E (Cuntz et al. 2002).

The comprehensive global three-dimensional model (ECHAM/BETHY) of $\delta^{18}O$ of atmospheric CO_2 by Cuntz et al. (2003) simulates diurnal variations and the transport of CO_2, $\delta^{18}O$ of CO_2 and $\delta^{18}O$ of H_2O. It consists of an Atmospheric General Circulation Model (ECHAM), which includes a simulation of the isotopic composition of different water reservoirs, a biosphere model (BETHY), which calculates the surface CO_2 fluxes, and a model, which calculates the $CO^{18}O$ fluxes (OFRAC). While the first part of the study validated the surface fluxes, the second part focused on the atmospheric signal. The calculated results agreed well with other estimates and measurements of net primary productivity (NPP), net ecosystem exchange (NEE), leaf-internal CO_2 mixing ratios and the isotopic signature of rain with the exception of northern latitudes. The large seasonal change in the isotopic signature of rain was almost completely leveled out in the soil because of the so called “soil bucket approach” of ECHAM. This led to results which showed almost no variation in the isotopic signature of soil-respired CO_2 and to too low $\delta^{18}O$ values of soil-respired CO_2 during the summer. Thus, the CO_2 fluxes and the leaf-internal mixing ratio were the main factors, which controlled the $\delta^{18}O$-values of atmospheric CO_2. The model results agreed well with the seasonal cycle of atmospheric CO_2, but preceded measured $\delta^{18}O$-CO_2 values by about two months. The model calculated the seasonal amplitude to be only 2/3 of the measured amplitude (Cuntz et al., 2003a+b).

Riley (2005) combined numerical model manipulations, regression analysis and an analysis of the time spans of relevant process in order to estimate the influences of several parameters on the $\delta^{18}O$ values of soil-respired CO_2. His findings contradicted the hypothesis of Miller et al. (1999) that a

steep gradient of the $\delta^{18}O$ values of soil water in the upper layer of the soil does not have a major effect on the oxygen isotopic composition of soil-respired CO_2. The author argued that the $\delta^{18}O$ value of soil water, which is close to the surface, can have a big impact on the $\delta^{18}O$ values of soil-respired CO_2, when CO_2 production close to the surface is high. The study thus highlighted the need for further soil column and field experiments and accurate measurements of $\delta^{18}O$ values of near surface soil water (Riley 2005).

1.2.5 Recent Studies at the Ecosystem Scale

Other studies have examined the influence of different processes on the $\delta^{18}O$ signature of CO_2 at the ecosystem scale. Flanagan and Varney (1995) measured the concentration and $\delta^{18}O$ values of CO_2 at two different canopy heights. The results showed large spatial and diurnal variations. Higher CO_2 concentrations and lower $\delta^{18}O$-CO_2 values were observed closer to the ground. The $\delta^{18}O$ values of CO_2 increased during the course of a day and depended on relative humidity. This reflected the effect of increasing photosynthetic activity during the day and the influence of the relative humidity on the oxygen isotope composition of chloroplast water. These results agreed well with a gas mixing model that calculated the relative amounts of CO_2 fluxes between forests and the bulk atmosphere (Flanagan and Varney 1995). In a similar study, Sternberg et al. (1998) took samples of ambient CO_2 at two sites in the tropical forest of the Amazon basin. The study tested whether the $\delta^{18}O$ values of plant stem water reflect the $\delta^{18}O$ values of bulk soil water, whether soil-respired CO_2 equilibrates with soil water before it diffuses to the atmosphere, the validity of a kinetic isotope fractionation of 8.8‰ during diffusion, and whether one can neglect the exchange reaction between CO_2 and wet surfaces or clouds and fogs. The results demonstrated that several assumptions from temperate regions do not hold true in the tropics. Namely ambient CO_2 can equilibrate with wet surfaces or fog, especially during nighttime condensation. The $\delta^{18}O$ values of soil-respired CO_2 cannot be derived from the $\delta^{18}O$ values of bulk soil water plus a constant diffusional fractionation factor because a big amount of the soil-respired CO_2 in the tropics is produced by very shallow roots (Sternberg et al., 1998). A survey in a boreal forest ecosystem examined the $\delta^{18}O$ values of soil-respired CO_2 and of CO_2 from the whole ecosystem. Short-term changes in the $\delta^{18}O$ values of rainwater and enrichment in ^{18}O during evaporation and transpiration showed strong effects on the $\delta^{18}O$ values of respired CO_2. Changes in the $\delta^{18}O$ values of water in the moss tissue on the forest floor also affected the $\delta^{18}O$ values of soil-respired CO_2. The authors concluded that isotopic fractionation processes during the CO_2 exchange between terrestrial ecosystems and atmosphere are influenced by large environmental changes, which may occur during a season or between years (Flanagan et al. 1999). Measurements and modeling in the tallgrass prairie in Oklohoma demonstrated large diurnal variations of the $\delta^{18}O$

values of ecosystem water pools and the CO_2 fluxes. The integrated land-surface and isotope model (ISOLSM) simulates ecosystem $H_2{}^{18}O$ and $C^{18}O$ fluxes. The prediction agreed well with measured values. The results of the study showed that the ecosystem isoflux was dominated by leaf fluxes and that the equilibration between CO_2 and leaf water is incomplete in grassland ecosystems. This is mainly due to the lack of carbonic anhydrase in C4 plants (Riley et al., 2003). In order to determine whether the $\delta^{18}O$-CO_2 values of nocturnal ecosystem respiration are more strongly influenced by evaporative processes or the oxygen isotopic signature of rain, Bowling et al. (2003) conducted measurements over a period of four years across a precipitation gradient from the coast to the inland of Oregon. The data revealed that the $\delta^{18}O$ values of the ecosystem respiration were more enriched at inland sites than at those sites which were closer to the coast. In contrast the $\delta^{18}O$ values of precipitation were more enriched at sites closer to the coast compared to the inland sites. This suggests that the evaporative enrichment of soil water has a bigger influence on the $\delta^{18}O$ values of nocturnal respired CO_2. Furthermore, the study examined the factors that influence short term variations of the $\delta^{18}O$ values of ecosystem respiration and the fractional contribution of soil respiration to total ecosystem respiration (Bowling et al., 2003a+b).

Two different techniques to measure the $\delta^{18}O$ values of soil CO_2 were tested and compared in a pine forest in Florida (Mortazawi et al. 2004). As first technique mini towers were applied that collected samples at a vertical gradient. The measured data was then used to draw Keeling plots in order to derive the $\delta^{18}O$ values of soil-respired CO_2. The other technique was the employment of flux chamber measurements and the estimation of a diffusional fractionation factor. The results of the chamber measurements yielded much higher $\delta^{18}O$ values of soil-respired CO_2 as compared to the results from the mini tower measurements (Mortazawi et al. 2004).

In order to estimate the errors of measurements of stable isotopes of CO_2 from photosynthesis and respiration, Ogee et al. (2004) accounted for and propagated uncertainties of all terms in the mass balance and isotopic mass balance equations for CO_2. The method was then applied to a study in a maritime pine forest in combination with nighttime Keeling plots to derive the $\delta^{18}O$-CO_2 values from respiration. For this particular ecosystem, an uncertainty of 2‰ of the oxygen isotopic composition of respired CO_2 was estimated (Ogee et al., 2004).

Ometto et al. (2005) measured seasonal variations of the $\delta^{18}O$ values of atmospheric CO_2 and different water pools in primary forests and pasture ecosystems in three different regions of the Amazonian basin over a time course of two years. The results showed that the $\delta^{18}O$ values of the source water for primary forests and pastures were similar within each region. In the forest, the $\delta^{18}O$ values of leaf water was influenced by the leaf height above ground. This was mainly due to variations in vapor pressure deficit within the forest canopies. Leaf water from the forest showed lower $\delta^{18}O$ values than leaf water from pastures during all seasons. During the dry season the

daytime leaf water was more enriched than during the wet season which reflected the lower relative humidity. During the dry season, aboveground vegetation seemed to have the dominant control on the $\delta^{18}O\text{-}CO_2$ of ecosystem respiration (Ometto et al. 2005).

Hoag et al. (2005) developed a model to partition gross terrestrial carbon fluxes by the use of the triple oxygen isotope composition of tropospheric CO_2. The advantage of this approach is that the anomalous relationship between ^{17}O and ^{18}O in tropospheric CO_2 does not depend directly on the $\delta^{18}O$ values of soil water or leaf water. Stratospheric CO_2 can therefore be used as a tracer of gross primary production and ecosystem response to interannual changes in precipitation and temperature (Hoag et al. 2005).

Bowling et al. (2003) demonstrated that a tunable diode laser (TDL) system is able to perfrom continuous measurements of the oxygen isotopic composition of atmospheric CO_2 with an unprecedented sampling frequency. Until then, the majority of CO_2 isotope studies applied flask sampling and isotopic analysis by mass spectrometry. These methods have limited the number and frequency of measurements and were comparatively expensive and time consuming. The new technology also proved to be suitable for field application and could operate with a precision of 0.25‰ (Bowling et al (2003). The first study, which applied this new method in the field, combined continuous flux measurements of $C^{18}OO$ with eddy covariance measurements over an agricultural ecosystem (soybean). The study demonstrated that the measurements had an adequate precision to resolve vertical gradients and diurnal variations of the isotopic composition of the CO_2 fluxes from ecosystem exchange above an agricultural ecosystem. The TDL allowed a full characterization of diurnal variations of atmospheric CO_2 and could detect the effects of combustion plumes and CO_2 retroflux from photosynthesis on the oxygen isotopic ratio (Griffis et al., 2005; Baker and Griffis, 2005).

Welp et al. (2006) explored the effect of post-fire stand age on the oxygen isotopic composition of soil released CO_2 in a boreal forest ecosystem. The study measured the isotopic composition of atmospheric CO_2 and ecosystem water pools at three different stands in a three-year burn. The analysis demonstrated that the expansion of deciduous forests due to an increased forest fire frequency influenced the $\delta^{18}O$ values of atmospheric CO_2. Hence an increase in deciduous forest area in northern latitudes would weaken the isotopic effect of photosynthesis during the early part of the growing season (Welp et al., 2006).

Lee et al. (2009) conducted measurements which indicated that canopy-scale fractionation has a balancing effect between the influence of air motion and the influence of stomata on gas exchange. At a given stomatal conductance the canopy kinetic fractionation for $\delta^{18}O\text{-}CO_2$ and of $\delta^{18}O\text{-}H_2O$ increases with increasing wind speed and surface roughness. This demonstrates that canopy fractionation can have a significant effect on the spatial and temporal variations of the $\delta^{18}O$ values of

atmospheric CO_2. The authors suggest that the $\delta^{18}O$ values of atmospheric CO_2 are not only closely linked to the hydrological cycle, but also to wind circulations on land (Lee et al., 2009).

Recently, an increased interest has been shown in the possible existence and the effect of carbonic anhydrase (CA) activity in soils. Experiments have shown that carbonic anhydrase catalyzes the reaction of atmospheric carbonic sulfide (COS) with soil water, forming CO_2 and H_2S (Kesselmeier et al. 1999). Badger et al. (1994) and Giordano et al. (2003) reported the presence of carbonic anhydrase in algae, which also exist in soils. Other studies have documented CA activity in roots (Victor and Cramer, 2005). The presence of carbonic anhydrase in soils would most likely also influence the reaction rate of soil-respired CO_2 with soil water. Seibt et al. (2006) measured the $\delta^{18}O$ values of soil CO_2 and soil water in a Sitka spruce plantation. The observed $\delta^{18}O$-CO_2 values showed variations over the course of one day. Calculations from a model, which included the atmospheric invasion of CO_2 into the soil, yielded simulated values close to the observation. Complete agreement of the simulated values with the observation was only achieved by including an acceleration term of the equilibrium reaction between CO_2 and soil water. This suggested the presence of carbonic anhydrase in the litter layer (Seibt et al., 2006).

Measurements with soil chambers in a Mediterranean forest showed diurnal patterns of the oxygen isotopic composition of net CO_2 fluxes. Additional model simulations indicated that the $\delta^{18}O$ values of soil-respired CO_2 are strongly influenced by the progressive enrichment of water in the upper soil layers due to evaporation and the presence of CA due to the acceleration of the isotopic exchange between CO_2 and soil water. The study highlighted the need for a better understanding of the role of enzymatic reactions in order to interpret the isotope signals of atmospheric CO_2 (Wingate et al., 2008). Furthermore, it became apparent that it is necessary to know the shallowest depth in the soil, where diffusing CO_2 molecules have enough time to fully equilibrate with the soil water. The presence of CA accelerates the equilibrium reaction of CO_2 and water and would thus the shallowest depth in the soil, where diffusing CO_2 molecules have enough time to fully equilibrate with the soil water, further towards the soil surface. This influences not only the CO_2 which diffuses from the soil to the atmosphere, but also the invasion flux from the atmosphere into the soil. Incorporating high CA activity in the global model by Cuntz et al. (2003) brought the simulated of $\delta^{18}O$-CO_2 values closer to the observed ones (Wingate et al, 2009). In another study, Wingate et al. (2010) investigated the extent of isotopic disequilibrium of the of $\delta^{18}O$-CO_2 values between CO_2 fluxes from leaves and soils within a forested ecosystem using a TDL system to guarantee continuous measurements. The results of the measurements demonstrated a significant disequilibrium between the of $\delta^{18}O$ values from photosynthetic and respiratory CO_2 fluxes during the day and also between foliage and soil respiratory CO_2 fluxes during the night. The observed isotopic compositions could be linked to

environmental fluctuations in the case of leaf water. In the case of the soil, though, there were indications that the extent of CA activity may vary significantly over the growing season. The authors highlighted that further research is necessary to better understand the drivers of CA activity in the soil (Wingate et al., 2010).

1.3 Goals of the Study

The first goal of this study was to establish and characterize an experimental setup for the simultaneous and continuous measurement of the isotopic composition of CO_2 and water vapor above soil columns by coupling a tunable diode laser absorption spectrometer (TGA200, Campbell Scientific, Inc., Logan, UT, USA) for CO_2 and a wavelength-scanned cavity ring-down spectrometer (Picarro L1102-I, Picarro, Inc., Sunnyvale, CA, USA) for H_2O as a new method for online analysis of the role of oxygen isotope exchange between CO_2 and soil water on soil-atmosphere CO_2 exchange under varying environmental conditions with high time resolution.

The second goal was to gain a more detailed understanding of the temporal and spatial variation of the $\delta^{18}O$ values of soil-respired CO_2 in dependence on soil-water content and soil texture under controlled laboratory conditions.

The third goal was to specifically explore the influence of soil moisture, organic litter layer and the presence of the enzyme carbonic anhydrase on the isotopic composition of CO_2 and water vapor above a soil column.

2. Theory

2.1 Isotope Notation

Isotopes are atoms with the same number of protons and electrons but a different number of neutrons. Stable Isotopes are those which do not decay over time but remain as they are. Most elements in the periodic table have more than one stable isotope. In nature each isotope of an element has a different abundance. The isotopes which have more neutrons are usually less abundant. For technical reasons it is difficult to reproduce precise measurements of the absolute isotopic abundance of elements in a sample. This is why measurements are rather expressed in the relative difference in the isotopic ratio of a sample compared to the isotopic ratio of an international standard. The relative difference is noted by the so called delta value which is given by:

$$\delta\ (‰) = \left(\frac{R_{sample}}{R_{standard}} - 1\right) \cdot 1000 \qquad (2.1)$$

R is the ratio of the heavy isotope to the light isotope. In most cases the heavy isotope is the less abundant isotope. The delta values are reported in per mil. A positive delta value thus means that the sample has a higher proportion of heavy isotopes compared to the standard, a negative value the opposite (Sharp, 2007). The study analyzes the stable isotopic composition of carbon dioxide and water and therefore deals with the stable isotopes of hydrogen, oxygen and carbon. For these elements different international standards are used to compare the stable isotope ratio (Table 1):

Table 2-1: Relative Abundance and International Standards of Stable Isotopes (Michener and Lajtha, 2004).

Element	Isotope	Abundance (%)	International Standard
Hydrogen	^{1}H	99.985	Vienna Standard Mean Ocean Water (V-SMOW)
	^{2}H	0.0155	
Carbon	^{12}C	98.892	Vienna Pee Dee Belemnite (V-PDB)
	^{13}C	1.108	V-PDB-CO_2
Oxygen	^{16}O	99.759	V-SMOW for O in all compounds except CO_2
	^{17}O	0.037	V-PDB or V-PDB-CO_2 for O in carbon dioxide
	^{18}O	0.204	

For technical reasons the $\delta^{17}O$ values were not analyzed, neither of water, nor of carbon dioxide. In the case of oxygen there are three different international standards which are expressed on different scales. The $\delta^{18}O$ values of water and all other oxygen-containing compounds except CO_2 are usually related to V-SMOW, whereas those of CO_2 are usually related to V-PDB or V-PDB-CO_2. The

international standard PDB or Pee Dee Belemnite was a rock from the Pee Dee formation in South Carolina which consisted of calcium carbonate from a Cretaceous belemnite. As PDB no longer physically exists, the so-called V-PDB (where V stands for Vienna, where the headquarters of the IAEA is located) has taken its place. Although it does not physically exist, it is used as the basis for the V-PDB scale with the same isotopic composition as PDB. The international standard V-PDB-CO_2 is derived from the CO_2, which would be liberated from the imaginary V-PDB with phosphoric acid at 25°C (Sharp 2007).

Isotopes of one element have different atomic masses because of their different number of neutrons. The mass difference leads to different reaction rates and bond strengths. This also applies to molecules which are made of different isotopes, so called isotopologues. The differences in reaction rates and bond strengths among isotopes or isotopologues lead to fractionations between substrates and products during chemical reactions or physical processes. The major fractionation processes can be classified as equilibrium fractionation and kinetic fractionation. Equilibrium fractionation, also called thermodynamic fractionation, occurs during equilibrium reactions in closed, well-mixed systems where the isotopic composition of the substrate differs from the one of the product. A typical example for an equilibrium exchange reaction is that between carbon dioxide and water. Kinetic fractionation, in contrast, occurs during irreversible, unidirectional processes in an open system, such as, for example, evaporation of a water body. The amount of fractionation is quantified by the fractionation factor α, given by:

$$\alpha = \frac{R_{product}}{R_{substrate}} \tag{2.2}$$

where *R* is the ratio of the heavy isotopes to the light isotopes in the product or substrate respectively. If $\alpha > 1$, it means the product is enriched in the heavier isotope compared to the substrate. And for $\alpha < 1$ it is the opposite (Michener and Lajtha, 2004). In order to express the result of the fractionation process in (‰), one uses the enrichment factor ε which is given by Michener and Lajtha (2004):

$$\varepsilon = (\alpha - 1) \cdot 1000. \tag{2.3}$$

The relevant processes in this study, which lead to fractionation, are the equilibrium reaction between carbon dioxide and soil water, the diffusion of CO_2 through a porous medium and the evaporation of water at the soil surface.

In this study $\delta^{18}O$ values of CO_2 and H_2O were analyzed. In order to make the data more transparent and to avoid a mixing of scales in the presentation of the oxygen isotope data the $\delta^{18}O$ values of CO_2 were transferred from the V-PDB-CO_2 scale to the V-SMOW scale. To convert the delta values of a

sample (*S*) from one scale (international standard *A*) to another scale (international standard *B*) one uses the following equation:

$$\delta_{S-B} = \delta_{S-A} + \delta_{A-B} + (000.1) \cdot \delta_{S-A} \cdot \delta_{A-B} \quad (2.4)$$

This equation can be rearranged to another format:

$$\delta_{S-B} = \alpha_{A-B} \cdot \delta_{S-A} + \delta_{A-B} \quad (2.5)$$

As mentioned above, in the case of oxygen there are three different international standards which can be used. The $\delta^{18}O$ values of water are usually referenced to the V-SMOW scale whereas those of CO_2 are usually referenced to the V-PDB or V-PDB-CO_2 scale. As mentioned above the international standard PDB or Peedee Belemnite is a rock from the Peedee formation in South Carolina which consisted of calcium carbonate from a Cretaceous belemnite. On the V-SMOW scale the zero point of V-PDB is 30.91‰. To convert a $\delta^{18}O$ value which is noted on the V-PDB scale into the $\delta^{18}O$ values on the V-SMOW scale one calculates analogous to equation (2.5):

$$\delta^{18}O_{V-SMOW} = 1.03091 \cdot \delta^{18}O_{V-PDB} + 30.91 \quad (2.6)$$

In order to convert a $\delta^{18}O$ value on the V-SMOW scale into a $\delta^{18}O$ value on the V-PDB scale, one first has to subtract the value of the zero point of the V-PDB scale on the V-SMOW scale from the measured $\delta^{18}O$ value on the V-SMOW scale. The term then has to be divided by the fractionation factor:

$$\delta^{18}O_{V-PDB} = (\delta^{18}O_{V-SMOW} - 30.91)/1.03091 \quad (2.7)$$

The international standard V-PDB-CO_2 was derived from the CO_2 which was liberated from PDB with phosphoric acid at 25°C. This process results in a fractionation factor of 1.01025. Thus the zero point of V-PDB-CO_2 is 10.25‰ on the V-PDB scale (Sharp, 2007). Figure (2.1-1) gives an overview of these three scales and the associated fractionation factors:

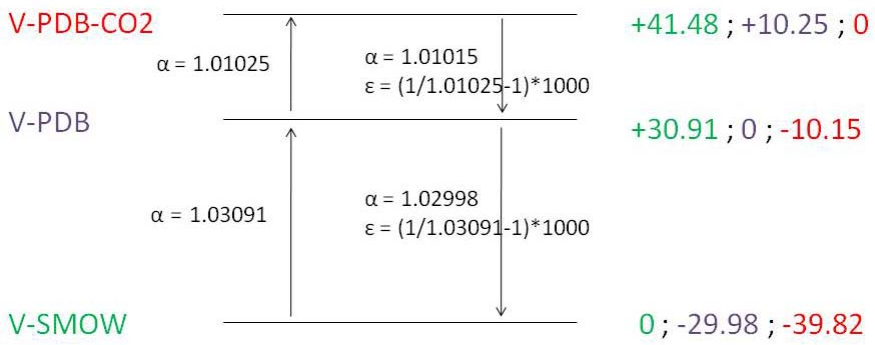

Figure 2.1-1: Three international standards to express $\delta^{18}O$ values.

In order to convert our measured $\delta^{18}O$ values of CO_2 from the VPDB-CO_2 scale to the V-SMOW scale one first has to convert the $\delta^{18}O$ values from the VPDB-CO_2 to the V-PDB scale and then from the V-PDB scale to the V-SMOW scale by the following equation:

$$\delta^{18}O_{V-SMOW} = 30.91 + 1.03091(\delta^{18}O_{V-PDB-CO2} \cdot 1.01025 + 10.25) \quad (2.8)$$

2.2 Ecosystem CO_2 Exchange

Atmospheric CO_2 undergoes several exchange processes with the terrestrial environment. During photosynthesis CO_2 diffuses from the atmosphere into the leaves (F_{AL}) where it equilibrates with the water in the chloroplasts, in the case of C3 leaves, or mesophyll, in the case of C4 leaves. While only approx. one third of the CO_2, which diffuses into the leaf, is fixed, two thirds diffuse back out from the leave to the atmosphere (F_{LA}) (Yakir et al. 2000). During autotrophic (root) and heterotrophic (microorganism) respiration, CO_2 is produced in the soils. After production, the CO_2 diffuses from the soil to the atmosphere (F_{SA}). During the diffusion through the soil the CO_2 equilibrates with soil water. In addition atmospheric CO_2 invades into the soil until a certain depth and then retrodiffuses back out to the atmosphere (F_{AS}). During the invasion, atmospheric CO_2 equilibrates with soil water as well (Ammundson et al. 1998). All these processes have an effect on the ^{18}O composition of CO_2 and lead to either kinetic fractionation, due to the diffusion of the molecules, or thermodynamic fractionation, because of the equilibrium reaction between CO_2 and water, or both. Hence it is important to note that the oxygen isotopic composition of atmospheric CO_2 does not only depend on the exchange processes but is closely linked to the hydrologic cycle (Yakir et al. 2000). Figure (2.2-1) gives an overview of the Ecosystem CO_2 exchange.

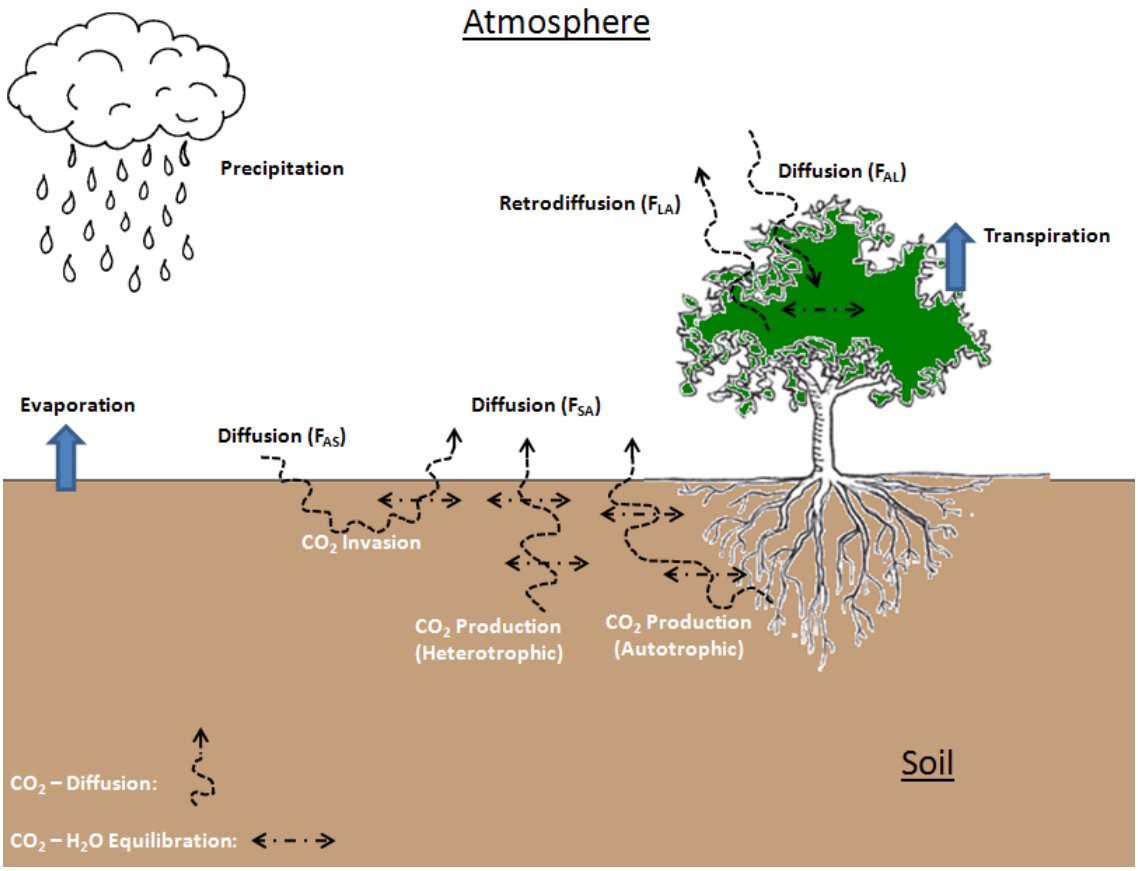

Figure 2.2-1: Processes which influence the oxygen isotopic composition of CO_2 in an ecosystem.

2.3 Isotopic Composition of Soil Water

The isotopic composition of soil water depends on the isotopic composition of the precipitation and is modified by evaporation. Craig and Gordon (1965) described the variations in the isotopic composition of water vapor (δ_V) and the water surface undergoing evaporation (δ_L) by:

$$\delta_V = [\alpha_{eq}\delta_L - rH\delta_A - \varepsilon_{eq} - (1-rH)\varepsilon_k]/[(1-rH) + \frac{(1-rH)\varepsilon_k}{1000}] \quad (2.9)$$

where:

V evaporating water vapor

L liquid water body

A ambient air

α_{eq} equilibrium fractionation factor

ε_{eq} equilibrium enrichment (at 20°C: ε_{eq} = 9.8‰ for $\delta^{18}O$, Majoube, 1971)

ε_k kinetic enrichment (at 20°C: ε_k = 15-30‰ for $\delta^{18}O$, Merlivat, 1978)

rH relative humidity of ambient air

In order to calculate the isotopic composition of a liquid water body at the water surface undergoing evaporation equation (2.9) can be rearranged to:

$$\delta_L = \delta_V[(1 - rH) + \frac{(1-rH)\varepsilon_k}{1000}]\frac{1}{\alpha_{eq}} + [rH\delta_A + \varepsilon_{eq} + (1 - rH)\varepsilon_k]\frac{1}{\alpha_{eq}} \quad (2.10)$$

From these equations follows that the evaporating body is strongly enriched in ^{18}O relative to the water vapor. The extent of this enrichment is influenced by the relative humidity, the isotopic composition of the atmospheric vapor and the fractionation associated with the diffusion of water molecules across the boundary layer (Yakir et al., 2000).

From the soil surface downwards the soil water becomes gradually enriched in ^{18}O. At about 0.1-0.5 meters below the surface a so called "evaporation front" develops. From there the $\delta^{18}O$ values decrease exponentially with depth until they reach the isotopic composition of the source water (Allison and Barnes, 1983; Barnes and Allison, 1988). No fractionation occurs during the uptake of water by roots. But transpiration usually is highest during spring and the summer months. This results in a seasonal selection of soil water by the roots which can lead to more ^{18}O-depleted water in deeper soil layers compared to the mean annual value because precipitation in winter usually has lower $\delta^{18}O$ values than precipitation in summer and contributes more to groundwater recharge (Gat, 1996).

2.4 Thermodynamic Fractionation during the Hydration of CO_2

As mentioned above the oxygen isotopic composition of CO_2 in the soil is strongly influenced by the $\delta^{18}O$ values of soil water with which it comes into contact. The oxygen isotopic exchange between CO_2 and water occurs because the dissolved CO_2 is hydrated to carbonic acid. In order for the equilibrium reaction to occur, water has to be in the liquid phase. This reaction is slow and strongly temperature dependent (Mills and Urey, 1940). The oxygen isotopic exchange during the hydration of CO_2 can be expressed by the following equation:

$$H_2{}^{18}O_{(l)} + CO_2 \leftrightarrow H^+ + [HCO_2{}^{18}O]^-_{(aq)} \leftrightarrow H_2O_{(l)} + CO^{18}O_{(g)} \quad (2.11)$$

The equilibrium fractionation between the oxygen of CO_2 and water has been experimentally determined by Brennikmeijer et al. (1983) and can be expressed by the following empiric equation:

$$\varepsilon_{eq-CO2}(T) = \frac{17604}{T} - 17.93 \qquad (2.12)$$

Thus, at 25°C (=298.15 K) equilibrium fractionation between the oxygen of CO_2 and water has a value of 41.11‰. It is important to note that the amount of water which is involved in the reaction is many magnitudes higher than the amount of CO_2 in the reaction. This is the reason why the CO_2 will adopt the $\delta^{18}O$ value of the water in which it is dissolved plus the enrichment caused by thermodynamic fractionation of the equilibrium reaction (Yakir et al, 2000).

The hydration of the CO_2 molecule is strongly catalyzed by the enzyme carbonic anhydrase (CA), which is present in leaves. In this case the equilibrium of equation (2.11) is reached almost instantaneously. There are several studies, which indicate a presence of carbonic anhydrase in soils, but there is no proof yet (Badger et al., 1994; Kesselmeier et al., 1999; Giordano et al., 2003; Victor and Cramer, 2005; Amoroso et al., 2005; Seibt et al., 2006; Wingate et al., 2008, 2009, 2010).

2.5 Kinetic Fractionation during the Diffusion of CO_2 through the Soil

The kinetic fractionation of CO_2 during diffusion is based on the binary diffusivities of the isotopologues of CO_2 in air. The idea is that lighter isotopologues diffuse faster through the soil column compared to the heavier ones (Yakir et al. 2000). The kinetic energy (E) of all molecules in an ideal gas is the same and can be given as:

$$E = \frac{1}{2}mv^2 \qquad (2.13)$$

m mass [g]

v velocity [ms^{-1}]

If the kinetic energies of the two isotopologues $C^{16}O^{16}O$ and $C^{18}O^{16}O$ are equal, the ratio of their velocity is $(46/44)^{1/2}$ or 1.022. This would mean that in a given time and a given temperature the $C^{16}O^{16}O$ molecule diffuses 2.2% further than the $C^{18}O^{16}O$ molecule. This holds true for an ideal gas, but in the case of air one has to mind the effect of molecular collision. In this case the ratio of the diffusion coefficients (D) of the two isotopologues equals the ratio of the square roots of the reduced masses (μ):

$$\frac{D_{C^{18}O^{16}O}}{D_{C^{16}O^{16}O}} = \frac{\sqrt{\mu_{C^{18}O^{16}O}}}{\sqrt{\mu_{C^{16}O^{16}O}}} = \frac{4{,}20847}{4{,}17212} = 1.0087 \quad (2.14)$$

where :

$$\mu = \frac{m_1 \cdot m_2}{m_1 + m_2} \quad (2.15)$$

with m_1 and m_2 the molecular weight of the isotopologue and air respectively. The mean molecular weight of air was assumed to be 28.8 (Hoefs, 2009).

Hence the fractionation because of gaseous diffusion for $C^{18}O^{16}O$ can be estimated to be approx. 8.7‰. Under the assumption that all other terms were known, global isotopic mass balance studies estimated the kinetic fractionation of diffusion through soils to be between 5.0‰ and 7.6‰ for $C^{18}O^{16}O$ (Ciais et al., 1997; Farquhar et al., 1993). Small scale, direct measurements suggested a value of 7.0‰ (Miller et al., 1999).

2.6 Mathematical Models

Assuming that the ratio of $C^{18}O^{16}O$/ $C^{16}O^{16}O$ in atmospheric CO_2 is at steady state one can derive following mass balance model for atmospheric CO_2:

$$M_A \frac{\partial CO_{2atm}^{18}}{\partial t} = 0 = (F_{LA} \cdot R_L \cdot \alpha_{LA}) - (F_{AL} \cdot R_A \cdot \alpha_{AL}) + (F_{SA} \cdot R_a \cdot \alpha_{SA}) - (F_{AO} \cdot R_A \cdot \alpha_{AO}) + (F_{OA} \cdot R_O \cdot \alpha_{OA}) + (F_{FA} \cdot R_F) \quad (2.16)$$

M_A moles of gas in the atmosphere

F_{XY} fluxes of CO_2 from reservoir *X* to reservoir *Y*

R_X ratio $C^{18}O^{16}O$/ $C^{16}O^{16}O$ in reservoir *X*

α_{XY} magnitude of fractionation during the transfer of CO_2 from one reservoir to another

A index for atmosphere reservoir

L index for leaf reservoir

S index for soil reservoir

O index for ocean reservoir

F index for fossil fuel reservoir

The soil component of this global mass balance model represents the greatest uncertainty (Ammundson et al., 1998). As shown above, the oxygen isotopic composition of soil CO_2 depends on various processes. It is generally assumed that biologically produced CO_2 in the soil is in isotopic

equilibrium with the soil water and that most of the CO_2 is produced in the upper parts of the soil column. In this case there is a competition between production, isotopic equilibrium with soil water and the diffusional transport of CO_2 through the soil to determine $\delta^{18}O$-CO_2 values. In order to include all relevant processes, Hesterberg and Siegenthaler (1991) developed the following diffusion–production–reaction equation:

$$\frac{\partial}{\partial t}(C^{18}) = \frac{D_s^{18}}{\varepsilon p}\frac{\partial^2}{\partial z^2}(C^{18}) + \phi\frac{R_p^{18}}{\varepsilon p} + kC(z)\cdot(R_{eq}^{18} - R^{18}(z)) \qquad (2.17)$$

Diffusion *Production* *Reaction*

where:

C^{18} concentration of $C^{18}O^{16}O$ [mol cm^{-3}]

D_s^{18} effective diffusion coefficient of $C^{18}O^{16}O$ in the soil [$cm^2\ s^{-1}$]

εp free air porosity

z depth increment [cm]

ϕ production (respiration) of CO_2 per depth increment [mol $cm^{-3}\ s^{-1}$]

R_p^{18} ratio of $^{18}O/^{16}O$ of CO_2 of the production

R_{eq}^{18} ratio of $^{18}O/^{16}O$ of CO_2 in equilibrium with soil water

k rate of CO_2-H_2O isotopic exchange

C concentration of CO_2 [mol cm^{-3}]

$R^{18}(z)$ ratio of $^{18}O/^{16}O$ of soil CO_2

This differential equation has been solved analytically under the conditions of (1) steady state, (2) R_{eq}^{18} is constant with depth, (3) the effective diffusivity is constant with depth (Hesterberg and Siegenthaler, 1991). The solution for the same equation for the more simple case of constant production with depth and isotopic identical water in the soil system has been derived by Ammundson et al. (1998).

Also under the assumption of steady state Tans (1998) developed following differential equation by using the Green function:

$$0 = \frac{\partial(\varepsilon_t RC)}{\partial t} = SR_s + k_H B\varepsilon_w C\left(R_{eq} - R\right) + \frac{\partial}{\partial z}(\varepsilon_a t D_{18}\frac{\partial(RC)}{\partial z}) \qquad (2.18)$$

Production *Reaction* *Diffusion*

where:

ε_t total porosity which equals $\varepsilon_a + B\varepsilon_w$

ε_a air-filled pore space

ε_w water-filled pore space

B dimensionless Bunsen coefficient (Weiss, 1974)

R isotopic ratio of CO_2

C concentration of CO_2 [moles cm^{-3}]

S rate of CO_2 production [moles cm^{-3} s^{-1}]

R_s isotopic ratio of CO_2 which is produced in the soil

R_{eq} isotopic ratio of CO_2 in equilibrium with soil water

k_H rate of isotopic equilibration, which takes place only in the dissolved phase

t tortuosity factor

D_{18} free air molecular diffusivity of $C^{18}O^{16}O$ [cm^2 s^{-1}]

Note that this differential equation also includes a production, reaction and diffusion term. Tans (1998) derived exact analytical solution for the cases that (1) CO_2 production in the soil decreases exponentially with depth, (2) CO_2 production in the soil as a function of depth is constant and (3) a zone of constant production underneath an inert surface layer (Tans, 1998). A detailed derivation and explanation of the analytical solutions of these differential equations would lead too far at this place. Other ways to solve differential equations are numerical solutions, for example the application of Taylor-series approximation. However, the equations developed by Hesterberg and Siegenthaler (1991) and Tans (1998) are the basis for many subsequent models including the most recent studies on the subject by Wingate et al. (2008, 2009, 2010).

3. Methods

3.1 Measurement Technology

In this study a new method was developed which allows the simultaneous and continuous measurement of the isotopic composition of CO_2 and water vapor above a soil column by coupling measurements of a tunable diode laser trace gas analyzer (TGA200, Campbell Scientific, Logan, UT, USA) and a wavelength-scanned cavity ring down spectrometer (G1102-*i* Isotopic H_2O Analyzer, Picarro, Sunnyvale, CA, USA).

3.1.1 TGA 200 Trace Gas Analyzer

The TGA 200 was used to measure the concentration and $\delta^{13}C$ and $\delta^{18}O$ values of CO_2. This technology analyzes the concentrations of trace gases by measuring the absorption of infrared radiation. The measuring technique is based on tunable diode laser absorption spectroscopy which provides a high sensitivity, selectivity and speed. Figure (3.1-1) gives a schematic overview of the optical system:

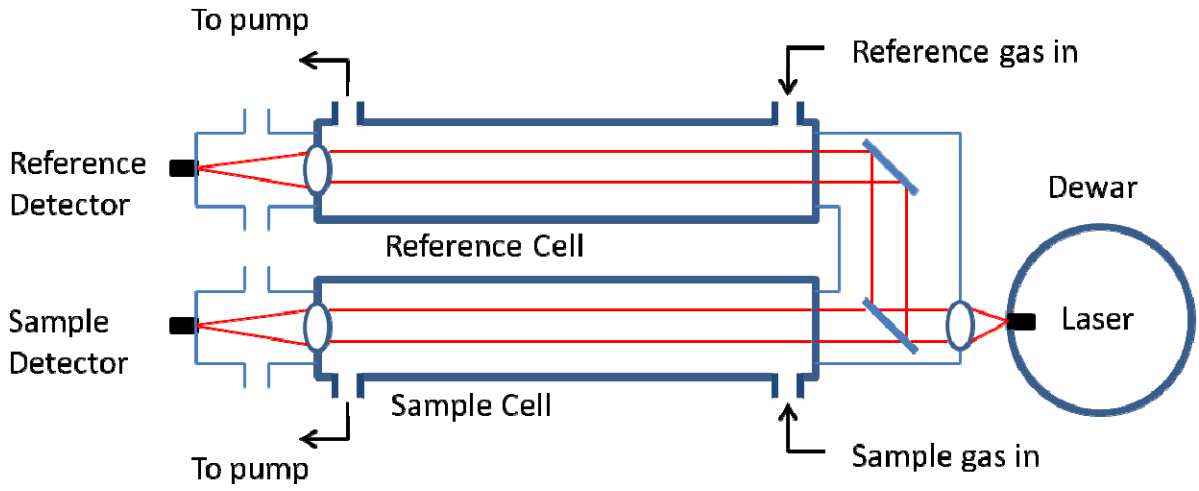

Figure 3.1-1: : Schematic overview of the optical system of the TGA200.

The optical source of the system is a lead-salt tunable diode laser. It produces a linear wavelength scan which is centered on the absorption line of the analyzed trace gas. The air space between the laser dewar and the sample cell is purged with synthetic air to avoid absorption by CO_2 in the ambient air. The infrared radiation of the laser is directed through a sample cell and a reference cell which are both about one and a half metres long. Both cells have a pressure of 25 hPa and a temperature of 30°C. It is important that both cells have the same temperature and pressure because the light absorption is influenced by these factors due to line broadening caused by the collision of the gas molecules. The reference gas has a known concentration of the trace gas to be

analyzed. The infrared radiation is absorbed in the two cells depending on the type and the concentration of the gas. The absorption is then measured by detectors at the end of the cells. The reference signal provides on the one hand a template for the spectral shape of the absorption line and the necessary information to maintain the center of the spectral scan at the center of the absorption line, and on the other hand the calculation basis for the concentrations of the measured gas species.

The wavelength of the laser depends on the laser temperature and current. Lead-salt tunable diode lasers usually operate at temperatures between 80 and 140 K and have thus to be cooled. The cooling can either be done with liquid nitrogen or a crycooler system which is based on a closed cycle refrigeration system. In this study the crycooler system was used because it has the advantage that no liquid nitrogen has to be refilled about every five to six days. The operating temperature of the laser in this study was 91 K.

The laser's emission wavenumber is the reciprocal of its wavelength. The emission is scanned over a small wavenumber range (usually +/- 0.03 to +/- 0.06 cm^{-1}). Because the emission wavelength does not only depend on its temperature but also on its current, the entire scan has three different phases: the zero current phase, the high current phase and the modulation phase as shown in Figure (3.1-2):

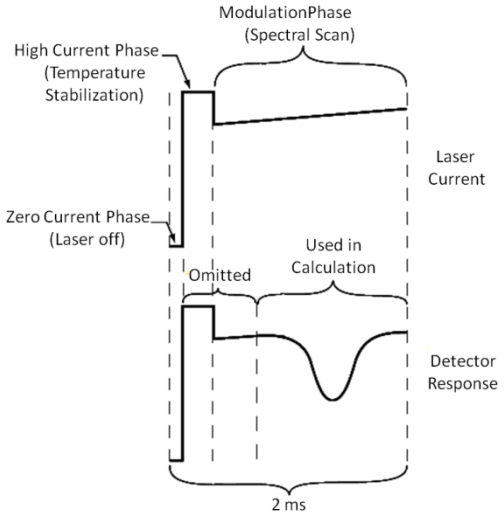

Figure 3.1-2: TGA200 laser scan sequence (www.campbellsci.com/tga200).

During the zero current phase, the laser does not emit any infrared radiation because the current is below the emission threshold. This is done in order to measure the detector's dark response. Because of the lower current the laser cools down slightly which again influences the laser's emission wavelength. Therefore the temperature needs to be stabilized again which happens during the high current phase. The actual spectral scan occurs during the modulation current when the laser current

is increased linearly over a small range usually between +/- 0.5 to 1.0 mA. The whole scan is repeated every 2 ms. Altogether, fifty consecutive scans are averaged which results in a sampling rate of 10 Hz. The TGA 200 can be configured to measure two or three gases simultaneously. To do so, one has to alternate the spectral wavelength between the absorption lines of the different gases. Prerequisite for this technique is that the absorption lines are close together within a range of about 1 cm^{-1}. In this study the laser was tuned at the adsorption lines at 2308.171 cm^{-1} for $^{13}C^{16}O^{16}O$, 2308.225 cm^{-1} for $^{12}C^{16}O^{16}O$ and 2308.416 cm^{-1} for $^{12}C^{18}O^{16}O$. It is thus also important to know the concentrations of each isotopologue in the reference gas. The software of the TGA then transfers the mole fractions of each isotopologue into the δ-values at the VPDB-CO_2 scale (TGA 100A User's Manual, Campbell Scientific).

3.1.2 Picarro G1102-*i* Isotopic H_2O Analyzer

The Picarro G1102-*i* Isotopic H_2O Analyzer was used in this study to measure the $\delta^{18}O$ and δD values of liquid water samples and water vapor. This wavelength-scanned cavity ring-down spectroscopy technology has some significant advantage compared to traditional isotope-ratio mass spectrometric analyses. It performs with very high precision and one can use it either for liquid samples or for continuous water vapor measurements. The use and maintenance of the instrument is comparably easy. Similar to the TGA 200 the Picarro G1102-*i* also uses a tunable diode laser to quantify spectral features of gases. Figure (3.1-3) shows the optical system of the Picarro G1102-*i*:

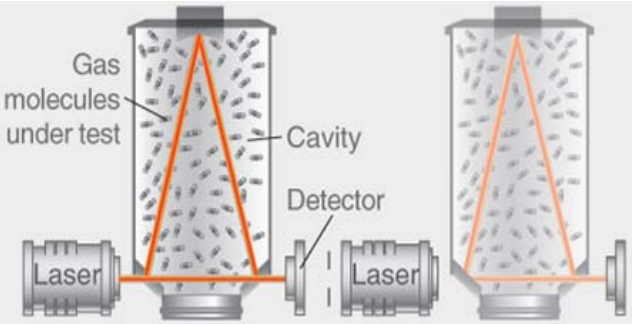

Figure 3.1-3: Optical System of a Picarro G1102-I Isotopic H2O Analyzer (www.picarro.com/technology)

The relevant isotopologues of water ($H_2{}^{16}O$, $H_2{}^{18}O$, $HD^{16}O$) each have a different absorption line. Laser light with a specific wavelength in the near-infrared is sent into the optical cavity, which is filled with the gas molecules under test. The cavity is equipped with three mirrors. The laser beam bounces from one mirror to the next which results in an effective path length of up to 20 kilometers.

The long effective path length of the laser beam guarantees that the absorption will be high enough to be measured. When the cavity fills with the laser light only a small proportional amount of the circulating light escapes the cavity and hits a photodetector. When the detector signal reaches a certain threshold the laser is turned off. The laser light inside the cavity continues to bounce from mirror to mirror but decays with time. This decay, the so called ring down, is accelerated if there is a specific gas in the cavity which absorbs the light at the laser's wavelength. The higher the concentration of this gas in the cavity, the faster is the ring down. The ring down time with the sample gas in the cavity is then compared to the ring down time without the gas in the cavity, which is simulated by the tuning of the laser to a wavelength which is not absorbed by the gas (Figure 3.1-4):

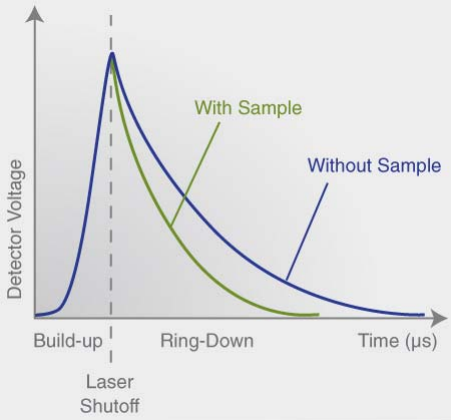

Figure 3.1-4: Light intensity as a function of time in a CRDS system (www.picarro.com/technology)

By comparing the different ring down times and a mathematical fitting to the shape of the absorption line the concentration of the specific isotopologue can be determined. Precise pressure and temperature control systems of the cavity ensure accurate measurements for a long period of time (Gupta et al., 2009; www.picarro.com/technology).

In order to measure liquid water samples, the samples are injected into a chamber where the water is evaporated. The chamber has a temperature of about 110°C and a volume of about 150 cm^3. After evaporation the water vapor is transported with a dry carrier gas to the cavity. In order to guarantee full evacuation of the chamber it is connected to a diaphragm vacuum pump. The injection is done with a 10-µl syringe and an auto sampler system (PAL Systems, CTC Analytics AG, Zwingen, Switzerland). After every injection, the syringe is rinsed with deionized water to avoid memory effects. Each measurement takes about 9 minutes, and every sample is measured six times.

3.1.3 Soil Moisture, Soil Temperature and Relative Air Humidity and Temperature Sensors

Six soil moisture sensors (ECH_2O EC-5, Decagon Devices, Inc., Pullman, WA, USA) were used in this study to measure the volumetric water content at three different heights in the soil columns. The sensor measures the dielectric constant of the soil. Since the dielectric constant of water is much higher than those of soil minerals and air, the volumetric water content can be. In order to reduce the influence of the soil texture on sensor readings, a soil-specific calibration for each sensor was performed. A combined relative air humidity and air temperature sensor (RFT-2, UMS GmbH, Munich, Germany) was used to measure the relative humidity (rH) and air temperature of the air above the soil columns. The RFT-2 works at temperatures between -30°C and +70°C and can measure relative humidities between 0 and 100%. The precision of the instrument is ±0.2K and ±2% rH, respectively. Soil temperature was measured with a soil temperature probe (Pt100, UMS GmbH, Munich, Germany) installed at 7cm depth. The sensor measures the change of resistance of platinum in dependence of temperature. The sensor was calibrated with ice water at 0°C and with boiling water at 100°C.

3.2 Experimental Design

Two gas-tight perspex cuvettes with a height of approx. 23 cm and an inner diameter of approx. 12 cm were filled with quartz sand. The left cuvette was filled with fine sand which had a grain size distribution of 0.1-0.5 mm and the right cuvette was filled with medium sand which had a grain size distribution of 1.0-1.8 mm. The lids of the cuvettes had a gas inlet and outlet. Additionally, at the center of the lids a RFT-2 air temperature and air moisture sensor was installed while three EC5 soil moisture sensors were installed at 1cm, 6cm and 11cm below the surface of the sand column at the sides of the cuvettes. (Figure 3.2-1) gives a schematic overview of the cuvettes:

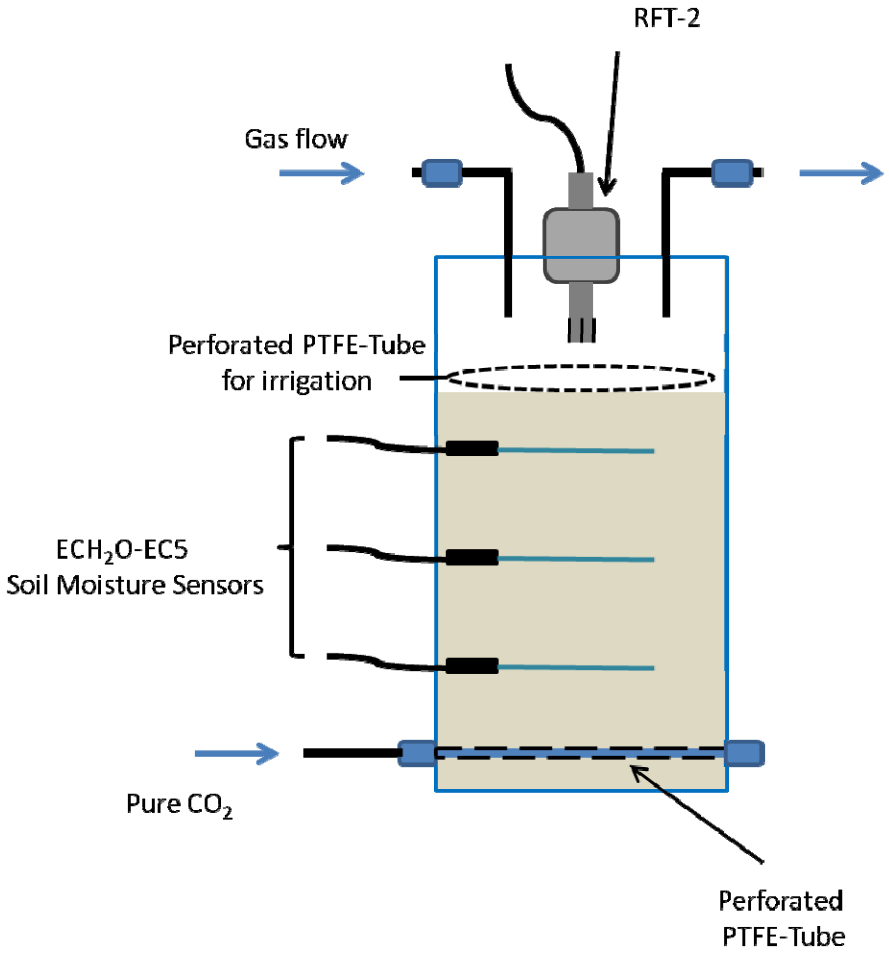

Figure 3.2-1: Schematic overview of the cuvettes

A perforated PTFE tube was installed at the bottom of the cuvettes, through which pure CO_2 was indcued in order to simulate soil respiration. Another perforated PTFE tube at the upper part of the cuvettes enabled the irrigation of the soil column without having to open the lids. The irrigation tube was installed in a circle in order to enable a uniform irrigation over the whole soil area. The gas which entered the cuvette from the top was a mixture of synthetic air and CO_2. The synthetic air consisted of 79% N_2 and 21% O_2. The admixture of pure CO_2 to the synthetic air was done with a pressure regulator. The flow rate of the gas mixture into the cuvettes was controlled by flow controllers and amounted to 1 l min^{-1}. In order to guarantee a complete mixing of synthetic air and CO_2 and to limit CO_2 concentration fluctuations, a compensation tank was installed before the inlet. The addition of pure CO_2 at the bottom of the cuvettes was also controlled by two pressure regulators. The gas fluxes were analyzed both at the inlet and the outlet. The concentration and isotopic composition of CO_2 were measured by the TGA 200 whereas the concentration and isotopic composition of H_2O were measured by the Picarro G1102-*i*. Figure (3.2-2) gives a schematic overview of the experiment setup:

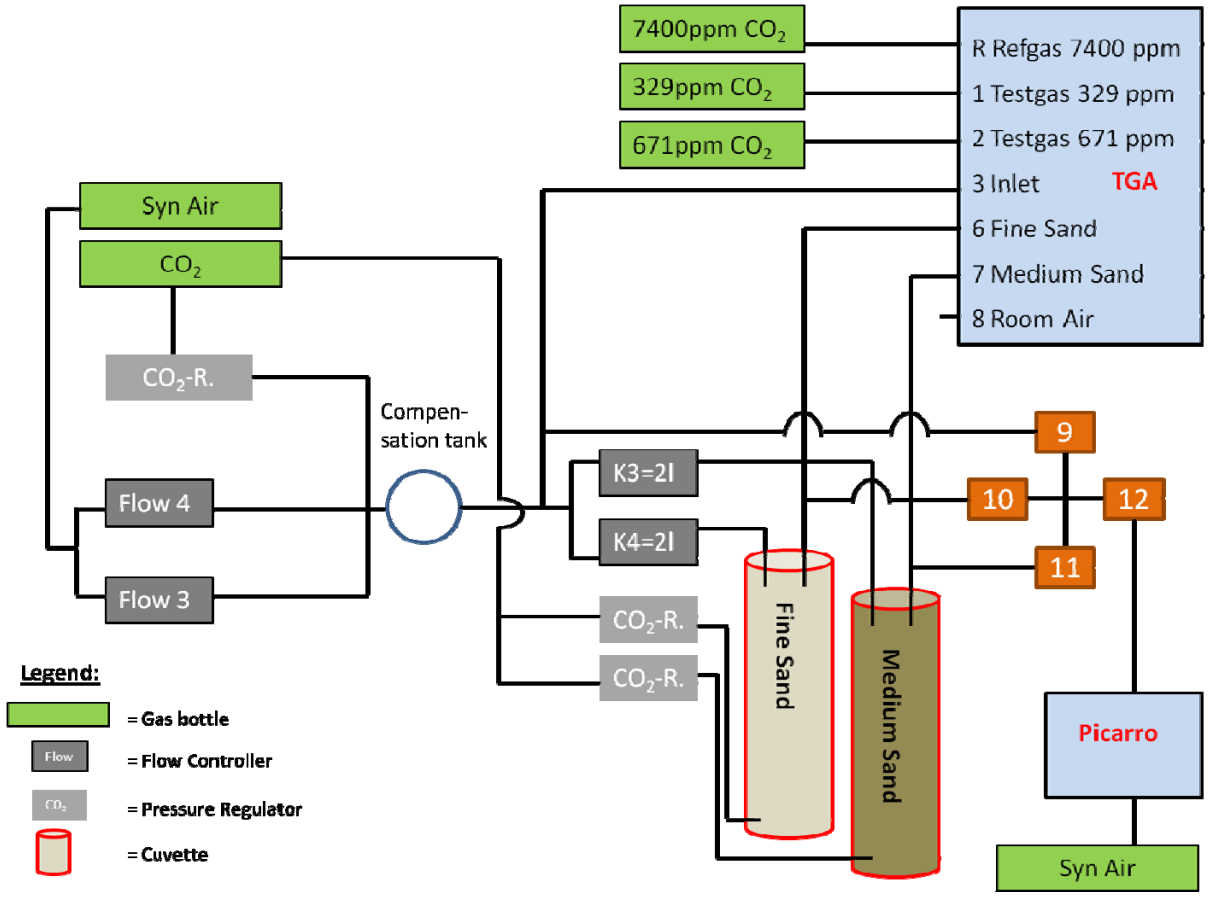

Figure 3.2-2: Schematic overview of the experiment setup

The flows were adjusted so that the CO_2 concentration at the outlet of the cuvettes was about 150 ppm higher than at the inlet. After the gas flow had stabilized, normal tap water and ^{18}O-enriched water was added through the irrigation tube on the top of the soil column in constant intervals. The reason for the irrigation with ^{18}O-enriched water was to make the isotopic effect of the equilibration reaction between CO_2 and soil water more visible. The purpose of this setup was to continuously observe the effect of soil moisture on the oxygen isotopic composition of CO_2 under controlled laboratory conditions with a high temporal resolution.

3.3 Measurement Procedure

3.3.1 Gaseous Measurements of CO_2 and H_2O

As mentioned above, the concentration and isotopic composition of CO_2 were measured by the TGA 200 whereas the concentration and isotopic composition of H_2O were measured by the Picarro

G1102-*i*. The TGA 200 measuring sequence consisted of 9 different measurements which were controlled by a CR3000 data logger (Campbell Scientific, Logan, UT, USA):

Measurement 1: Channel 1 = Calibration gas 1 (329ppm)

Measurement 2: Channel 2 = Calibration gas 2 (671ppm)

Measurement 3: Channel 3 = Cuvette inlet air

Measurement 4: Channel 4 = Simultaneous experiment

Measurement 5: Channel 5 = Simultaneous experiment

Measurement 6: Channel 3 = Cuvette inlet air

Measurement 7: Channel 6 = Cuvette outlet air (fine sand)

Measurement 8: Channel 7 = Cuvette outlet air (medium sand)

Measurement 9: Channel 8 = Room air

Measurements (4) and (5) were conducted for a simultaneous experiment of gas exchange in the canopy of trees. Each measurement lasted for 20 seconds of which the first 10 seconds were omitted. The whole measurement loop thus took 3 minutes. The two calibration gases were measured in order to correct for drift of the TGA 200. Their isotopic composition was determined with an isotope-ratio mass spectrometer (GasBench II, coupled to a Delta Plus XP, Thermo Scientific, Bremen, Germany). Calibration gas I had a CO_2 concentration of 329 ppm, a $\delta^{13}C$ value of -46.71‰ ± 0.05‰ (vs. VPDB-CO_2) and a $\delta^{18}O$ value of -33.65 ± 0.19‰ (vs. VPDB-CO_2). Calibration gas II had a CO_2 concentration of 671 ppm, a $\delta^{13}C$ value of -46.83‰ ± 0.05‰ (vs. VPDB-CO_2) and a $\delta^{18}O$ value of -33.26 ± 0.09‰ (vs. VPDB-CO_2). Note that there is no difference between the V-PDB and V-PDB-CO_2 scale for $\delta^{13}C$ values because for the carbon stable isotopes there is no fractionation during the liberation of CO_2 from carbonate by treatment with phosphoric acid. The transformation of the $\delta^{18}O$ values from the V-PDB-CO_2 scale to the V-SMOW scale was carried out according to equation 2.8.

The correction of the instrument drift was done via the two-point form of the linear equation:

$$\frac{y_2 - y_{sample}}{x_2 - x_{sample}} = \frac{y_2 - y_1}{x_2 - x_1} \tag{3.1}$$

which can be rearranged to:

$$y_{sample} = y_2 - \frac{(y_2 - y_1)(x_2 - x_{sample})}{x_2 - x_1} \tag{3.2}$$

where *x* stands for the measured value and *y* for the correct value and the subscripts *1* and *2* stand for the calibration gas I and II respectively. The calibration gases were measured every 3 minutes.

Thus, for the time of the sample measurements the *x*-values of the calibration gas I and II were determined by linear interpolation. Bowling et al. (2003) and Marron et al. (2009) recommend calibrating the instrument every 60 seconds. But calculating the arithmetic mean of the instrument drift for three minutes proofed that this time interval is sufficient.

It was assumed that the CO_2 of the gas mixture which enters the cuvette at the inlet does not invade into the soil column and equilibrate with the soil water. For this reason the measured $\delta^{18}O$-CO_2 values had to be corrected for the proportion of the respired CO_2 which actually does equilibrate with soil water. This is done via the following equation:

$$\delta^{18}O_{resp} = \frac{\delta^{18}O_O \cdot [CO_2]_O - \delta^{18}O_I \cdot [CO_2]_I}{[CO_2]_O - [CO_2]_I} \quad (3.3)$$

where:

$\delta^{18}O_{resp}$ $\delta^{18}O$ of respired CO_2

$\delta^{18}O_O$ $\delta^{18}O$ of CO_2 at the cuvette outlet

$\delta^{18}O_I$ $\delta^{18}O$ of CO_2 at the cuvette inlet

$[CO_2]_O$ concentration of CO_2 at the cuvette outlet

$[CO_2]_I$ concentration of CO_2 at the cuvette inlet

The Picarro G1102-*i* measuring sequence comprised six different measurements, for which sample air was directed to the analyzer by a custom-made sampling manifold, consisting of six relay-switched valves. The sampling manifold was also controlled by the CR3000 data logger:

Measurement 1 = Channels 9 and 12 = Inlet

Measurement 2 = Channels 10 and 12 = Simultaneous experiment

Measurement 3 = Channels 11 and 12 = Simultaneous experiment

Measurement 4 = Channels 9* and 12* = Inlet

Measurement 5 = Channels 10* and 12* = Cuvette with fine sand

Measurement 6 = Channels 11* and 12* = Cuvette with medium sand

Each measurement lasted for 5 minutes, of which only minute 3 and 4 were used for the data evaluation in order to avoid memory effects of the previous measurement as well as effects of the next measurement because the clocks of the two instruments (TGA 200, Picarro G1102-*i*) differed slightly. This is why after every experiment the clocks of the two instruments had to be reset to the same time again.

3.3.2 Additional Measurements

One big advantage of the Picarro G1102-*i* is that it is possible to measure gaseous and liquid H_2O with the same instrument. The irrigation water was sampled, and aliquots were filled into 2-ml glass vials with PTFE/silicon septa. Every sample was measured six times. The first two measurements were ignored due to possible memory effects. The values of the last four measurements were then averaged.

The soil moisture measurements with the EC5 sensors were conducted at 2 cm, 6 cm and 10 cm below the surface of the soil column. The air humidity and air temperature measurements were conducted in the center of the cuvette headspace. Both instruments were controlled by ICP CON data acquisition and control modules (ICP DAS, Hukou, Taiwan). The soil temperature was measured with the PT100 at 7 cm below the surface of the soil column.

Because the EC5 soil moisture sensors were newly purchased they had to be calibrated for the two types of sands which were used in this study in order to reduce the effect of soil texture on sensor readings. The sensors were placed into the cuvettes which were filled with fine sand and medium sand respectively. The sensors were then calibrated with dry and saturated sands. Figure (3.3-1) shows the calibration lines for the six sensors which were installed in the two cuvettes. The first letter and the number stand for the hexadecimal position at the ICP-Con unit which controls the measurements of the soil moisture sensors:

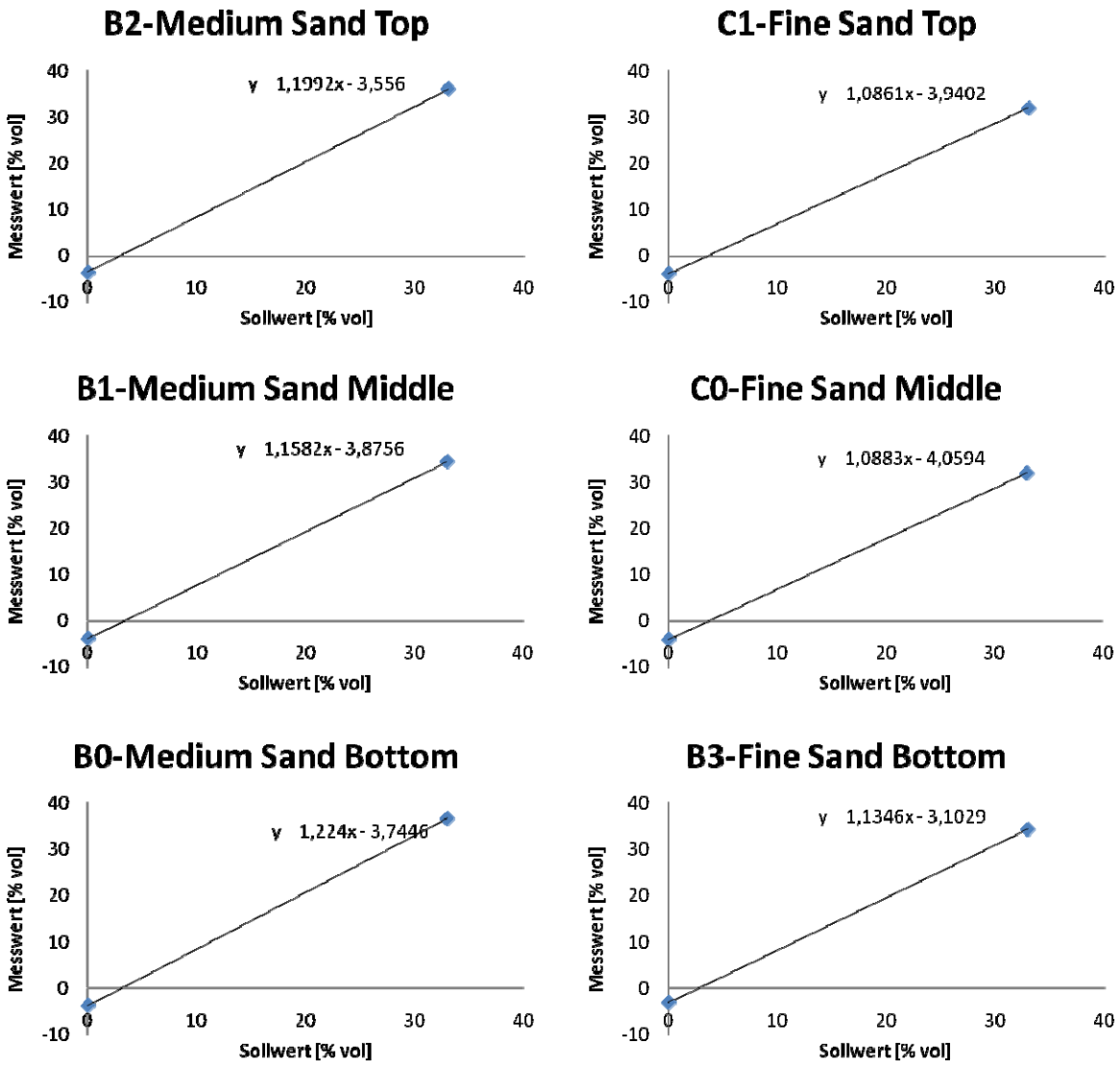

Figure 3.3-1: Calibration lines of the soil moisture sensors (EC-5) installed in the two cuvettes.

3.4 Experiment I – Concentration Dependence and Cross Sensitivity

The purpose of the first experiment was to test for a CO_2 and H_2O concentration dependency of the measurements of the TGA 200 and the Picarro. For this purpose the CO_2 concentration was increased in regular time intervals by 50 ppm from about 280 ppm up to about 530 ppm. The admixture of CO_2 was controlled manually by a pressure regulator. The H_2O concentration was increased by mixing various fractions of dry and moist synthetic air, which was generated by directing dry synthetic air through a water tank, temperature-stabilized with a water bath (Table 3-1). The total flow rate of the gas mixture through the cuvettes was held at 5 l min^{-1}. The gas mixture was directed into two empty cuvettes which were placed on top of each other.

Table 3-1: : Cross sensitivity experiment. Concentrations are in ppm and gas flows in l·min^{-1}.

Date	H_2O concentration	Minimum concentration	Maximum concentration	Flow synair	Flow moist Air	Temperature water bath
22.03.2010	14685	14492	14969	2	3	18°C
23.03.2010	15264	15057	15456	1.5	3.5	18°C
24.03.2010	16919	16692	17190	1	4	18°C
25.03.2010	18532	18273	18750	0.5	4.5	18°C
26.03.2010	19196	18993	19404	0	5	18°C
31.03.2010	26206	25802	26811	0	5	22°C
01.04.2010	22247	22076	22390	0.5	4.5	22°C
08.04.2010	23809	23294	24125	0	5	21°C
09.04.2010	21167	21069	21363	1	4	19°C

3.5 Experiment II – Empty Cuvettes

In order to test whether the experimental setup of the cuvettes did not have a bias on isotope analysis, the δ-values of CO_2 were measured in empty cuvettes. Each channel was measured 20 times alternatingly for five minutes. Afterwards, an analysis of variance (ANOVA) and a post-hoc test to identify homogeneous subgroups was carried out with the dataset in order to test whether the means of the results from the measurements of the inlet and the outlet of the two cuvettes were the same. The statistical analysis was done with the statistical software SPSS (SPSS 8.0, SPSS Inc., Chicago, IL, USA).

3.6 Experiment III – Cuvettes Filled with Sand, without CO_2 Addition and Irrigation

To test whether the gas flows could be maintained stable both cuvettes were filled with quartz sand. The left cuvette was filled with 1750 ml fine sand which had a grain size distribution of 0.1-0.5 mm and the right cuvette was filled with 1750 ml medium sand which had a grain size distribution of 1.0-1.8 mm. This resulted in a height of the soil column in the cuvette of approximately 15 cm. A gas mixture of dry synthetic air and CO_2 was directed through the inlet at the top of cuvette. No additional pure CO_2 was inducted into the cuvette through the perforated PTFE tube at the bottom. The CO_2 concentration of the gas mixture ranged from about 460 ppm to about 500 ppm. In this experiment only the δ-values of CO_2 were measured over a period of eight hours because only dry gas was directed into the cuvettes.

3.7 Experiment IV – Drying of Soil Columns After Irrigation

The setup was basically the same as in Experiment III, with the difference that pure CO_2 was inducted at the bottom of the cuvettes in order to simulate soil-respired CO_2. The CO_2 concentration at the inlet ranged approximately from 400 ppm to 500 ppm. The CO_2 concentration at the outlet was about 150 ppm higher than at the inlet. The soil column was irrigated once 24 hours after the flows had stabilized with 200 ml of water. The δ-values of the irrigation water were 10.72‰ vs. V-SMOW for $\delta^{18}O$ and -78.60‰ vs. V-SMOW for δD. The whole experiment lasted 96 hours. In addition, the soil moisture sensors as well as the air humidity and temperature sensors were installed. Also a soil temperature sensor PT100 was installed into the cuvette with the medium sand at a height of 7cm below the surface of the soil column. The purpose of this experiment was to analyze the effect of drying on the δ-values of CO_2 and H_2O.

3.8 Experiment V – Soil Columns with CO_2 Addition and Irrigation with ^{18}O-enriched Water

The purpose of Experiment V was to test the effect of soil moisture on the oxygen isotopic composition of soil released CO_2. Experiment V had the same setup as the previous one, with the difference that the soil columns were irrigated three times with 100 ml water every 24 hours. The irrigation water was enriched in ^{18}O and had a δ-value of 58.64‰ vs. V-SMOW for $\delta^{18}O$ and -79.71‰ vs. V-SMOW for δD.

3.9 Experiment VI – The Effect of a organic Litter Layer (Spruce Needles)

The purpose of Experiment VI and VII was to explore the effect of organic litter layer on the δ- values of CO_2 and H_2O. The setup and procedure was basically the same as during Experiment V but the cuvettes were only filled with 1600ml of sand which resulted in a soil column height of about 13.5 cm. On top of the soil column a spruce needle litter layer of about 3 cm height was placed. The litter was collected on a dry day from the forest floor close by the institute. Before it was applied to the cuvette the litter was autoclaved and dried at 60°C for two days. The irrigation water had a δ-value of 58.15‰ vs. V-SMOW for $\delta^{18}O$ and -80.24‰ vs. V-SMOW for δD.

3.10 Experiment VII – The Effect of a organic Litter Layer (Beech Leaves)

This experiment was the same as Experiment VI, with the only difference that the litter layer consisted of beech leaves instead of spruce needles. The irrigation water had a δ-value of 58.61‰ vs. V-SMOW for $\delta^{18}O$ and -79.65‰ vs. V-SMOW for δD.

3.11 Experiment VIII – The Effect of Application of Carbonic Anhydrase

Experiment VIII had the same setup and procedure as Experiment V but this time 100 mg of lyophilized powder of the enzyme carbonic anhydrase from bovine erythrocytes (C3934 Carbonic Anhydrase, Sigma Aldrich Chemie GmbH, Steinheim, Germany) were dissolved in 800 ml of the enriched irrigation water. The purpose of this experiment was to examine the effect of dissolved carbonic anhydrase on the $\delta^{18}O$ values of CO_2 released in the soil. The irrigation water had a δ-value of 59.16‰ vs. V-SMOW for $\delta^{18}O$ and -79.32‰ vs. V-SMOW for δD.

4. Results

4.1 Experiment I – Concentration Dependence and Cross Sensitivity

Experiment I was conducted to test for a CO_2 and H_2O concentration dependency of the measurements of the TGA 200 and the Picarro. As one can clearly see in Figure (4.1-1), the CO_2 concentration had only a small effect on the δ-values of CO_2 and H_2O. However, with rising CO_2 concentration there appeared to be a slight tendency of decreasing $\delta^{18}O\text{-}CO_2$ values and increasing $\delta^{18}O\text{-}H_2O$ and $\delta D\text{-}H_2O$ values. In contrast, the $\delta^{13}C\text{-}CO_2$ values were hardly affected at all.

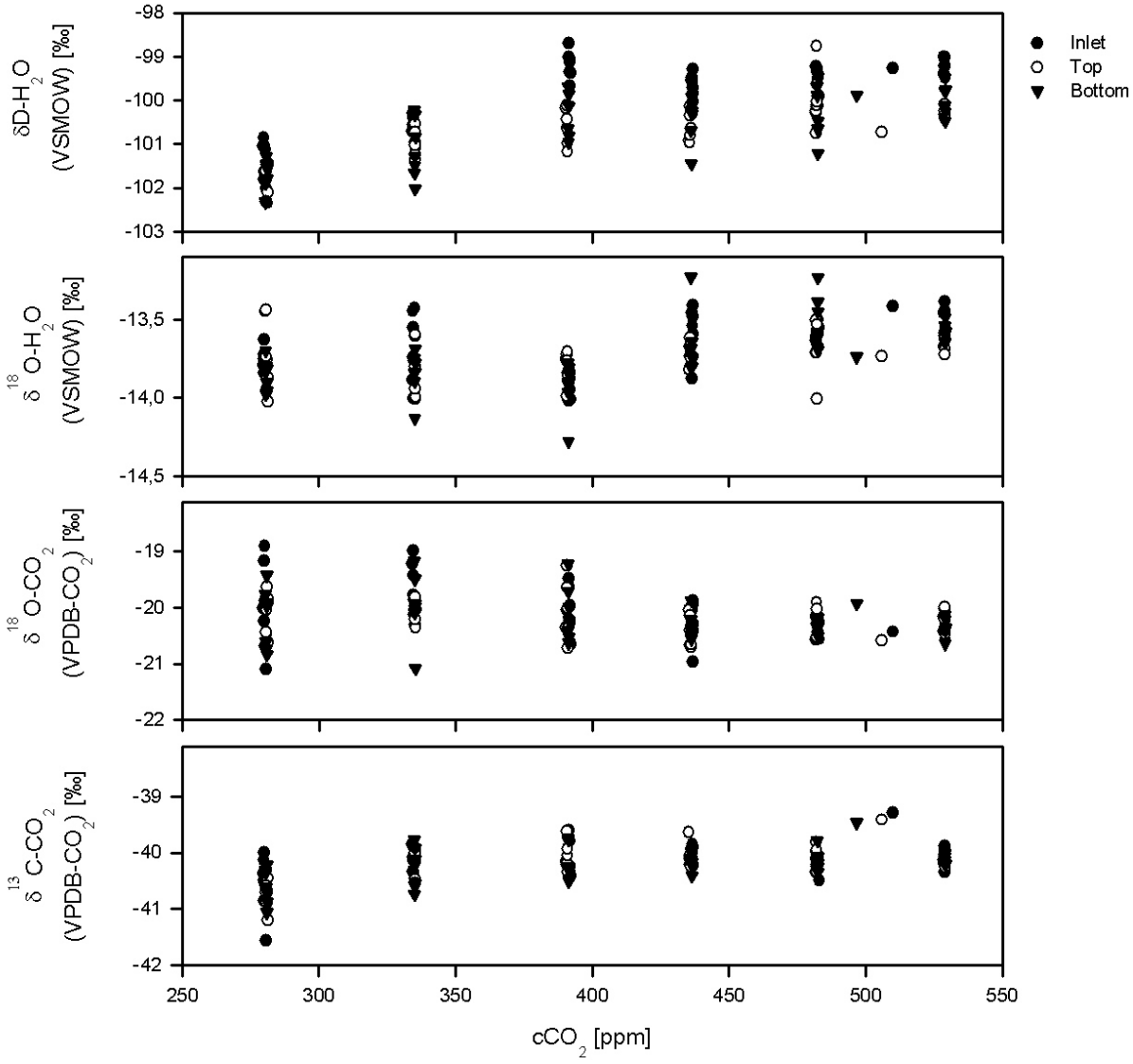

Figure 4.1-1: Dependence of H_2O and CO_2 isotope measurements on CO_2 concentrations.

Linear regression for the range between 380 and 530 ppm CO_2, which was about the range of the measured CO_2 concentrations during the experiments, resulted in following linear equations, coefficients of linear determination and levels of significance (Table 4-1). The p-values of $\delta^{18}O\text{-}CO_2$ and $\delta^{18}O\text{-}H_2O$ are both lower than 0.05. Hence there was a significant trend.

Table 4-1: Linear equations, linear regression coefficients and levels of significance of the dependence of the δ –values on the CO_2 concentration.

	Linear Equation	r^2	p	Δδ-value
$\delta^{13}C\text{-}CO_2$	0.00025x-40.2	0.0028	0.6325	0.0350
$\delta^{18}O\text{-}CO_2$	-0.0017x-19.5	0.0733	0.0127	-0.2380
$\delta^{18}O\text{-}H_2O$	0.0022x-14.7	0.3761	0.0000	0.3080
$\delta D\text{-}H_2O$	0.0022x-101	0.0327	0.0997	0.3080

Figure (4.1-2) shows the result of the cross sensitivity analysis. The $\delta^{13}C\text{-}CO_2$ values and $\delta^{18}O\text{-}CO_2$ values were neither affected by H_2O concentration nor by CO_2 concentration. The CO_2 concentrations did not have any effect on the $\delta^{18}O\text{-}H_2O$ and $\delta D\text{-}H_2O$ values either. However, the $\delta^{18}O\text{-}H_2O$ and $\delta D\text{-}H_2O$ values showed a dependency on H_2O concentration and increased with rising H_2O concentration.

Linear regression for the range between 14000 and 27000 ppmv H_2O resulted in following linear equations, coefficients of linear determination and levels of significance (Table 4-2). The p-values of all δ values were lower than 0.05. Hence there was a significant trend.

Table 4-2: Linear equations, linear regression coefficients and levels of significance of the dependence of the δ –values on the H_2O concentration.

	Linear Equation	r^2	p	Δδ-value
$\delta^{13}C\text{-}CO_2$	-0.000004715x-40.1	0.0050	0.02545	0.0613
$\delta^{18}O\text{-}CO_2$	-0.00001169x-19.94	0.0105	0.00111	0.1520
$\delta^{18}O\text{-}H_2O$	0.0002571x-19.58	0.7124	0.00000	3.3423
$\delta D\text{-}H_2O$	0.001378x-101	0.5005	0.00000	17.9140

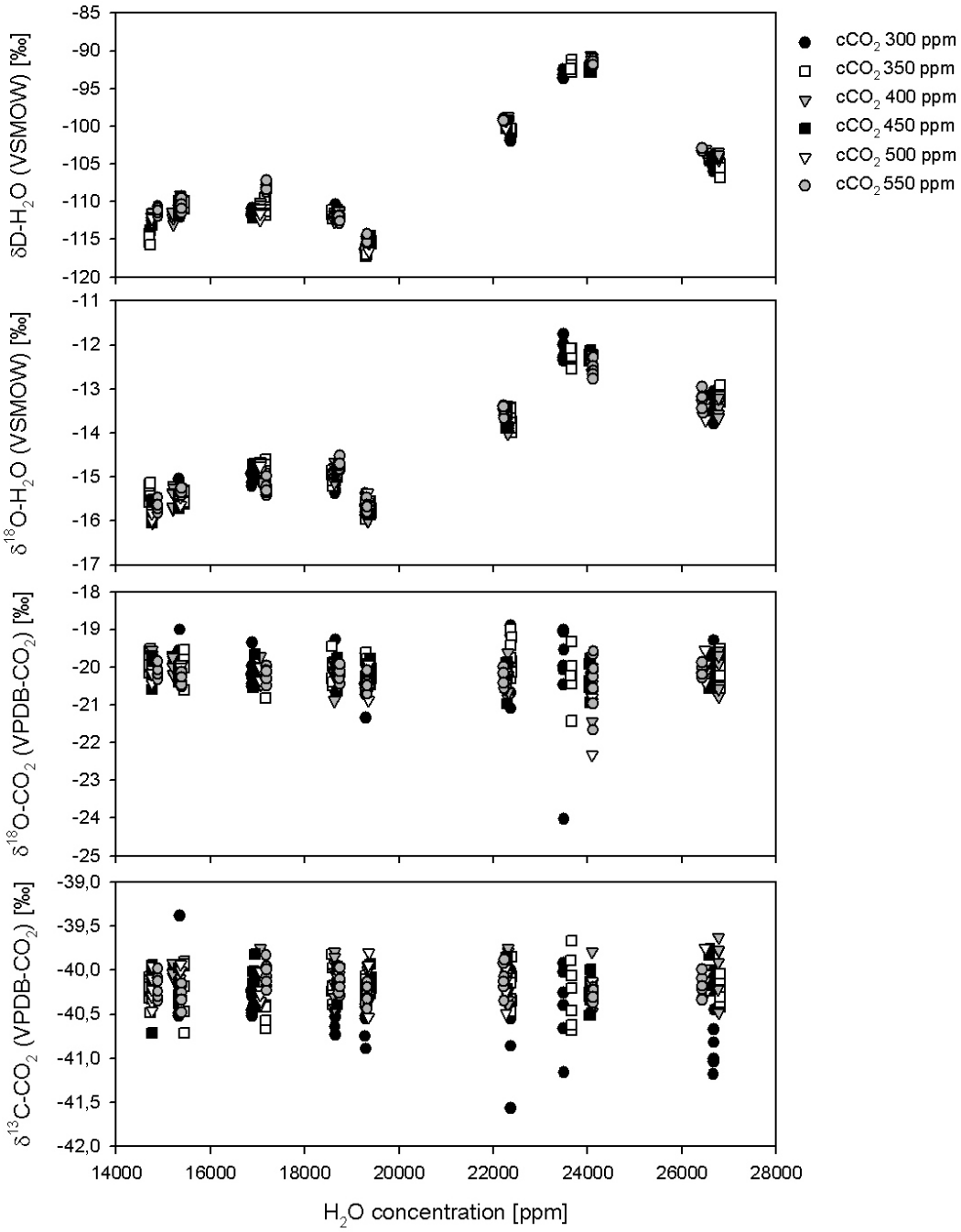

Figure 4.1-2: Cross sensitivity of CO_2 and H_2O isotope measurements at different CO_2 and H_2O concentrations.

4.2 Experiment II – Characterization of Empty Cuvettes

In order to test whether the experimental setup of the cuvettes did not have a bias on isotope analysis, the δ-values of CO_2 were measured in empty cuvettes. Figure (4.2-1) shows the homogenous subgroups of the results of the measurements 1-10:

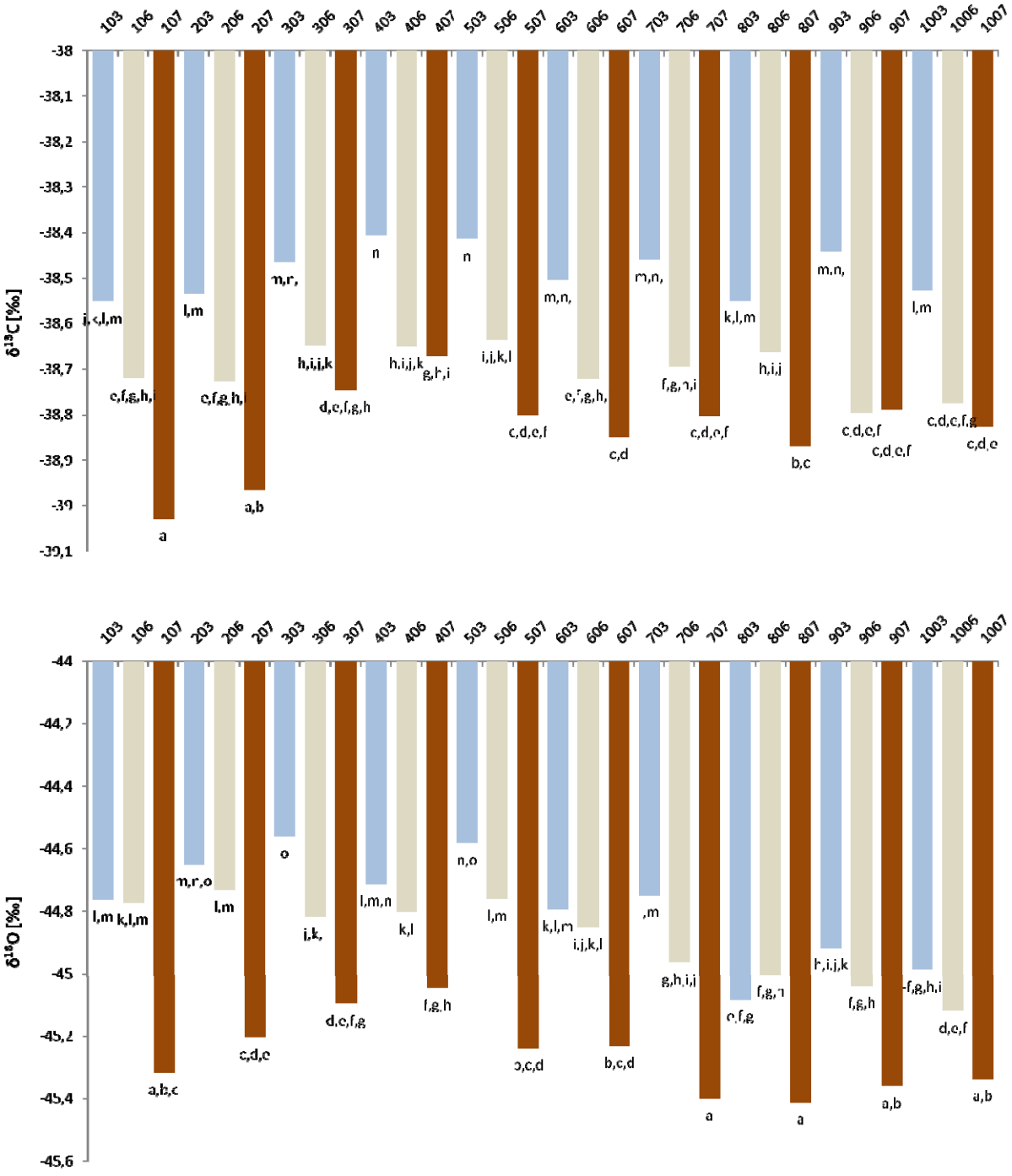

Figure 4.2-1: Homogenous subgroups of the means of the measured values of $\delta^{13}C\text{-}CO_2$ and $\delta^{18}O\text{-}CO_2$ for the measurements 1-10. The x-axis represents the code for the number and the site of the measurement, where 03 stands for the inlet, 06 for the left cuvette and 07 for the right cuvette. For example, 803 stands for the eighth measurement of the inlet. The light blue column represents the value of the inlet, the light brown column represents the value of the left cuvette and the dark brown column represents the value of the right cuvette.

Figure (4.2-2) shows the homogenous subgroups of the results of the measurements 11-20 of Experiment II:

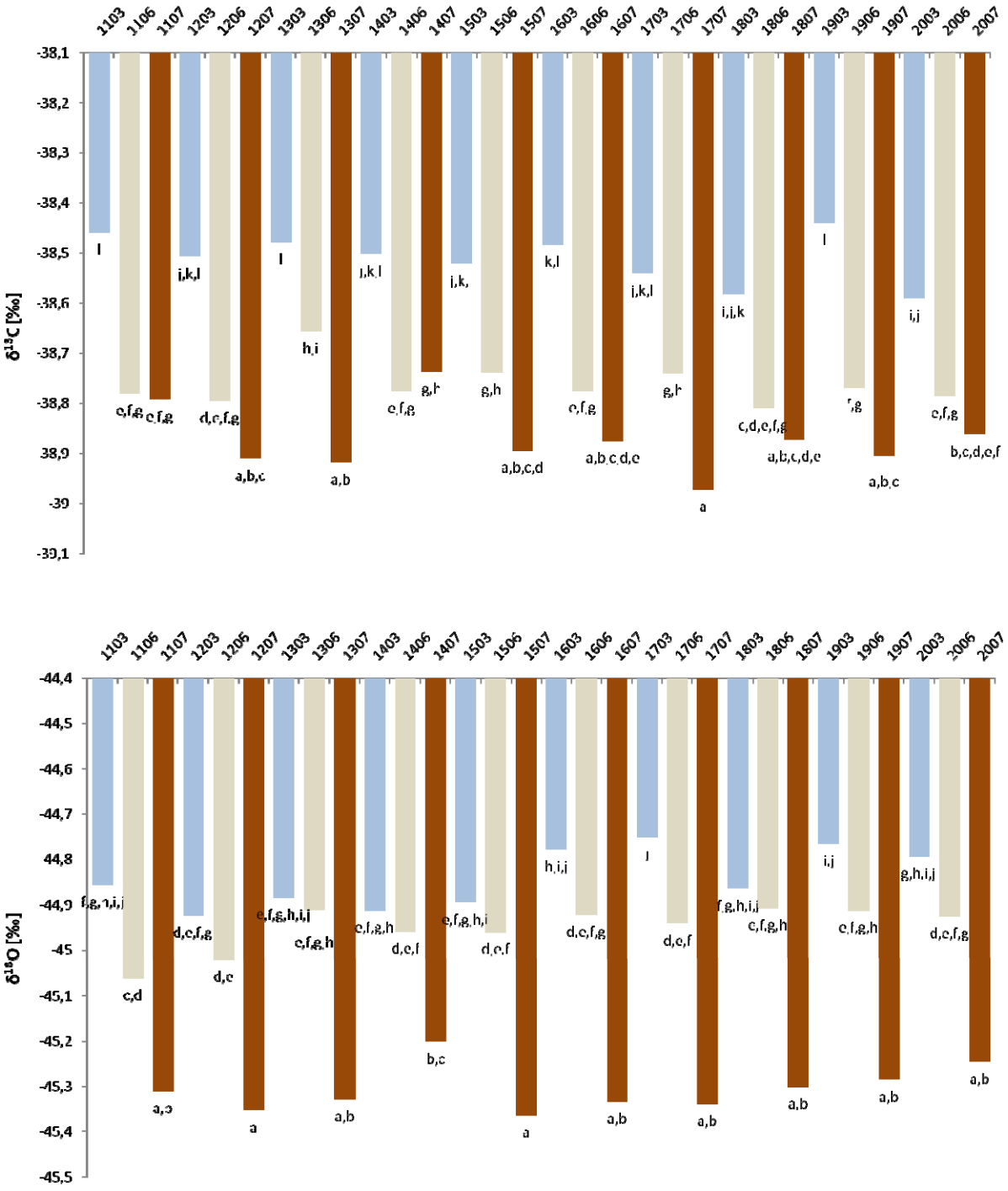

Figure 4.2-2: Homogenous subgroups of the means of the measured values of $\delta^{13}C\text{-}CO_2$ and $\delta^{18}O\text{-}CO_2$ for the measurements 11-20. The x-axis represents the code for the number and the site of the measurement, where 03 stands for the inlet, 06 for the left cuvette and 07 for the right cuvette. For example, 1603 stands for the sixteenth measurement of the inlet. The light blue column represents the value of the inlet, the light brown column represents the value of the left cuvette and the dark brown column represents the value of the right cuvette.

During the first 10 measurements, the maximum deviation of the inlet values from the outlet values of the two cuvettes was approx. 0.5‰ for $\delta^{13}C\text{-}CO_2$, and approx. 0.7‰ for $\delta^{18}O\text{-}CO_2$. In the case of $\delta^{13}C\text{-}CO_2$, the values of the right cuvette and the left cuvette were close together and deviated from those of the inlet by approx. 0.3‰. In the case of $\delta^{18}O\text{-}CO_2$ the values of the inlet and the left cuvette were close together, whereas those of the right cuvette deviated by approx. 0.4‰.

During the measurements 11-20, the maximum deviation of the inlet to the two cuvettes was approx. 0.5‰ for $\delta^{13}C\text{-}CO_2$ and approx. 0.6‰ for $\delta^{18}O\text{-}CO_2$. The $\delta^{13}C\text{-}CO_2$ values of the right cuvette and the left cuvette were close together. They deviated from the inlet by approx. 0.3‰. The $\delta^{18}O\text{-}CO_2$ values of the inlet and the left cuvette were close together. The $\delta^{18}O\text{-}CO_2$ values of the right cuvette deviated by approx. 0.4‰.

4.3 Experiment III – Cuvettes filled with Sand, with CO_2 Addition and Irrigation

Experiment III was conducted to test whether the gas flows of the experimental setup could be maintained stable over a longer period for several hours. As figure (4.3-1) shows, the gas flows could be maintained stable. It took approx. one hour to bring the CO_2 concentration to the desired level. From this point on, the CO_2 concentration remained stable and did not deviate between the inlet and the two cuvettes. At about 11:00 h a breakdown of the fluxes occurred for about 15 minutes because thegas bottle with synthetic air was changed.

The $\delta^{13}C\text{-}CO_2$ values did not deviate between the inlet and the two cuvettes. With the exception of a few outliers, the range of the $\delta^{13}C$ values remained between -41.0‰ and -42.0‰ vs. V-PDB-CO_2, with a small tendency to increase towards the end of the experiment.

The $\delta^{18}O\text{-}CO_2$ values during the first four hours also showed no deviations between the inlet and the two cuvettes. Towards the end of the experiment, the $\delta^{18}O\text{-}CO_2$ values of the cuvette with fine sand tended to be slightly higher compared to the other two measurements. The total range of the values was between -39.5‰ and 41.0‰ vs. V-PDB-CO_2, again with the exception of a few outliers.

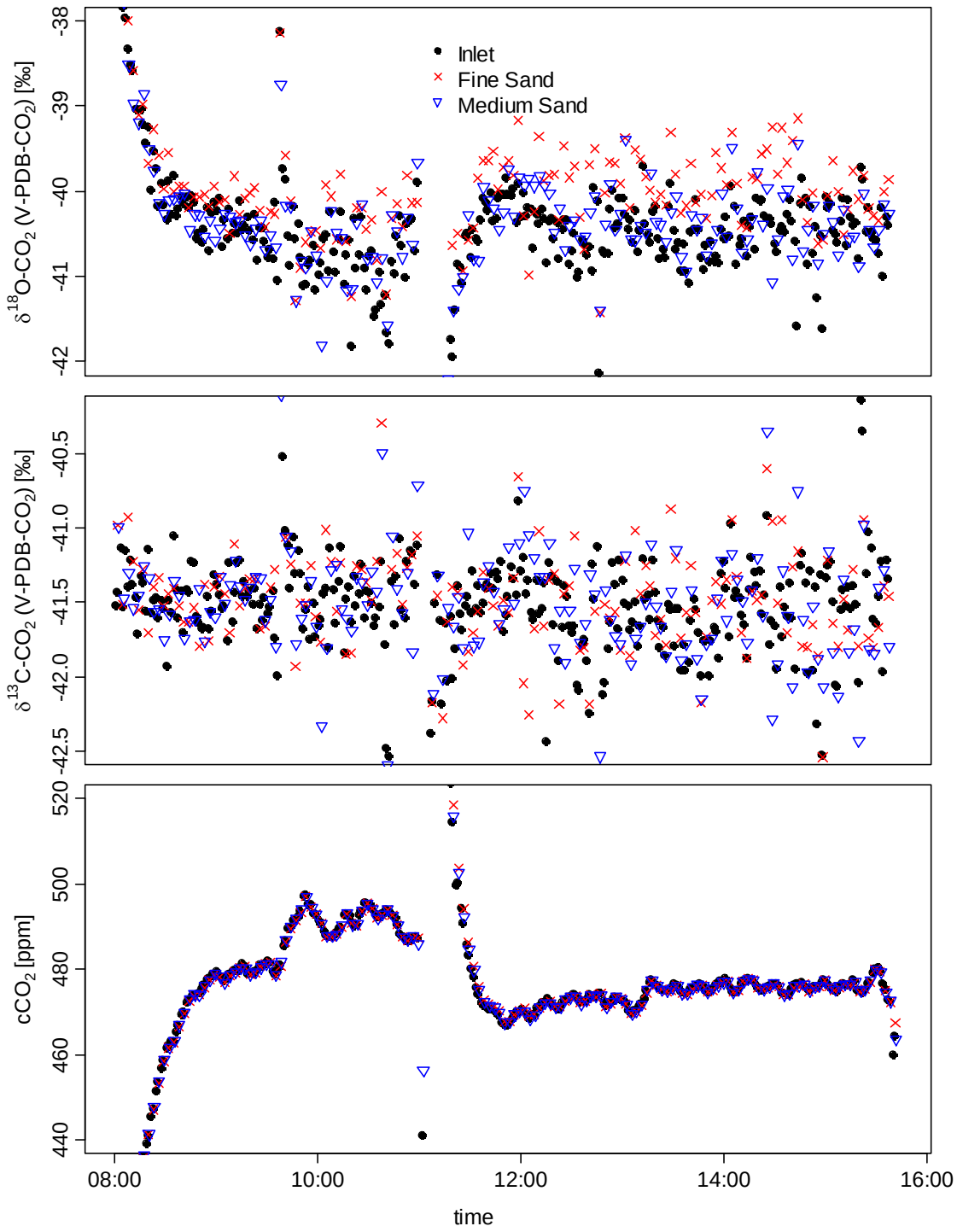

Figure 4.3-1: Concentration and isotopic composition of CO_2 after stabilization of flows through cuvettes with dry fine and medium sand over a period of eight hours.

4.4 Experiment IV – Drying of Soil Columns After Irrigation

The purpose of Experiment IV was to test the effect of the drying-out of soil columns on the oxygen isotopic composition of soil-released CO_2. Figure (4.4-1) shows the concentration and δ-values of CO_2, Figure (4.4-2) displays the concentration and δ-values of H_2O, and Figure (4.4-3) depicts the volumetric water content and the temperature of the soil columns, the relative humidity and the temperature of the air. The CO_2 concentrations could be maintained very stable during the whole experiment, and the concentrations of CO_2 of the two cuvettes hardly deviated at all. One could see clearly the effect of irrigation after 24 hours. The CO_2 concentrations of the two cuvettes dropped immediately after the irrigation, but returned to their original level and stabilized again after a few hours.

The $\delta^{13}C$ values did not deviate between the inlet and the two cuvettes and were not affected by irrigation at all. Values ranged between approx. 41.0‰ and 42.0‰ vs. V-PDB-CO_2. In contrast, the $\delta^{18}O$ values exhibited a diffusional effect during the first 24 hours of the experiment. This effect appeared to be more pronounced in the cuvette with fine sand compared to the cuvette with medium sand. In contrast to $\delta^{13}C$, $\delta^{18}O$ values were affected by the irrigation, reflected in the increase directly after the addition of water. This effect was more pronounced in the cuvette with medium sand, where the $\delta^{18}O$ values rose from approx. 10‰ to approx. 20‰, compared to the cuvette with fine sand, where the $\delta^{18}O$ values rose from approx. 17‰ to approx. 20‰. Evaporation on the surface and the concomitant drying-out of the soil column did not have an effect on the δ-values of CO_2.

Figure (4.4-2) shows the concentration and δ-values of H_2O. The H_2O concentration in the gas mixture rose directly after irrigation to approx. 25,000 ppm. After approx. 60 h, the H_2O concentration in the cuvette with medium sand started to decrease to a value of approx. 12,000 ppm, whereas the concentration in the cuvette with fine sand remained stable for the whole experiment. The δD values started to increase directly after the irrigation from approx. -140‰ vs. V-SMOW to approx. 75‰ vs. V-SMOW. The increase of the δD values of the cuvette with medium sand was larger and faster compared to the cuvette with fine sand. After approx. 70 h, the δD values of the cuvette with medium sand suddenly decreased slowly by approx. 10‰, whereas they continued to rise in the cuvette with fine sand. The behavior of the $\delta^{18}O$ values was very similar to the one of the δD values, only the absolute values differed.

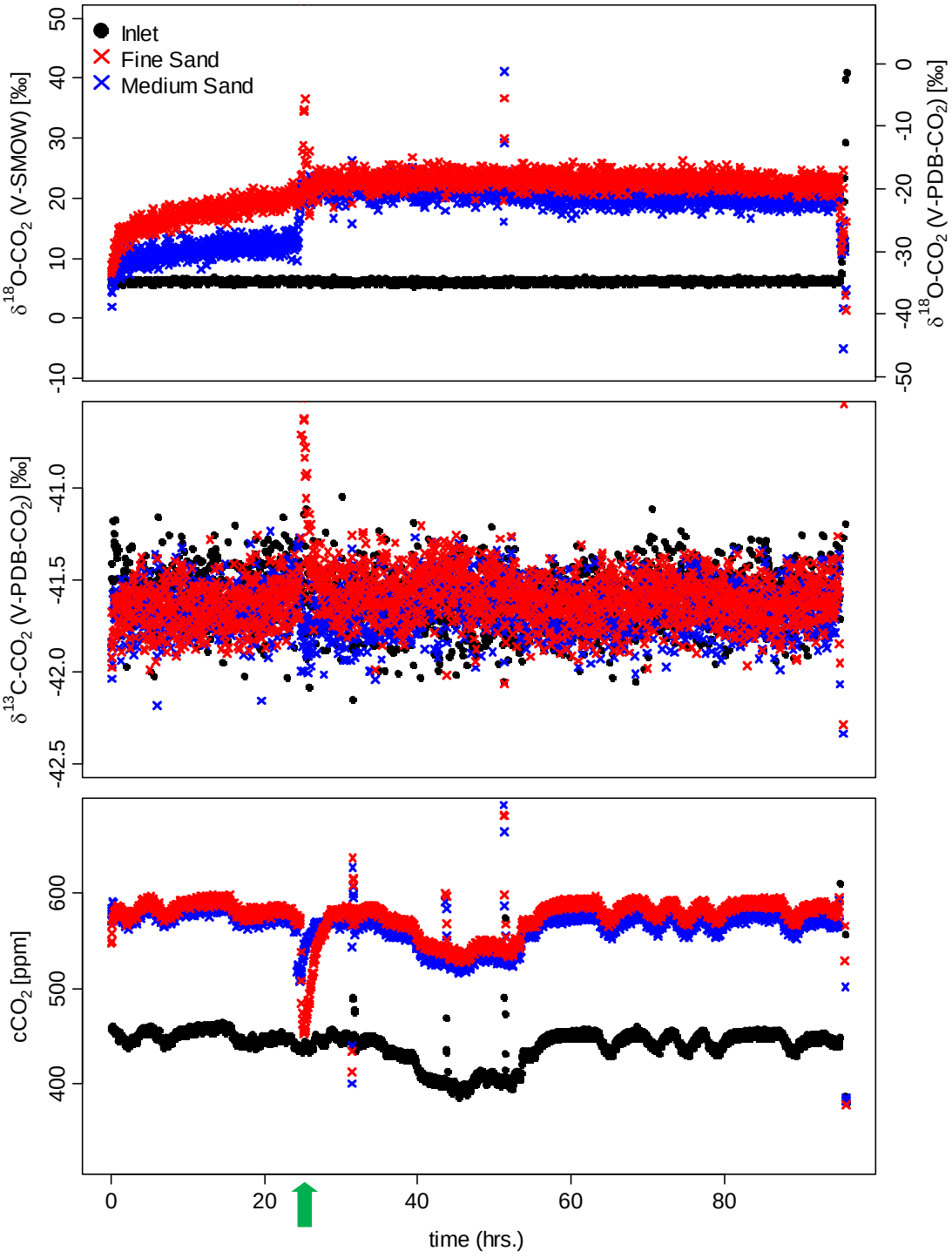

Figure 4.4-1: Concentration and δ-values of CO_2 during Experiment IV; $\delta^{18}O$ values are expressed on the V-SMOW scale on the left y-axis and on the V-PDB-CO_2 scale on the right y-axis. The green arrow represents the time of irrigation.

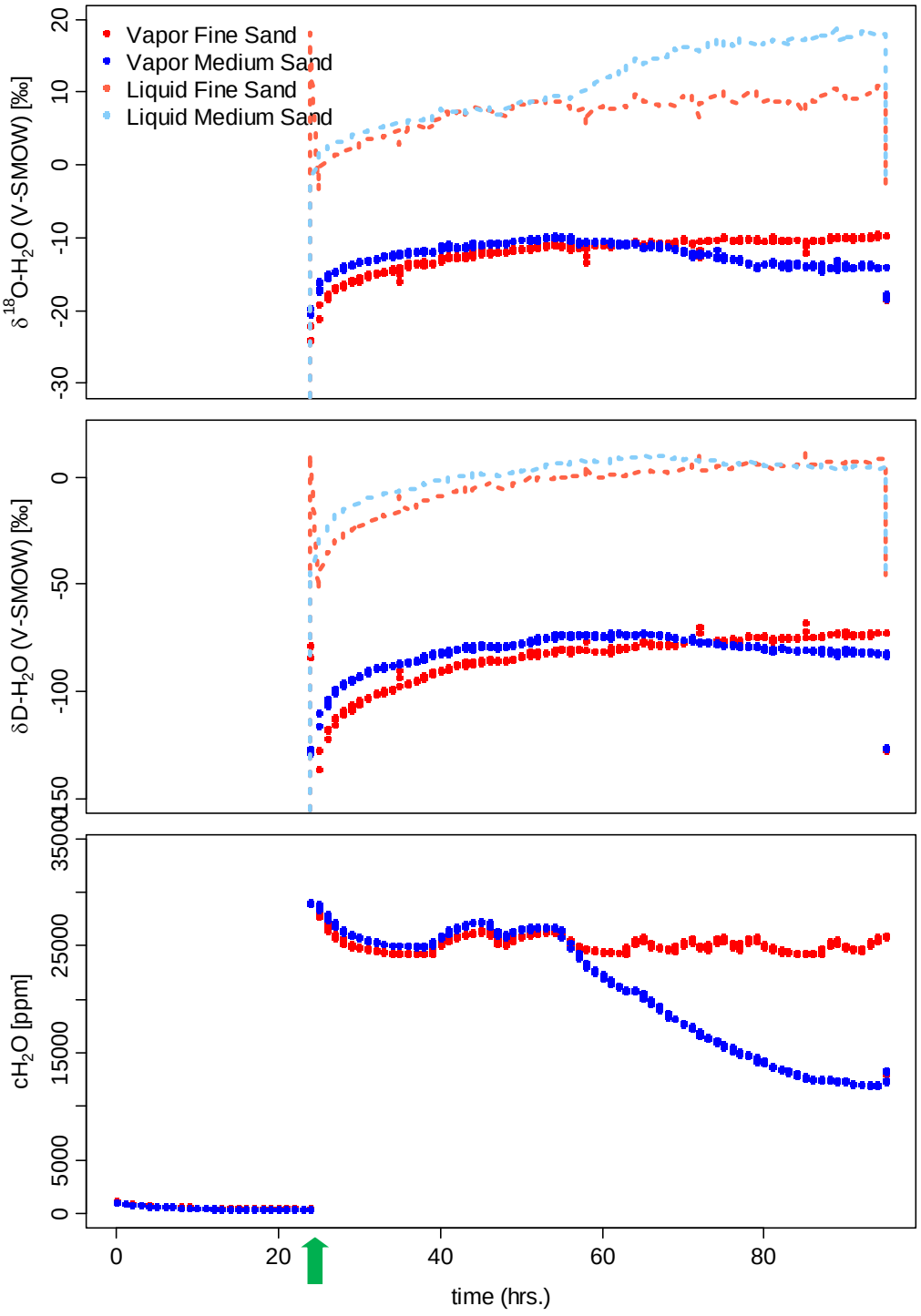

Figure 4.4-2: Concentration and δ-values of H_2O during Experiment IV. The pale colored lines represent the δ-values of the soil water at the site of evaporation calculated according to the Craig-Gordon model (Craig and Gordon, 1965). The green arrow represents the time of irrigation.

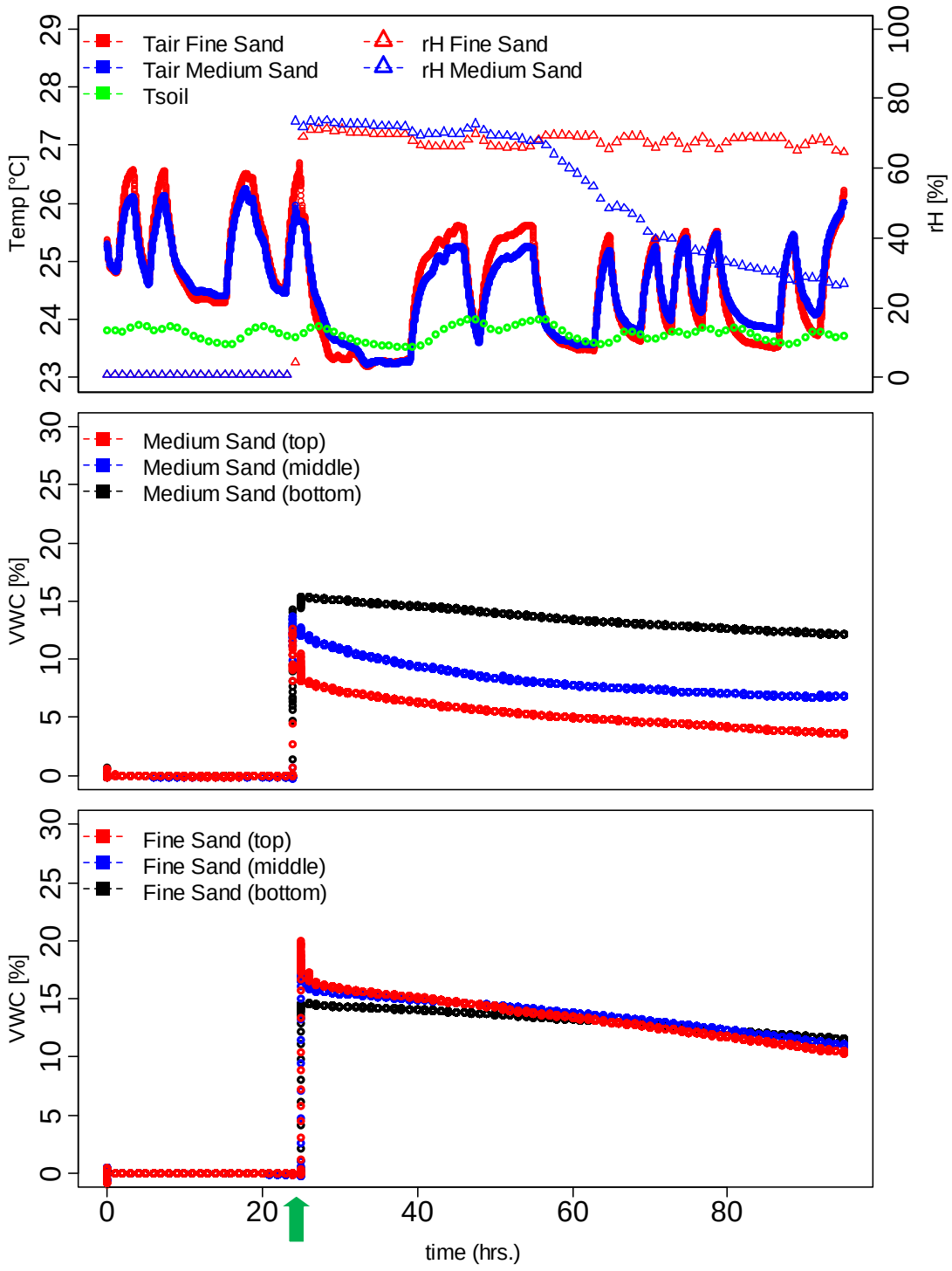

Figure 4.4-3: Volumetric soil water content, soil temperature, air temperature and relative air humidity in the cuvettes during Experiment IV. The green arrow represents the time of irrigation.

One could clearly see the evaporative enrichment of the water body for both δD and $\delta^{18}O$ values. The enrichment was more pronounced and faster in the cuvette with medium sand compared to the cuvette with fine sand in the case of δD values. The δD values of the cuvette with medium sand rose from approx. -50‰ vs. V-SMOW to approx. 10‰ vs. V-SMOW whereas the δD values of the cuvette with fine sand rose from approx. -50‰ vs. V-SMOW to approx. 5‰ vs. V-SMOW. In the case of the $\delta^{18}O$ values of the liquid water body of the two types of sand did not lead to any differences during the first 60 h. They rose from approx. -1‰ vs. V-SMOW to approx. 9‰ vs. V-SMOW. But at the time when the H_2O concentration in the cuvette with medium sand started to decrease, a big increase in the $\delta^{18}O$ values of the soil water to approx. 19‰ occurred, whereas they continued to rise much less, i.e. to a value of approx. 10‰, in the cuvette with fine sand.

Figure (4.8) shows the volumetric soil water content, soil temperature, air temperature and relative humidity of air in the cuvettes. The volumetric water content (VWC) of the two types of sand showed very different developments. The VWC in the cuvette with fine sand did not differ very much between the different depths and decreased very constantly from approx. 18% to approx. 12%. In contrast, VWC in the cuvette with medium sand showed large variations at the different depths. Shortly after irrigation, VWC at the bottom of the cuvette with fine sand was already higher than at the middle and the top of the soil column. It then decreased at the top from approx. 7.5% to approx. 5%, at the middle from approx. 12.5% to approx. 7.5% and at the bottom from approx. 15% to approx. 12.5%. While headspace air temperature fluctuated between 23°C and 27°C, soil temperature fluctuations were less pronounced, ranging from approx. 23.5°C to 24°C. Relative humidity matched H_2O concentrations in the headspace of the cuvettes.

4.5 Experiment V – Soil Columns with CO_2 Addition and Irrigation with ^{18}O-enriched Water

The aim of Experiment V was to test the effect of soil moisture on the oxygen isotopic composition of soil released CO_2. Figure (4.5-1) shows the concentration and δ-values of CO_2, Figure (4.5-2) displays the concentration and δ-values of H_2O and Figure (4.5-3) illustrates the volumetric water content and the temperature of the soil columns, the relative humidity and the temperature of the air. The CO_2 concentrations could be maintained very stable during the whole experiment, and the concentrations of CO_2 of the two cuvettes hardly deviated at all. One could clearly see the effect of irrigation after every 24 hours. Right after the irrigation the CO_2 concentrations of the two cuvettes dropped, but stabilized again after a few hours as in Experiment IV.

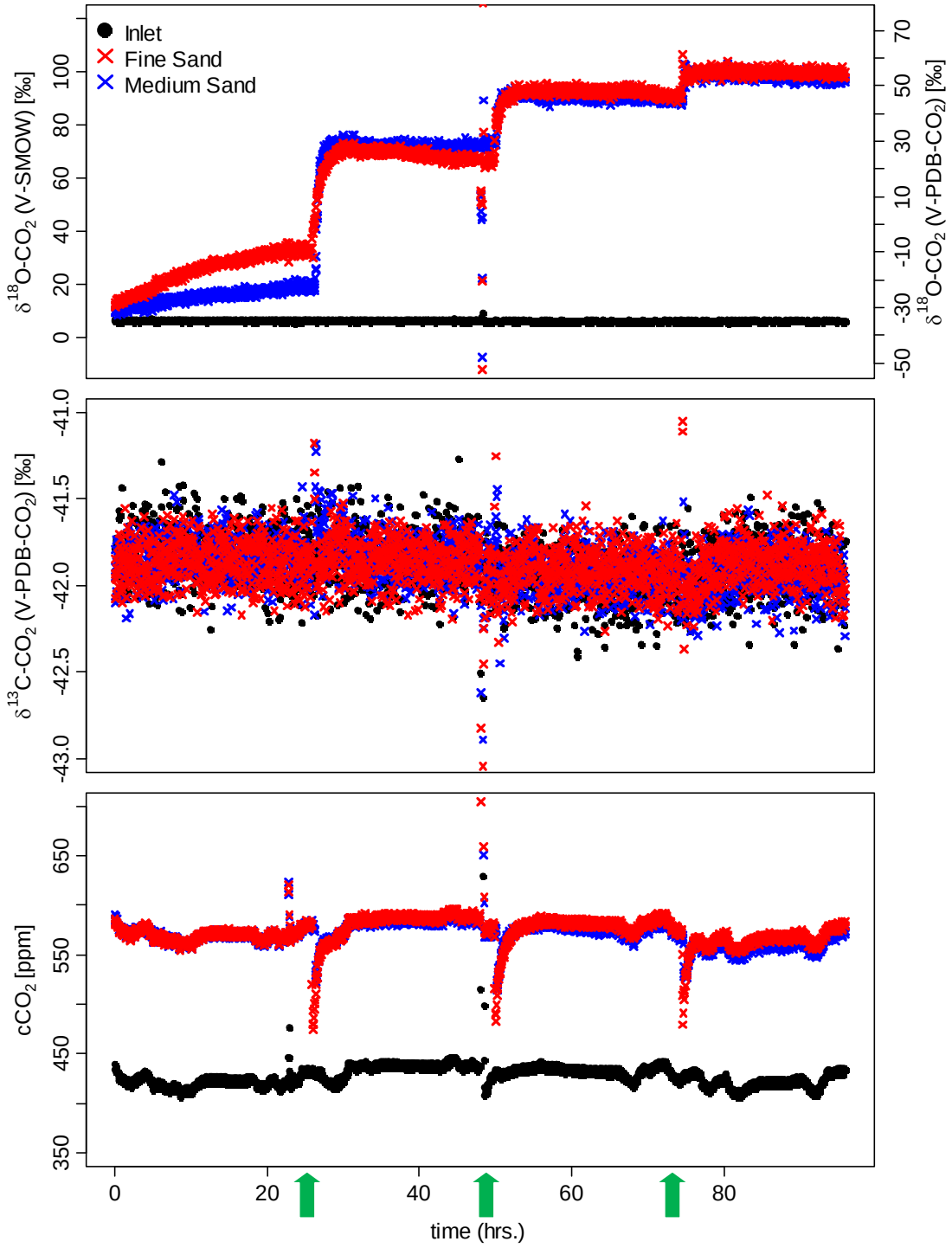

Figure 4.5-1: Concentration and δ values of CO_2 during Experiment V. The green arrows represent the time of irrigation.

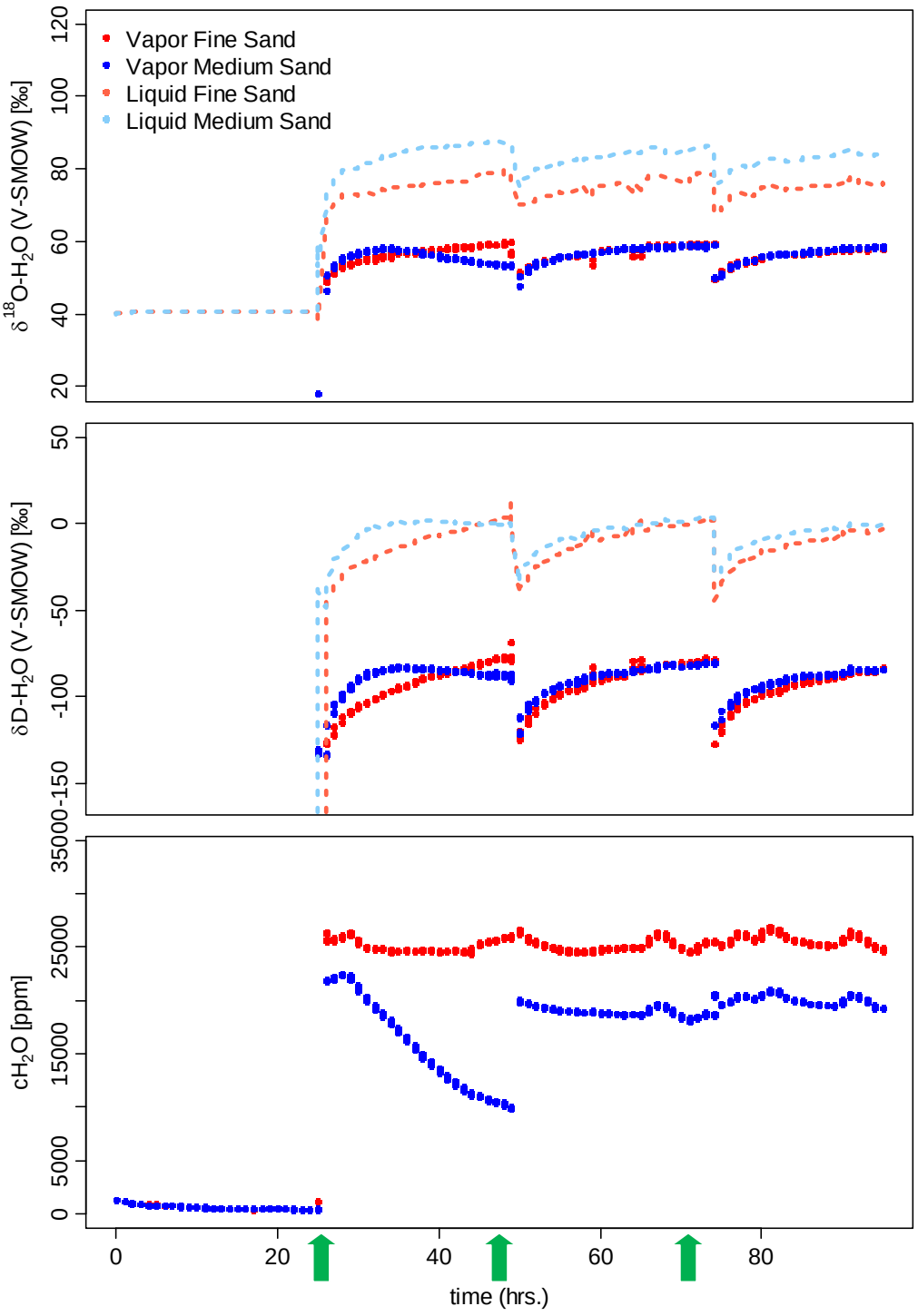

Figure 4.5-2: Concentration and δ-values of H_2O during Experiment V. The pale colored lines represent the δ values of the soil water at the site of evaporation calculated after the Craig-Gordon modell (Craig and Gordon, 1965). The green arrows represent the time of irrigation.

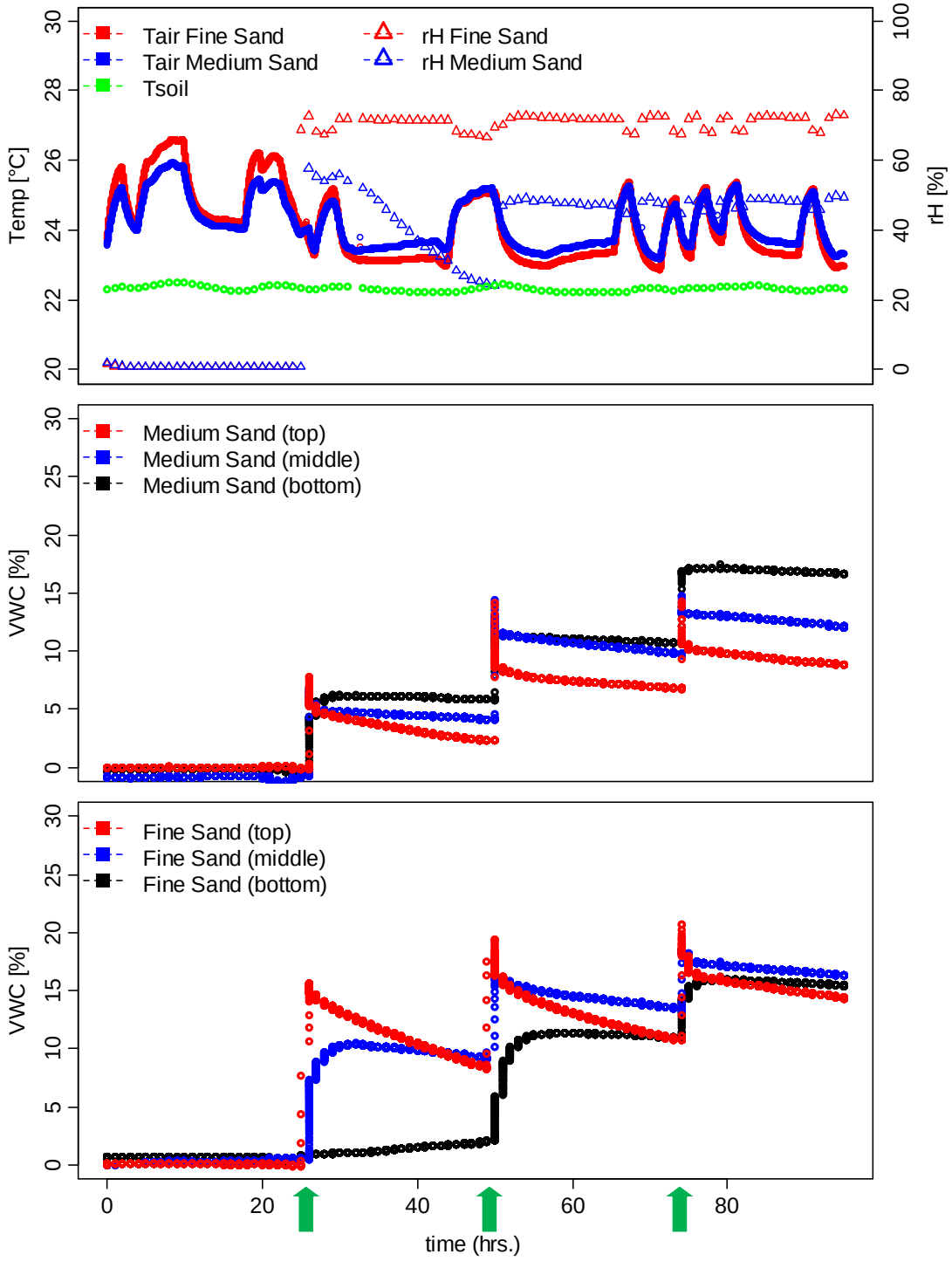

Figure 4.5-3: Volumetric soil water content, soil temperature, air temperature and relative humidity of air in the cuvettes during Experiment V. The green arrows represent the time of irrigation.

Again, the $\delta^{13}C$ values did not deviate between the inlet and the two cuvettes and were not affected by irrigation at all. The total range of the values in Experiment V was between approx. 41.5‰ and 42.25‰ vs. V-PDB-CO_2. As in Experiment IV, the $\delta^{18}O$-CO_2 values did showed a diffusional effect during the first 24 h of the experiment. This effect was much more pronounced in the cuvette with fine sand compared to the cuvette with medium sand. In this experiment the diffusional effect was more pronounced as compared to the previous experiment. The $\delta^{18}O$-CO_2 values were strongly affected by irrigation. They increased directly after the first addition of water by 35‰ to 70‰ vs. V-SMOW in the case of the cuvette with fine sand and by about 45‰ to 73‰ vs. V-SMOW in the case of medium sand. From this point on, $\delta^{18}O$-CO_2 values of both cuvettes hardly deviated any more. After the next two irrigation events, $\delta^{18}O$-CO_2 values increased again, but not as much as after the first irrigation event. After the last irrigation, they reached a $\delta^{18}O$-CO_2 value of about 98‰ vs. V-SMOW.

Figure (4.5-2) shows the concentration and δ-values of H_2O. As in the previous experiment, the H_2O concentration in the gas mixture rose directly after irrigation to approx. 25,000 ppm in the case of the cuvette with fine sand and to approx. 24,000 ppm in the case of the cuvette with medium sand. In Experiment V, the concentration started to decline again after only a few hours in the cuvette with medium sand to a level of approx. 10,000 ppm. After the second irrigation the concentration increased to approx. 20000 ppm and remained stable at this level. The δD values showed a behavior very similar to the previous experiment. One could see an evaporative enrichment after every irrigation event. The same was the case for the $\delta^{18}O$-H_2O values, only this time the values were larger due to the enriched irrigation water. Much stronger during this experiment though was the evaporative enrichment of the liquid water body for both, the δD values and the $\delta^{18}O$-H_2O values. Again the enrichment was more pronounced and faster in the cuvette with medium sand compared to the cuvette with fine sand in the case of δD. The δD values of the cuvette with medium sand rose from approx. 50‰ vs. V-SMOW to approx. 85‰ vs. V-SMOW, whereas the δD values of the cuvette with fine sand rose from approx. -50‰ vs. V-SMOW to approx. 0‰ vs. V-SMOW. A similar behavior with different values could be observed in the case of the $\delta^{18}O$-H_2O values of the liquid water body.

Figure (4.5-3) shows the volumetric water content, soil temperature, air temperature and relative humidity of air in the cuvettes. After the first irrigation the volumetric water content at the bottom of the cuvette with fine sand hardly changed at all whereas those of the middle and the top did. After the second irrigation, the volumetric water content at the bottom of the cuvette increased abruptly. Over the whole course of the experiment the volumetric water content at the three different heights converged to a very similar value of approx. 15%. In contrast, in the cuvette with medium sand the volumetric water content at the bottom reacted directly after the first irrigation and remained at the

highest level compared to the other two heights during the whole experiment. Over the whole course of the experiment the volumetric water content at the three different heights diverged from each other with a value of approx. 17.5%, 14% and 10% at the bottom, at the middle and at the top, respectively. Air temperature, relative humidity and soil temperature showed a similar behavior compared to the previous experiment.

4.6 Experiment VI – The Effect of an Organic Litter Layer (Spruce Needles)

In Experiment VI and VII, the effect of an organic litter layer on the δ-values of CO_2 and H_2O was examined. Figure (4.6-1) shows that the litter layer did not have any effect on CO_2 concentrations or $\delta^{13}C$ values. The change of the $\delta^{13}C$ values was due to the fact that the gas bottle with the pure CO_2 had to be changed before the experiment. In the case of $\delta^{18}O$-CO_2 values, the kinetic fractionation due to diffusion appeared to be less pronounced in the presence of a litter layer as compared to the situation without. The $\delta^{18}O$-CO_2 values showed a similar behavior after irrigation like in the previous experiment. The soil CO_2 flux in the cuvette with medium sand was broke down after the third irrigation, which caused a significant increase and deviation of the δ-values.

In contrast, concentration and δ-values of H_2O were significantly influenced by the litter layer, as demonstrated in Figure (4.6-2). The H_2O vapor concentration was very similar in both cuvettes and much lower as compared to the previous experiment. It remained close to approx. 7,500 ppm after the first irrigation, and close to 8,500 ppm after the second and third irrigation event. The evaporative enrichment of the vapor was also much less pronounced compared to the previous experiment, reaching only values of approx. -120‰ and 45‰ vs. V-SMOW for δD and $\delta^{18}O$-H_2O, respectively. The evaporative enrichment of the δ-values of H_2O in the cuvette with medium sand was slightly higher than in the cuvette with fine sand. The evaporative enrichment of the liquid water body was much less variable than in the previous experiments without litter layer.

As can be seen from Figure (4.6-3), the volumetric water content of at the top of the cuvette with fine sand did not decrease as much as in the experiment without litter layer after each irrigation. The behavior at the other two depths was very similar to the previous experiment. In the case of the cuvette with medium sand, the volumetric water content reacted similar to the previous experiment, but on a higher level. The inhibiting influence of the litter layer on evaporation was also reflected in relative humidity.

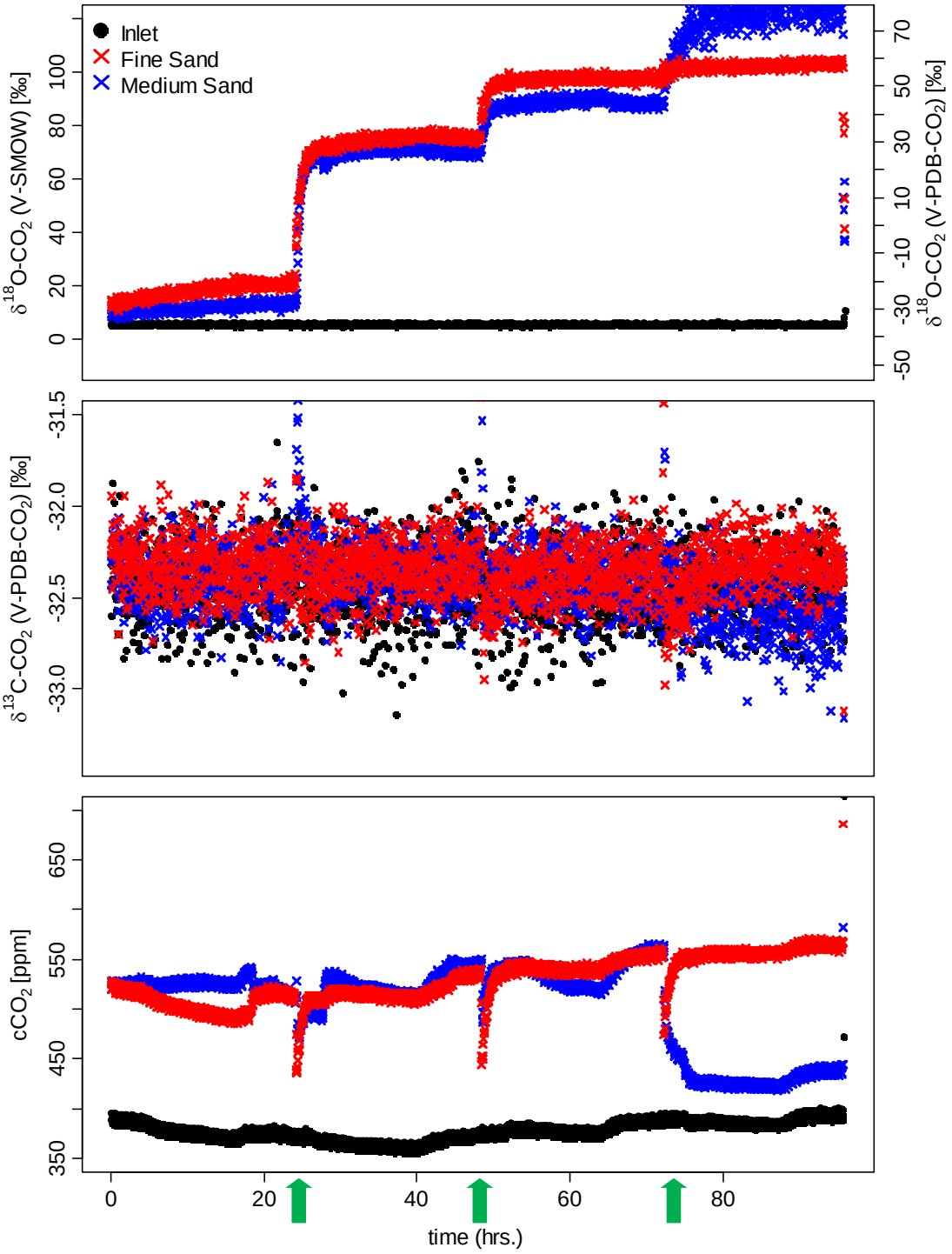

Figure 4.6-1: Concentration and δ values of CO_2 during Experiment VI. The green arrows represent the time of irrigation.

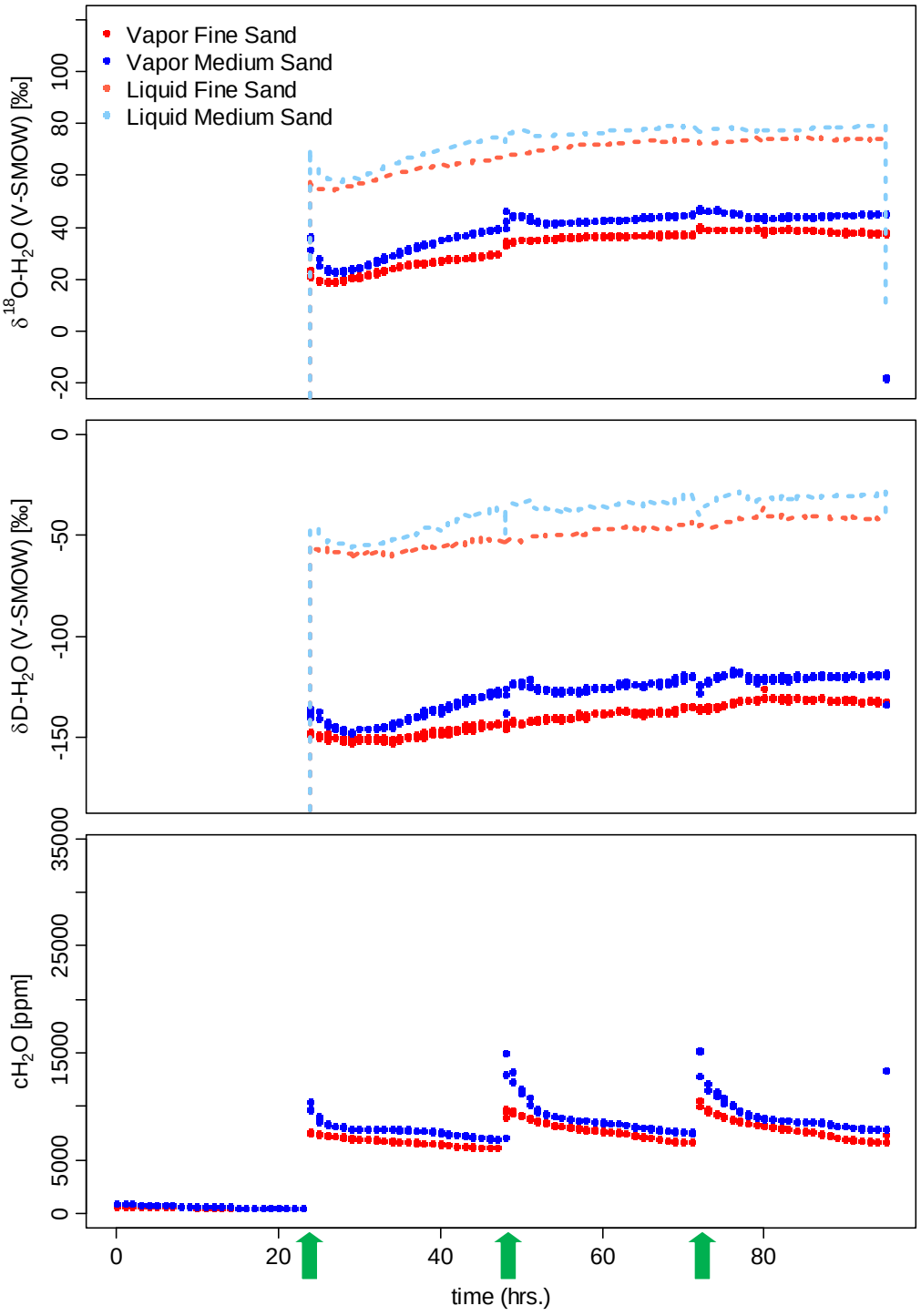

Figure 4.6-2: Concentration and δ-values of H_2O during Experiment VI. The pale colored lines represent the δ values of the soil water at the site of evaporation calculated after the Craig-Gordon modell (Craig and Gordon, 1965). The green arrows represent the time of irrigation.

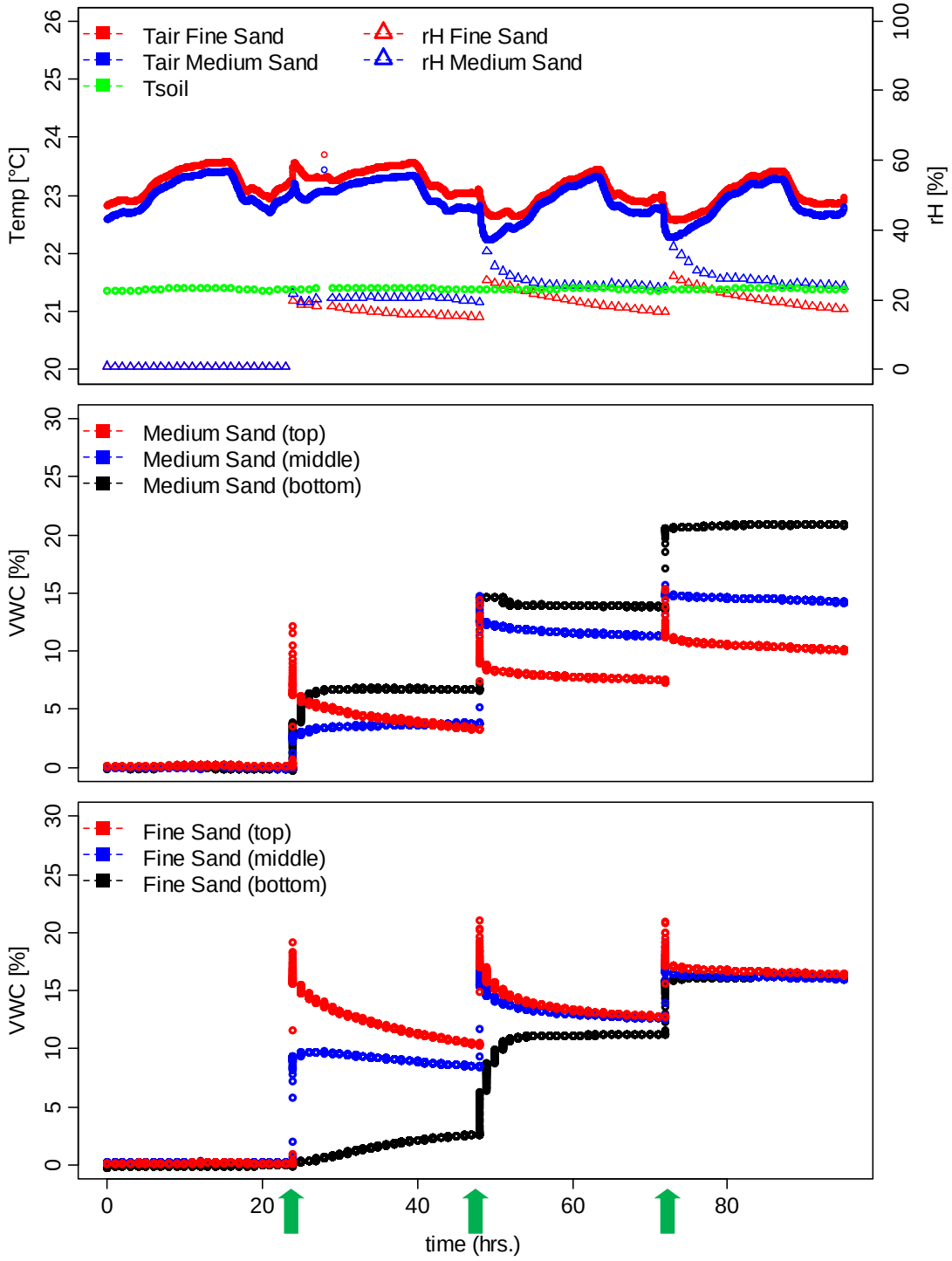

Figure 4.6-3: Volumetric water content, soil temperature, air temperature and relative humidity of air in the cuvettes during Experiment VI. The green arrows represent the time of irrigation.

4.7 Experiment VII – The Effect of an Organic Litter Layer (Beech Leaves)

The concentration and δ-values of CO_2 during Experiment VII were very similar to those of Experiment VI (Figure 4.7-1). Only the $\delta^{13}C$ values were slightly higher. The inhibitory effect of the beech litter layer on evaporation, and hence on concentration and δ-values of H_2O was not as pronounced as compared to the experiment with spruce needle litter layer (Figure 4.7-2). The change of the volumetric water content at each depth over time showed the same pattern in both experiments, albeit the volumetric water content under the beech leaf litter layer was higher as compared to the experiment with spruce needle litter layer. Air temperature, soil temperature and relative humidity of air were very similar to the previous experiment (Figure 4.7-3).

4.8 Experiment VIII – The Effect of Application of Carbonic Anhydrase

In Experiment VIII, the effect of carbonic anhydrase, dissolved in irrigation water, on $\delta^{18}O\text{-}CO_2$ values was explored. Because the data logger did not record soil moisture, soil temperature, relative humidity and air temperature, only the results of the TGA 200 and the Picarro are presented for this experiment. Hence the δ-values of the liquid water body at the site of evaporation could not be calculated for this experiment. Figure (4.8-1) shows the concentration and δ-values of CO_2 during Experiment VIII. The CO_2 concentrations could again be maintained stable during Experiment VIII, with the exception of the disruption right after irrigation.

The $\delta^{13}C$ values at the inlet were approx. 1‰ lower than at the outlet of the two cuvettes and showed a decreasing trend with time. The $\delta^{18}O\text{-}CO_2$ values showed a similar kinetic fractionation due to diffusion as in the previous experiments during the first 24 h. But already after the first irrigation event, $\delta^{18}O\text{-}CO_2$ increased to about 180‰ vs. V-SMOW, much higher than in the previous experiments. In the cuvette with medium sand, $\delta^{18}O\text{-}CO_2$ values decreased to about 140‰ vs. V-SMOW 10 h after the first irrigation. After the second and third irrigation event, $\delta^{18}O\text{-}CO_2$ values further increased to a maximum of about 230‰ vs. V-SMOW, after having passed through a very high peak directly after irrigation. The δ-values of H_2O showed a very similar behavior to those of Experiment V. Only the H_2O concentration in the headspace of the cuvette with medium sand decreased this time directly after each irrigation.

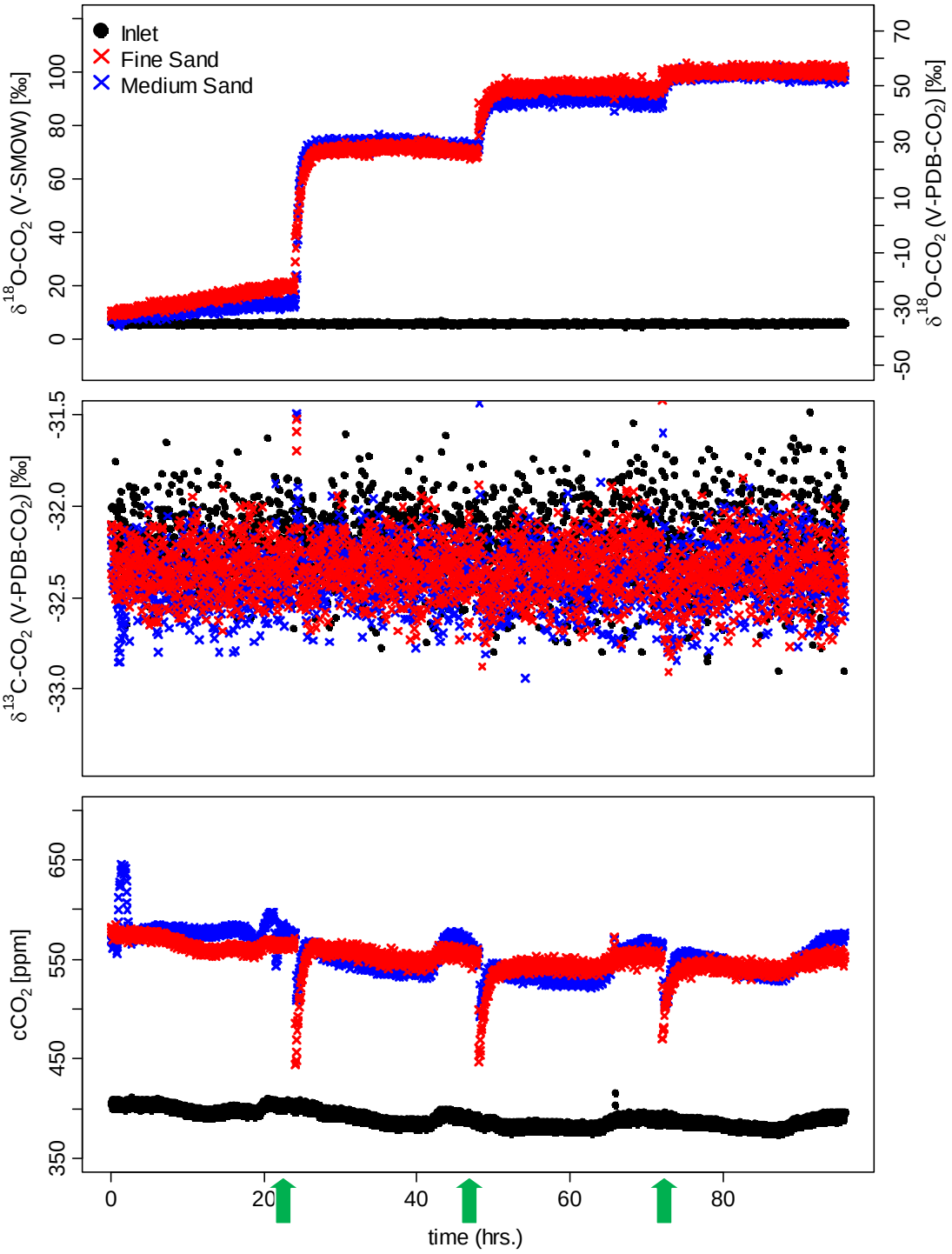

Figure 4.7-1: Concentration and δ values of CO_2 during Experiment VII. The green arrows represent the time of irrigation.

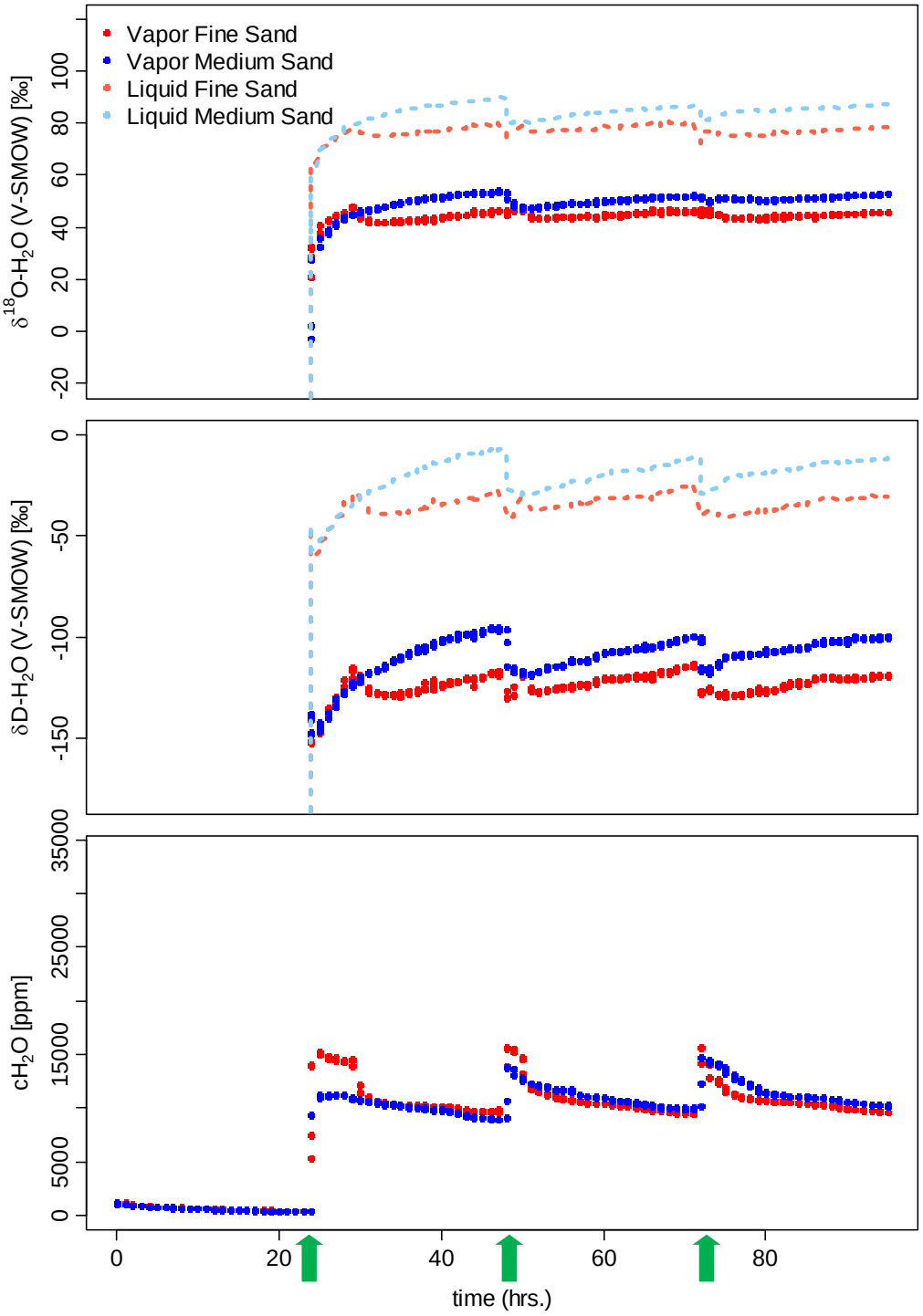

Figure 4.7-2: Concentration and δ-values of H_2O during Experiment VII. The pale colored lines represent the δ values of the soil water at the site of evaporation calculated after the Craig Gordon Modell (Craig and Gordon, 1965). The green arrows represent the time of irrigation.

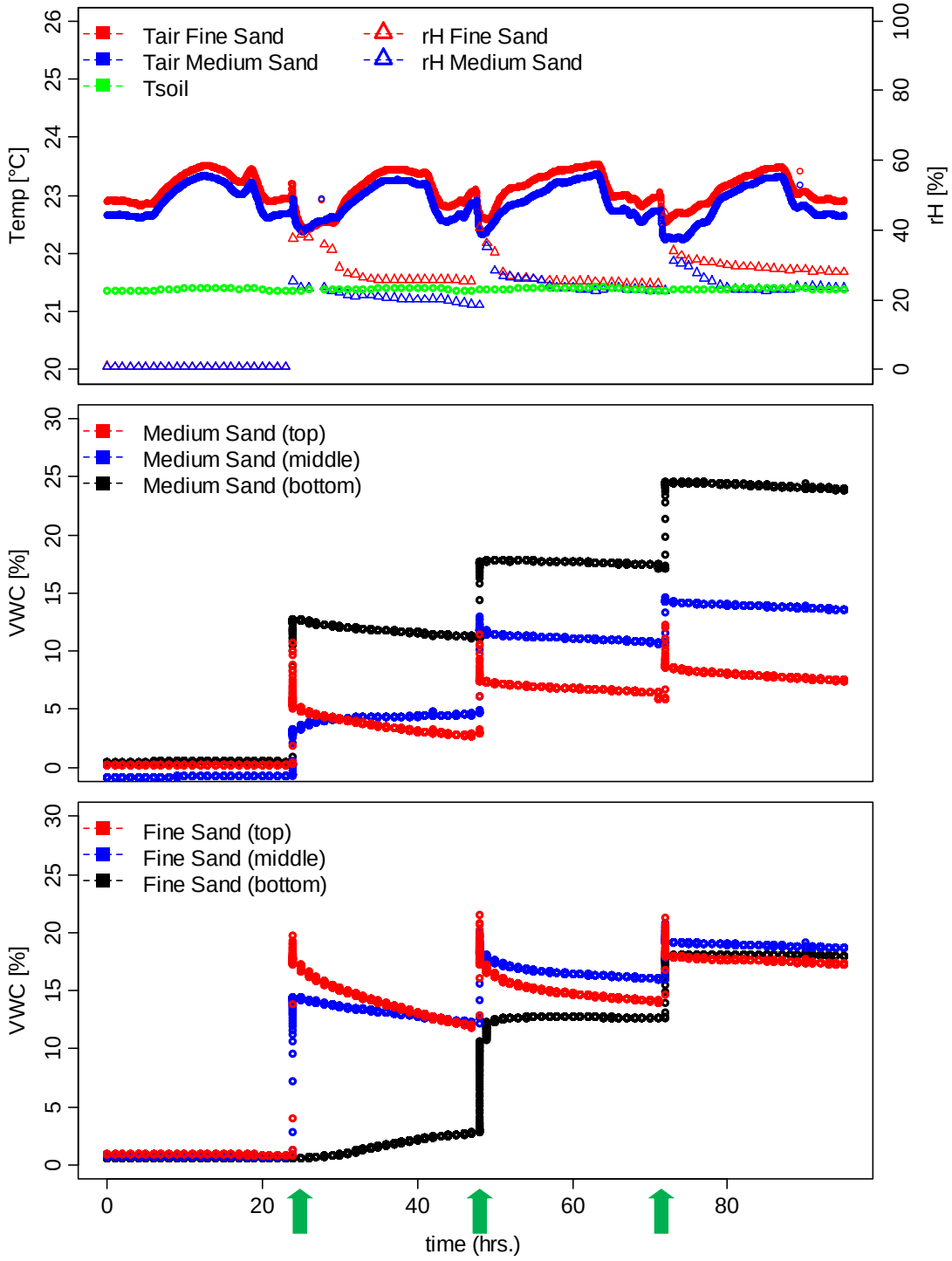

Figure 4.7-3: Volumetric water content, soil temperature, air temperature and relative humidity of air in the cuvettes during Experiment VII. The green arrows represent the time of irrigation.

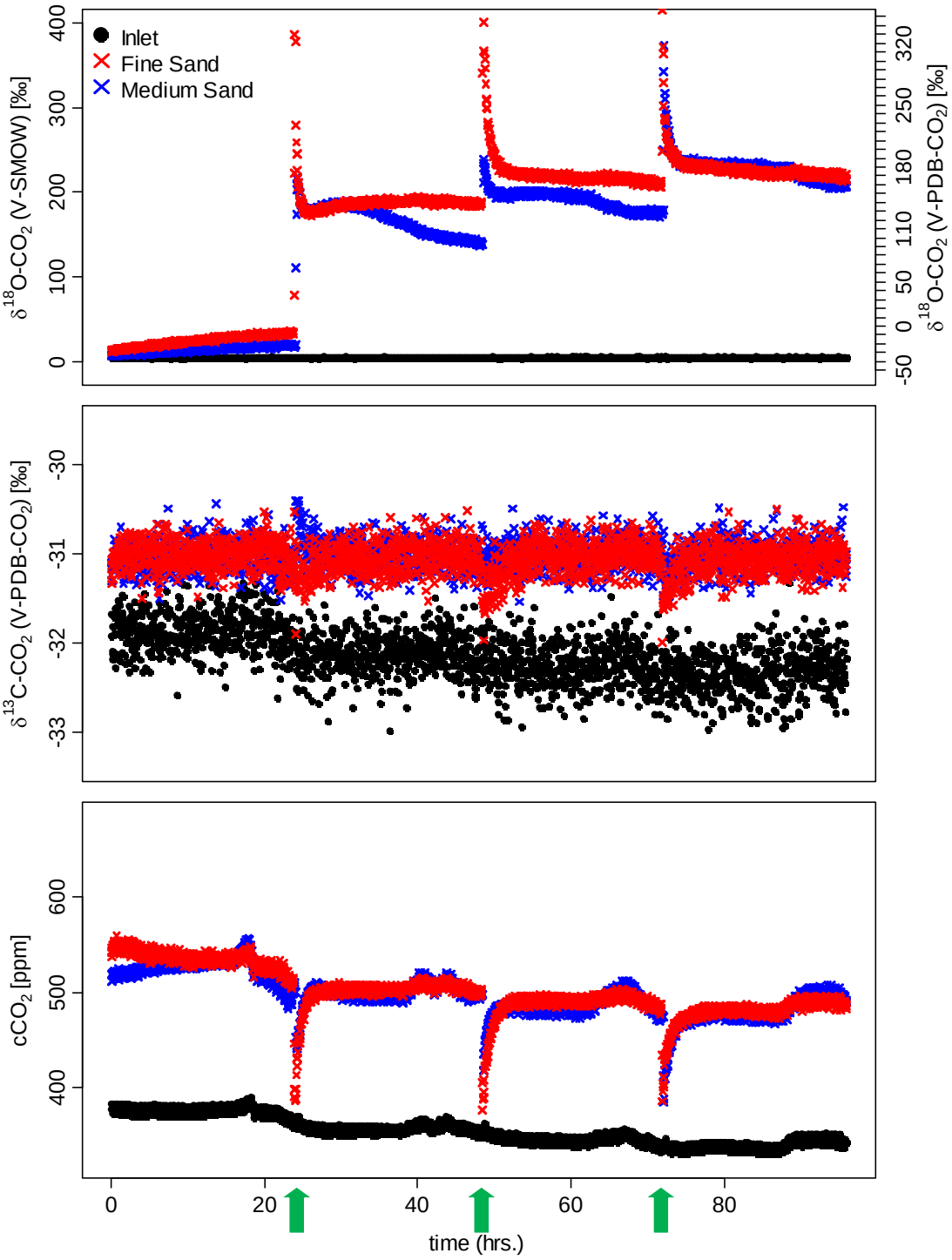

Figure 4.8-1: Concentration and δ values of CO_2 during Experiment VIII. The green arrows represent the time of irrigation.

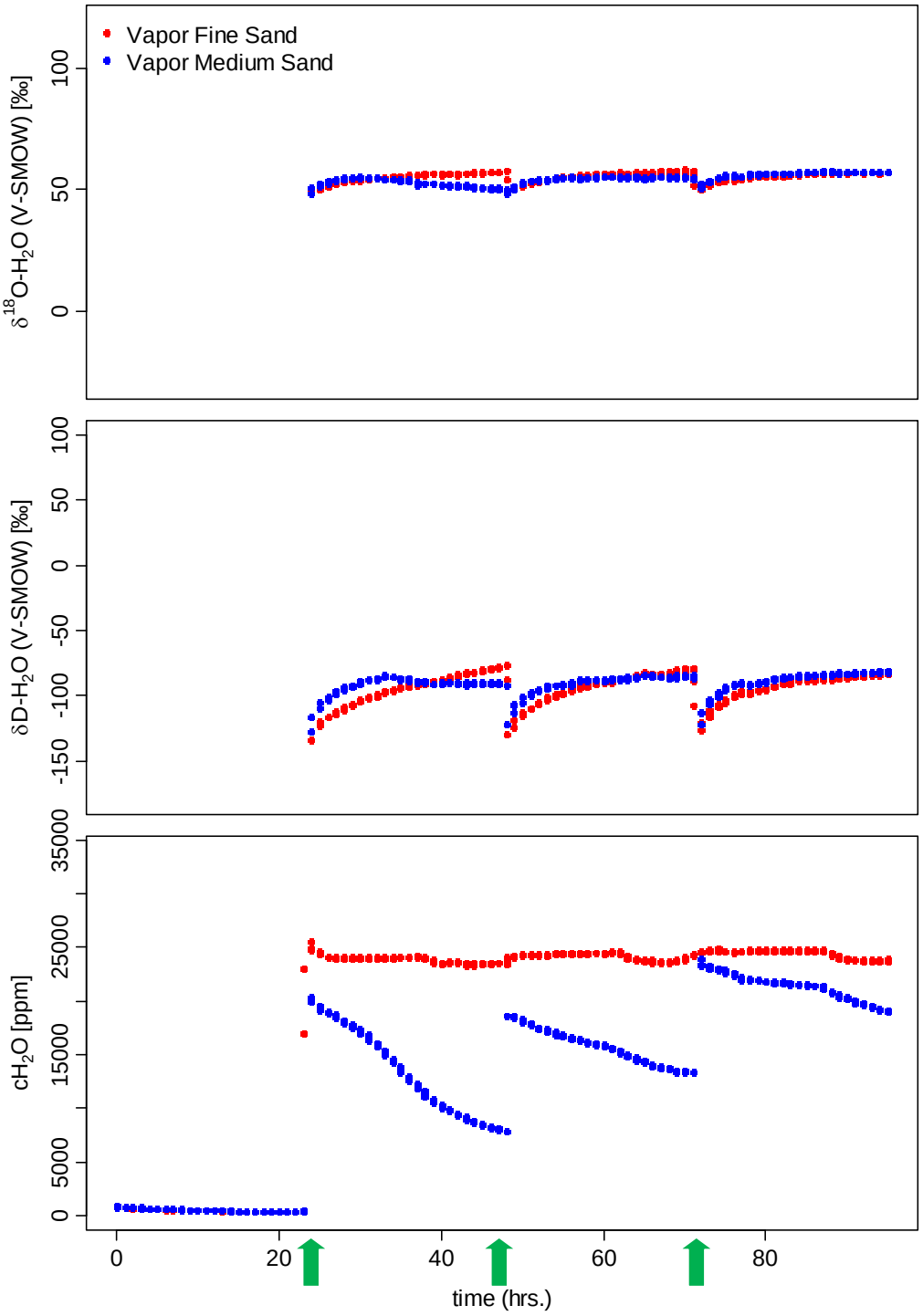

Figure 4.8-2: Concentration and δ-values of H_2O during Experiment VIII. The green arrows represent the time of irrigation.

5. Discussion

5.1 Isotopic Composition of CO_2

5.1.1 Kinetic fractionation of the isotopic composition of CO_2 due to diffusion

Most of the gas exchange between soils and the atmosphere occurs via a network of air-filled pores which connect the surface of the soils with deeper layers. Diffusion is the most important process, which controls the gaseous movement in soils (Hillel, 1998). As noted above, several studies developed a production-diffusion-reaction model to describe the oxygen isotopic composition of soil released CO_2. These models all included a diffusion term, which described the kinetic fractionation due to diffusion (Hesterberg and Siegenthaler, 1991; Tans, 1998, Ammundson et al., 1998). One of these models developed by Tans (1998) applied following differential equation:

$$0 = \frac{\partial(\varepsilon_t RC)}{\partial t} = SR_s + k_H B\varepsilon_w C\left(R_{eq} - R\right) + \frac{\partial}{\partial z}\left(\varepsilon_a t D_{18} \frac{\partial(RC)}{\partial z}\right) \qquad (2.18)$$

Production *Reaction* *Diffusion*

where:

ε_t total porosity which equals $\varepsilon_a + B\varepsilon_w$

ε_a air-filled pore space

ε_w water-filled pore space

B dimensionless Bunsen coefficient (Weiss, 1974)

R isotopic ratio of CO_2

C concentration of CO_2 [moles cm^{-3}]

S rate of CO_2 production [moles cm^{-3} s^{-1}]

R_s isotopic ratio of CO_2 which is produced in the soil

R_{eq} isotopic ratio of CO_2 in equilibrium with soil water

k_H rate of isotopic equilibration, which takes place only in the dissolved phase

t tortuosity factor

D_{18} free air molecular diffusivity of $C^{18}O^{16}O$ [cm^2 s^{-1}]

Hence the kinetic fractionation of the oxygen isotopic composition of soil released CO_2 due to diffusion depends on the air-filled pore space and the tortuosity factor of the porous medium, through which the CO_2 molecule diffuses (Hesterberg and Siegenthaler, 1991; Tans, 1998, Ammundson et al., 1998). The pore space of a porous medium varies with the size of particles and

the state of aggregation. In a homogenous medium with quasi-spherical sand grains the size of the pores is approximately equal to the size of the grains (Dingman, 2008). The tortuosity depends on the fractional volume of air filled pores. The tortuous gas path length of a diffusing gas increases as the air-filled porosity decreases (Baver et al.,1972). The different grain size distributions of the two sands in the cuvettes hence cause different pore spaces, which again lead to different kinetic fractionations due to diffusion. The pore space of the soil column with fine sand is smaller compared to the one of the soil column with medium sand. Hence the kinetic fractionation during the diffusion was larger in the cuvette with fine sand which could be observed in Experiment IV-VIII.

In theory the kinetic fractionation due to diffusion is estimated to be about 8.7‰ (Hoefs, 2009). Global isotopic mass balance studies estimated the kinetic fractionation of diffusion through soils to be between 5.0‰ and 7.6‰ for $C^{18}O^{16}O$ (Ciais et al., 1997; Farquhar et al., 1993). Small scale, direct measurements suggested a value of 7.0‰ (Miller et al., 1999). Our measurements suggested values of approx. 5‰ in the cuvette with medium sand and approx. 7‰ in the cuvette with fine sand during Experiment IV, approx. 8‰ in the cuvette with medium sand and approx. 15‰ in the cuvette with fine sand during Experiment V, approx. 7‰ in the cuvette with medium sand and approx. 10‰ in the cuvette with fine sand during Experiment VI and VII, approx. 8‰ in the cuvette with medium sand and approx. 14‰ in the cuvette with fine sand during Experiment VIII. There is hence a large fluctuation of kinetic fractionation due to diffusion. The presence of an organic litter layer appears to lessen the diffusional effect on the oxygen isotopic composition of soil released CO_2. More measurements with the current setup should hence be conducted to get more certainty.

But no diffusional effect could be observed in the case of $\delta^{13}C$. Due to the different reduced mass of $^{13}C^{16}O^{16}O$ compared to $C^{18}O^{16}O$ equation (2.14) has to be corrected to:

$$\frac{D_{^{13}C^{16}O^{16}O}}{D_{C^{16}O^{16}O}} = \frac{\sqrt{\mu_{^{13}C^{16}O^{16}O}}}{\sqrt{\mu_{C^{16}O^{16}O}}} = 1.0044 \qquad (2.14)$$

The kinetic fractionation of the carbon isotopic composition of CO_2 due to diffusion can thus be estimated to be 4.4‰, only about the half of the oxygen isotopic composition (Hoefs, 2009). Still, a small diffusional effect should be visible in the $\delta^{13}C$ values if this effect is so omnipresent in the case of $\delta^{18}O$. But during the whole time of Experiment IV to VII the $\delta^{13}C$ values remained stable and did not show any deviations between the inlet and the two cuvettes. The exception was Experiment VIII where the $\delta^{13}C$ values at the inlet were lower compared to the two cuvettes. The reason for this deviation during Experiment VIII is not known. Because no diffusional effect on the $\delta^{13}C$ values could be observed the results of the kinetic fractionation of diffusion for $C^{18}O^{16}O$ should be regarded with care.

5.1.2 Thermodynamic fractionation of the isotopic composition of CO_2 due to equilibration with soil water

The increase in $\delta^{18}O$-CO_2 in the two cuvettes directly after irrigation was due to the thermodynamic fractionation caused by the equilibration of the soil released CO_2 with the soil water. The oxygen isotopic exchange during the hydration of CO_2 can be expressed by the following equation:

$$H_2{}^{18}O_{(l)} + CO_2 \leftrightarrow H^+ + [HCO_2{}^{18}O]^-_{(aq)} \leftrightarrow H_2O_{(l)} + CO^{18}O_{(g)} \quad (2.11)$$

Because the amount of water, which is involved in the reaction is many magnitudes higher than the amount of CO_2, the CO_2 will adopt the $\delta^{18}O$ value of the water in which it is dissolved plus an enrichment caused by the thermodynamic fractionation of the equilibrium reaction (Yakir et al, 2000). This thermodynamic fractionation has been experimentally determined by Brennikmeijer et al. (1983) and can be expressed by the following empiric equation:

$$\varepsilon_{eq-CO2}(T) = \frac{17604}{T} - 17.93 \quad (2.12)$$

Thus, at 25°C (=298.15 K) equilibrium fractionation between the oxygen of CO_2 and water has a value of 41.11‰. As one can see from the reaction term of the differential equation (2.18) by Tans et al. (1998) the isotopic ratio of soil released CO_2 strongly depends on the rate of isotopic equilibration.

It is important to note that the $\delta^{18}O$-CO_2 values which are presented in the graphs of Experiment IV-VIII are not the actual measured values but are derived from equation (3.3):

$$\delta^{18}O_{resp} = \frac{\delta^{18}O_O \cdot [CO_2]_O - \delta^{18}O_I \cdot [CO_2]_I}{[CO_2]_O - [CO_2]_I} \quad (3.3)$$

This equation assumes that the CO_2, which invades the soil column from the headspace of the cuvette, does not equilibrate with the soil water, because all the CO_2, which enters the cuvette from the inlet ($[CO_2]_I$) is assumed to have the δ-value of the CO_2 at the inlet ($\delta^{18}O_I$), which did not equilibrate with soil water. Several studies though describe that CO_2, which invades into the soils, most likely equilibrates, at least partly, with the soil water (Ammundson et al., 1998; Miller et al., 1999, Seibt et al., 2006; Wingate et al. 2009). Hence the assumption is most likely wrong but at this point of the study it is necessary in order to be able to differentiate between the soil released CO_2, which equilibrates with the soil water, and the CO_2 which doesn't, because the TGA 200 measures the mixture of these two gas fluxes. Hence there is another unknown variable, namely the proportional amount of the CO_2 in the headspace of the cuvette, which invades the soil and equilibrates with the soil water.

The observed thermodynamic fractionation after the irrigation during Experiment IV was about 12‰ in the cuvette with medium sand and about 8‰ in the cuvette with fine sand and thus below the theoretical fractionation of 41.11‰. Hence it can be concluded that the equilibration reaction did not reach completion during Experiment IV. Interestingly, evaporative enrichment of the liquid water body at the site of evaporation appeared not to have an effect on the $\delta^{18}O\text{-}CO_2$ values. This can be clearly be seen in the case of the cuvette with medium sand. Hence the CO_2 which diffuses through the soil column might not have enough time to equilibrate with the water at the surface of the soil column. But before and during the course of this experiment a lot of technical problems occurred including a leak in the pressure regulator of the CO_2, which was induced from the bottom of the cuvette with medium sand. The results of this experiment should hence be regarded with care and the whole experiment should be repeated again.

During the Experiments V-VII these troubles could be eliminated. During all these experiments a large increase of the $\delta^{18}O\text{-}CO_2$ values could be observed directly after the first irrigation, which showed that soil-released CO_2 underwent oxygen isotopic exchange with the soil water. Because ^{18}O enriched water was used for irrigation, the isotopic effect of the equilibrium reaction between soil water and soil released CO_2 was much more visible. The $\delta^{18}O\text{-}CO_2$ values of the Experiments V-VII reached a limit of approx. 100‰ vs. V-SMOW after the third irrigation. This value fit in well with the theory that CO_2, which equilibrates completely with the soil water, adopts the oxygen isotopic composition of the soil water it equilibrates with, in the case of the experiments approx 59‰ vs. V-SMOW, plus a thermodynamic fractionation of 41.1‰. This would result in a $\delta^{18}O\text{-}CO_2$ value of approx. 100‰ vs. V-SMOW. In the case that all of the CO_2, which has been induced from the bottom of the cuvette and which diffused through the soil column, equilibrated completely with the soil water, only a very small, negligible amount, of the CO_2, which invaded the soil column from the headspace of the cuvette, actually equilibrated with the soil water. These findings hence would prove our assumption of equation (3.3) to be right. Interestingly, an organic litter layer appeared not to have an effect on the oxygen isotopic composition of soil released CO_2 after the irrigation started. This finding contradicts the results of Sternberg et al. (1998) which indicated that there is an isotopic exchange between soil-released CO_2 and wet organic litter layer.

During all experiments the evaporative enrichment of the liquid water body at the soil surface did not have an effect on the oxygen isotopic composition. This concurs with the findings of Miller et al. (1999), which state that the zone between 5 and 15 cm below the surface have the biggest influence on the $\delta^{18}O$ values of soil-respired CO_2. Below 15 cm the oxygen isotopic composition of CO_2 was readjusted during the diffusion process towards the surface. This indicated that a steep gradient of the $\delta^{18}O$ values of soil water in the upper layer of the soil does not have a major effect on the oxygen

isotopic composition of soil respired CO_2 (Miller et al., 1999). Simultaneously these findings contradict the suggestion by Riley (2005) who argued that the $\delta^{18}O$ value of soil water, which is close to the surface, can have a big impact on the $\delta^{18}O$ values of soil respired CO_2.

5.1.2 The Effect of the Presence of Carbonic Anhydrase

One could clearly see the effect of carbonic anhydrase on the $\delta^{18}O$-CO_2 values because they increased to much higher levels compared to the experiments without the application of the enzyme. The $\delta^{18}O$-CO_2 values that were calculated by equation (3.3) reached a value of up to 220‰ vs. V-SMOW. But according to theory, as discussed above, the maximum $\delta^{18}O$-CO_2 value of soil released CO_2 could only be approx. 100‰ vs. V-SMOW. Hence in the presence of carbonic anhydrase the assumption of equation (3.3) that the CO_2, which invades the soil from the headspace of the cuvette, does not equilibrate with the soil water is wrong. If we assume now that the acceleration of the equilibration reaction between CO_2 and soil water due to the presence of carbonic anhydrase is so strong that actually all the CO_2, which invades the soil column from the headspace of the cuvette, equilibrates with the soil water, one can derive the proportional amount of the CO_2, which invades the soil column from the headspace of the cuvette, by rearranging equation (3.3) to:

$$100‰ = \frac{\delta^{18}O_O \cdot [CO_2]_O - \delta^{18}O_I \cdot [CO_2]_I}{[CO_2]_O - [CO_2]_I} \tag{3.4}$$

The δ-value of 100‰ is the approx. expected $\delta^{18}O$ value of the CO_2, which equilibrated with the soil water. This includes both, the CO_2, which was induced at the bottom of the cuvette and diffused through the soil column to the surface, and the CO_2, which invaded the soil column from the headspace of the cuvette and equilibrated then with the soil water. In this case the fractional amount of the CO_2, which did not equilibrate with the soil water can be calculated by:

$$100‰ = \frac{66‰ \cdot 500[ppm] - 5.7‰ \cdot x}{500[ppm] - x} \tag{3.5}$$

which can be solved for x:

$$x = \frac{34‰ \cdot 500[ppm]}{94.3‰} = 180.3\ [ppm] \tag{3.6}$$

Hence 180.3 ppm of a total of approx. 370 ppm, the concentration of CO_2 at the inlet, did not equilibrate with the soil water. Hence approx. 52% of the CO_2 in the headspace of the cuvette invaded the soil and equilibrated with the soil water. This indicates the significant effect of the

presence of carbonic anhydrase in the soil on the oxygen isotopic composition of soil released CO_2 due to the accelerated equilibrium reaction between CO_2 and soil water.

This simple model concurs in theory with several studies that have explored the effect of a presence of carbonic anhydrase in the soils on the oxygen isotopic composition of soil released CO_2. Seibt et al. (2006) measured the $\delta^{18}O$ values of soil CO_2 and soil water in a forest and then simulated the measured values with a model. The study showed that complete agreement between measured and simulated values was only achieved if an acceleration term of the equilibrium reaction between CO_2 and soil water was included. This acceleration was attributed to the presence of carbonic anhydrase in the soils. Wingate et al. (2009) stressed the importance of the shallowest depth in a soil where CO_2 still equilibrates with soil water. As we have shown, this shallowest depth is moved dramatically in direction to the soil surface in the presence of carbonic anhydrase as at least a very big amount of the CO_2, which invades the soil column from the atmosphere above, equilibrates with the soil water. Hence the presence of carbonic anhydrase has a twofold effect on the oxygen isotopic composition of soil released CO_2. On the one hand quantitatively more CO_2 equilibrates with the soil water because more invasive CO_2 equilibrates with soil water. On the other hand, if the shallowest depth where CO_2 equilibrates with soil water moves further towards the soil surface, the CO_2 equilibrates with soil water which is progressively enriched in ^{18}O due to evaporation (Allison and Barnes, 1983; Barnes and Allison, 1988; Gat, 1996).

However a proportional amount of approx. 50% of CO_2, which invades the soil column from the headspace of the cuvette and then equilibrates with the soil water, appears to be very much. This could maybe be explained by the fact that the gas mixture is directed into the cuvette with a gas flow of 1 l min^{-1} through a one eighth inch diameter gas line. This flow most likely results in an air current and a pronounced advective flow into the soil column. Under natural conditions this advective flow into the soils might be much lower compared to the laboratory conditions in Experiment VIII. Hence the extent of the advective flow into the soil columns in the cuvettes should be analyzed in future studies and compared to natural conditions. Another explanation might be that the concentration of carbonic anhydrase in the irrigation water (0.125 $mgml^{-1}$) was much higher than it probably would be the case in natural soils.

In general these findings concur very well with the hypothesis by Hesterberg and Siegenthaler (1991), Ammundson et al. (1998) and Tans (1998) that the $\delta^{18}O$ values of soil released CO_2 are determined by a competition between production, isotopic equilibrium with soil water and the diffusional transport of CO_2. Ammundson et al. (1998) emphasized the importance of the reaction rate of isotopic exchange between CO_2 and soil water. They suggested that for reaction rates $k > 0.001s^{-1}$ in soils with

CO_2 production in the top 30 cm, full equilibration between CO_2 and H_2O occurs (Ammundson et al., 1998). Experiment VIII has shown that in case of a presence of carbonic anhydrase the reaction rate might be even higher.

5.2 Soil Moisture and Evaporation

After irrigation a soil dries both by drainage and evaporation. Drainage is the flow of water in an unsaturated porous medium which is described by Darcy's Law:

$$q_x = -K_h \cdot \frac{d(z_e + \frac{p}{y_w})}{dx}$$

where:

q_x volumetric flow rate in the direction x per unit cross sectional area of medium [cms^{-1}]

K_h hydraulic conductivity of the medium [cms^{-1}]

z_e elevation above arbitrary datum [cm]

p water pressure [Pa]

y_w weight density of water [$Pacm^{-1}$]

As conditions in both cuvettes were the same with the exception of the type sand, the hydraulic conductivity is the only variable in this equation which differed in the two cuvettes. The hydraulic conductivity is the rate at which water moves through a porous medium. This rate is controlled by the pore space and the degree of saturation. As discussed above the pore space depends on the grain size of the porous medium. Hence the hydraulic conductivity of the medium sand was higher compared to the fine sand, which led to a higher infiltration rate in the medium sand (Dingman, 2008). This concurred well with the development of the volumetric soil water content measurements. During all experiments the volumetric water content at the bottom of the cuvettes changed much faster after the irrigation in the case of the cuvette with medium sand compared to the cuvette with fine sand. There is no explanation for the higher values of the volumetric water content during the experiment with beech leaf litter layer compared to the experiment with spruce needle litter layer.

The other treason for the drying of a soil is evaporation. Evaporation from bare soils occurs in two distinct phases. During the first phase the evaporation rate is mostly determined by the surface

energy balance, the wind and the humidity. In this case evaporation is largely independent of the soil-water content and can be described by approaches of free-water evaporation after Penman (1948). During the second phase evaporation is mostly controlled by the rate at which water can be conducted to the soil surface and hence depends on soil moisture and soil properties. The transition from phase one to phase two of evaporation occurs abruptly and can often be observed by an increase of brightness of the soil surface (Dingmann, 2008). The parameters of the first phase of evaporation were the same in both cuvettes. But the soil properties and hence the drainage and the soil moistures of the two types of sand in the two cuvettes differed. This could clearly be observed at the values of water concentration and relative humidity during the experiments with bare soil columns. During the Experiments IV, V and VIII the concentration of water vapor in the cuvette with fine sand was more or less stabile and remained at the same level. Hence the evaporation in the cuvette with fine sand remained in evaporation phase one for the whole time. In contrast the concentration of water vapor in the cuvette with medium sand dropped several times significantly a few hours after irrigation. This indicated that evaporation in the cuvette with medium sand shifted to phase two very abruptly. This shift could be observed after approx. 60 hours after the irrigation during Experiment IV, after approx. 2 hours after the irrigation during Experiment V and shortly after all three irrigations during Experiment VIII. These differences of the evaporation rates in the two cuvettes over the course of those three experiments are hence due to different infiltration rates of the two types of sands, because of the different grain size distribution. Interestingly one could observe the visual effect of the transition from evaporation phase 1 to evaporation phase 2 in the cuvette with medium sand as the color of the surface brightened a few hours after the first irrigation. This visual effect should be documented in future experiments.

The presence of organic litter layer not only weakened the total rate of evaporation during Experiment VI and VII compared to the other experiments but also inhibited this transition into phase two of the evaporation. The evaporation rates of the two types of sands did not show a significant difference during Experiment VI and VII. This weakening effect of the organic litter layer was more pronounced in the case of spruce needles compared to the beech leaves, because the spruce needle layer is much more compacted compared to the beech leaves. Hence more air was exchanged through the beech litter layer which led to higher evaporation rates and hence a stronger rate of evaporation.

5.3 Isotopic Composition of the Water Vapor and the Liquid Water Body

According to the equation by Craig and Gordon (1965) the isotopic composition of water vapor is strongly related to relative humidity and thus the rate of evaporation and the isotopic composition of the liquid water body as well:

$$\delta_V = [\alpha_{eq}\delta_L - rH\delta_A - \varepsilon_{eq} - (1 - rH)\varepsilon_k]/[(1 - rH) + \frac{(1-rH)\varepsilon_k}{1000}] \quad (2.9)$$

where:

V evaporating water vapor

L liquid water body

A ambient air

α_{eq} equilibrium fractionation factor

ε_{eq} equilibrium enrichment (at 20°C: ε_{eq} = 9.8‰ for $\delta^{18}O$, Majoube, 1971)

ε_k kinetic enrichment (at 20°C: ε_k = 15-30‰ for $\delta^{18}O$, Merlivat, 1978)

rH relative humidity of ambient air

One could clearly observe the evaporative effect on the isotopic composition of the water vapor during all experiments. After each irrigation the $\delta^{18}O$-H_2O and δD values experienced a pronounced enrichment with time during all experiments. The isotopic composition of the water vapor showed no significant difference between the two cuvettes with the exception that the δ-values of water vapor in the cuvette with medium sand started to decrease directly after the H_2O concentration in the headspace of the cuvette decreased abruptly. It is difficult to explain why this happened, because the liquid water body became more and more enriched in heavy isotopes as the top layer was getting drier, which should have led to a further increase of the δ-values of the water vapor. One reason for the decrease of the δ-values of water vapor in the cuvette with medium sand could be the H_2O concentration dependence of the measurements of the Picarro, which has been shown in Experiment I. The presence of an organic litter layer influenced the isotopic composition of water vapor significantly as well. The evaporative enrichment of the water vapour was much less pronounced in particular in the presence of the spruce needle litter layer. In general the evaporative enrichment of the liquid water body, which was calculated after equation (2.10) from the Craig-Gordon Model, Craig and Gordon (1965), showed a very similar pattern compared to the evaporative enrichment of the water vapor. The calculated results indicate and progressive enrichment of soil water in ^{18}O due to evaporation. This fit in well with the findings of several previous studies (Allison and Barnes, 1983; Barnes and Allison, 1988; Gat, 1996).

6. Conclusion

This study established a new method to continuously measure the isotopic composition of CO_2 and water vapor above a soil column under laboratory conditions by applying the coupled use of a Tunable Diode Laser Spectroscopy (TDLAS) and Wavelength-scanned Cavity Ring Down Spectroscopy (WS-CRDS). The gas flows and measurements could be maintained stable over a period of 96 h or longer. This method thus can also be very valuable for future studies in the field to explore the processes involved in CO_2 gas exchange between the biosphere and atmosphere at the plot or ecosystem scale. The successful conduction of several experiments showed detailed results about the influence of soil moisture on the isotopic composition of soil released CO_2 as well as the water vapor above the soil column under laboratory conditions. The presence of organic litter layer showed a significant influence on the isotopic composition of soil released CO_2 and water vapor above a soil column. The effect of the litter layer was more pronounced in the case of spruce needles compared to beech leaves. The final experiment showed a significant influence of the enzyme carbonic anhydrase (CA) on the oxygen isotopic composition of soil released CO_2. These findings indicated that the most important parameter which controls the oxygen isotopic composition of soil released CO_2 is the exchange rate between CO_2 and H_2O. The presence of CA hence moves the shallowest depth in the soil, where CO_2 molecules have enough time to equilibrate fully with soil water, closer to the surface of the soil. In addition, a simple model was developed to determine the proportional amount of atmospheric CO_2 which invades the soil column under laboratory conditions. Due to technical difficulties many experiments had to be conducted several times, yielding many consistent results. Nonetheless, some of the described experiments should be repeated in order to have more certainty about the results. In particular the kinetic fractionation of the oxygen isotopic composition of soil released CO_2 caused by diffusion should be explored in more detail in future experiments since there is still big uncertainty. An important step forward would be the installation of gas-permeable tubing line inside the soil column at different depths which would enable the sampling of the gaseous phase inside the soil column, allowing for a direct analysis of the soil profile of $\delta^{18}O\text{-}H_2O$ and $\delta^{18}O\text{-}CO_2$. In addition, a comparison of the production, diffusion and reaction models of Hesterberg and Siegenthaler (1991) and Tans (1998) with the actual measured values could be done. Finally, one could use the experimental setup to analyze the gas flows above natural soil columns.

Bibliography

Allison, G. B., & Barnes, C. J. (1983). Estimation of evaporation from non-vegetated surfaces using natural deuterium. *Nature*, *301*(5896), 143-145.

Allison, G., & Barnes, C. (1985). Estimation of evaporation from the normally "dry" Lake Frome in South Australia. *Journal of Hydrology*, *78*(3-4), 229-242.

Allison, G., Barnes, C., & Hughes, M. (1983). The distribution of deuterium and ^{18}O in dry soils 2. Experimental. *Journal of Hydrology*, *64*(1-4), 377-397.

Amundson, R., Stern, L., Baisden, T., & Wang, Y. (1998). The isotopic composition of soil and soil-respired CO_2. *Geoderma*, *82*(1-3), 83-114.

Badger, M. R., & Price, G. D. (1994). The Role of Carbonic Anhydrase in Photosynthesis. *Annual Review of Plant Physiology and Plant Molecular Biology*, *45*(1), 369-392.

Baker, J., & Griffis, T. (2005). Examining strategies to improve the carbon balance of corn/soybean agriculture using eddy covariance and mass balance techniques. *Agricultural and Forest Meteorology*, *128*(3-4), 163-177.

Barnes, C. J., & Allison, G. B. (1983). The distribution of deuterium and ^{18}O in dry soils : 1. Theory. *Journal of Hydrology*, *60*(1-4), 141-156.

Barnes, C., & Allison, G. (1988). Tracing of water movement in the unsaturated zone using stable isotopes of hydrogen and oxygen. *Journal of Hydrology*, *100*(1-3), 143-176.

Baver, L.D., Gardener W. H., & Gardener, W. R. (1972). *Soil Physics*. John Wiley and Sons Inc., New York, 498 pp.

Bottinga, Y., & Craig, H. (1968). Oxygen isotope fractionation between CO_2 and water, and the isotopic composition of marine atmospheric CO2. *Earth and Planetary Science Letters*, *5*, 285-295.

Bowling, D. R., Pataki, D. E., & Ehleringer, J. R. (2003). Critical evaluation of micrometeorological methods for measuring ecosystem-atmosphere isotopic exchange of CO_2. *Agricultural and Forest Meteorology*, *116*(3-4), 159-179.

Bowling, D. R., Sargent, S. D., Tanner, B. D., & Ehleringer, J. R. (2003). Tunable diode laser absorption spectroscopy for stable isotope studies of ecosystem-atmosphere CO_2 exchange. *Agricultural and Forest Meteorology*, *118*(1-2), 1-19.

Brenninkmeijer, C., Kraft, P., & Mook, W. (1983a). Oxygen isotope fractionation between CO_2 and H_2O. *Chemical Geology*, *41*, 181-190.

Buchmann, N., & Ehleringer, J. R. (1998). CO_2 concentration profiles and carbon and oxygen isotopes in C3 and C4 crop canopies. *Agricultural and Forest Meteorology*, *89*(1), 45-58.

Ciais, P., Denning, A. S., Tans, P. P., Berry J. A., et al. (1997). A three-dimensional synthesis study of $\delta^{18}O$ in atmospheric CO_2 1. Surface fluxes. *Journal of Geophysical Research*, *102*(D5), 5857-5872.

Ciais, P., Tans, P. P., Denning, A. S., Francey, R. J., et al., (1997). A three-dimensional synthesis study of $\delta^{18}O$ in atmospheric CO_2 2. Simulations with the TM2 transport model. *Journal of Geophysical Research*, *102*(D5), 5873-5883.

Clark, I. D., & Fritz, P. (1997). *Environmental isotopes in hydrogeology*. Lewis Publishers,Boca Raton, New York, 328 pp.

Cuntz, M., Ciais, P., & Hoffmann, G. (2002). Modelling the continental effect of oxygen isotopes over Eurasia. *Tellus B*, *54*(5), 895-911.

Cuntz, M., Ciais, P., Hoffmann, G., Allison, C. E., Francey, et al., (2003). A comprehensive global three-dimensional model of $\delta^{18}O$ in atmospheric CO_2: 2. Mapping the atmospheric signal. *Journal of Geophysical Research*, *108*, 4527.

Cuntz, M., Ciais, P., Hoffmann, G., & Knorr, W. (2003). A comprehensive global three-dimensional model of $\delta^{18}O$ in atmospheric CO_2: 1. Validation of surface processes. *Journal of Geophysical Research*, *108*, 4528.

Dingmann, S. L., (2008). Physical Hydrology. Waveland Press Inc., Long Grove, IL, 646 pp.

Doney, S. C., Fabry, V. J., Feely, R. A., & Kleypas, J. A. (2009). Ocean Acidification: The Other CO_2 Problem. *Annual Review of Marine Science*, *1*(1), 169-192.

Ehleringer, J. R., Bowling, D. R., Flanagan, L. B., Fessenden, J., Helliker, B., Martinelli, L. A., & Ometto, J. P. (2002a). Stable Isotopes and Carbon Cycle Processes in Forests and Grasslands. *Plant Biology*, *4*(2), 181-189. Ehleringer, J. R., Bowling, D. R., Flanagan, L. B., Fessenden, J., Helliker, B., Martinelli, L. A., & Ometto, J. P. (2002b). Stable Isotopes and Carbon Cycle Processes in Forests and Grasslands. *Plant Biology*, *4*(2), 181-189.

Ehleringer, J. R., Buchmann, N., & Flanagan, L. B. (2000). Carbon isotope ratios in belowground carbon cycle processes. *Ecological Applications*, *10*(2), 412-422.

Farquhar, G. D., Lloyd, J., Taylor, J. A., Flanagan, L. B., Syvertsen, J. P., Hubick, K. T., Wong, S. C., u. a. (1993). Vegetation effects on the isotope composition of oxygen in atmospheric CO_2. *Nature*, *363*(6428), 439-443.

Flanagan, L. B., Brooks, J. R., Varney, G. T., Berry, S. C., & Ehleringer, J. R. (1996). Carbon isotope discrimination during photosynthesis and the isotope ratio of respired CO_2 in boreal forest ecosystems. *Global Biogeochemical Cycles*, *10*(4), PP. 629-640.

Flanagan, L. B., Brooks, J. R., Varney, G. T., & Ehleringer, J. R. (1997). Discrimination against $C^{18}O^{16}O$ during photosynthesis and the oxygen isotope ratio of respired CO_2 in boreal forest ecosystems. *Global Biogeochemical Cycles*, *11*(1), PP. 83-98.

Flanagan, L. B., Ehleringer, J. R., & Pataki, D. E. (2005). *Stable isotopes and biosphere-atmosphere interactions: processes and biological controls*. Academic Press. San Diego, California, 333 pp.

Flanagan, L. B., & Ehleringer, J. R. (1998a). Ecosystem-atmosphere CO_2 exchange: interpreting signals of change using stable isotope ratios. *Trends in Ecology & Evolution*, *13*(1), 10-14.

Flanagan, L. B., Kubien, D. S., & Ehleringer, J. R. (1999). Spatial and temporal variation in the carbon and oxygen stable isotope ratio of respired CO_2 in a boreal forest ecosystem*. *Tellus B*, *51*(2), 367-384.

Francey, R. J., & Tans, P. P. (1987). Latitudinal variation in oxygen-18 of atmospheric CO_2. *Nature*, *327*(6122), 495-497.

Fraser, P. J., Pearman, G. I., & Hyson, P. (1983). The Global Distribution of Atmospheric Carbon Dioxide 2. A Review of Provisional Background Observations, 1978–1980. *Journal of Geophysical Research*, *88*(C6), 3591-3598.

Friedli, H., Siegenthaler, U., Rauber, D., & Oeschger, H. (1987). Measurements of concentration, $^{13}C/^{12}C$ and $^{18}O/^{16}O$ ratios of tropospheric carbon dioxide over Switzerland. *Tellus B*, *39B*(1-2), 80-88.

Friedlingstein, P., Cox, P., Betts, R., Bopp, L., von Bloh, W., Brovkin, V., Cadule, P., u. a. (2006). Climate–Carbon Cycle Feedback Analysis: Results from the C4 MIP Model Intercomparison. *Journal of Climate*, *19*(14), 3337-3353.

Galewsky, J., Strong, M., & Sharp, Z. D. (2007). Measurements of water vapor D/H ratios from Mauna Kea, Hawaii, and implications for subtropical humidity dynamics. *Geophysical Research Letters*, *34*(22).

Gat, J. R. (1996). Oxygen and Hydrogen isotopes in the hydrologic cycle. *Annual Review of Earth and Planetary Sciences*, *24*(1), 225-262.

Gillon, J., & Yakir, D. (2001). Influence of Carbonic Anhydrase Activity in Terrestrial Vegetation on the ^{18}O Content of Atmospheric CO_2. *Science*, *291*(5513), 2584-2587.

Giordano, M., Norici, A., Forssen, M., Eriksson, M., & Raven, J. A. (2003). An Anaplerotic Role for Mitochondrial Carbonic Anhydrase in Chlamydomonas reinhardtii. *Plant Physiol.*, *132*(4), 2126-2134.

Griffis, T., Baker, J., & Zhang, J. (2005a). Seasonal dynamics and partitioning of isotopic CO_2 exchange in a C3/C4 managed ecosystem. *Agricultural and Forest Meteorology*, *132*(1-2), 1-19.

Griffis, T., Lee, X., Baker, J., Sargent, S., & King, J. (2005). Feasibility of quantifying ecosystem-atmosphere $C^{18}O^{16}O$ exchange using laser spectroscopy and the flux-gradient method. *Agricultural and Forest Meteorology*, *135*(1-4), 44-60.

Gupta, P., Noone, D., Galewsky, J., Sweeney, C., & Vaughn, B. H. (2009). Demonstration of high-precision continuous measurements of water vapor isotopologues in laboratory and remote field deployments using wavelength-scanned cavity ring-down spectroscopy (WS-CRDS) technology. *Rapid Communications in Mass Spectrometry*, *23*(16), 2534-2542.

Harwood, K. G., Gillon, J. S., Griffiths, H., & Broadmeadow, M. S. J. (1998). Diurnal variation of $\Delta^{13}CO_2$, $\Delta C^{18}O^{16}O$ and evaporative site enrichment of $\delta H_2{}^{18}O$ in Piper aduncum under field conditions in Trinidad. *Plant, Cell and Environment*, *21*(3), 269-283.

Harwood, K. G., Gillon, J. S., Roberts, A., & Griffiths, H. (1999). Determinants of isotopic coupling of CO_2 and water vapour within a Quercus petraea forest canopy. *Oecologia*, *119*(1), 109-119.

Hesterberg, R., & Siegenthaler, U. (1991). Production and stable isotopic composition of CO_2 in a soil near Bern, Switzerland. *Tellus B*, *43*(2), 197-205.

Hillel, D. (1998). *Environmental Soil Physics*. Academic Press, San Diego,CA, 771 pp.

Hoag, K. J., Still, C. J., Fung, I. Y., & Boering, K. A. (2005). Triple oxygen isotope composition of tropospheric carbon dioxide as a tracer of terrestrial gross carbon fluxes. *Geophysical Research Letters*, *32*, 5 PP.

Hoefs, J. (2009). *Stable isotope geochemistry*. Springer, Berlin Heidleberg, 293 pp.

Ishizawa, M., Nakazawa, T., & Higuchi, K. (2002). A multi-box model study of the role of the biospheric metabolism in the recent decline of delta ^{18}O in atmospheric CO_2. *Tellus B*, *54*(4), 307-324.

Intergovernmental Panel on Climate Change, 2007. Climate Change 2007 – The Physical Science basis: Contribution of Working Group I to the Fourth Assessment Report of the Intergovernmental Panel on Climate Change. Cambridge Univ Press, Cambridge, UK.

Kesselmeier, J., Teusch, N., & Kuhn, U. (1999). Controlling variables for the uptake of atmospheric carbonyl sulfide by soil. *Journal of Geophysical Research*, *104*(D9),11,577-11,584.

Lai, C., Riley, W., Owensby, C., Ham, J., Schauer, A., & Ehleringer, J. R. (2006). Seasonal and interannual variations of carbon and oxygen isotopes of respired CO_2 in a tallgrass prairie: Measurements and modeling results from 3 years with contrasting water availability. *Journal of Geophysical Research*, *111*(D8).

Langendorfer, U., Cuntz, M., Ciais, P., Peylin, P., Bariac, T., Milyukova, I., Kolle, O., u. a. (2002). Modelling of biospheric CO_2 gross fluxes via oxygen isotopes in a spruce forest canopy: a 222Rn calibrated box model approach. *Tellus B*, *54*(5), 476-496.

Lee, X., Griffis, T. J., Baker, J. M., Billmark, K. A., Kim, K., & Welp, L. R. (2009). Canopy-scale kinetic fractionation of atmospheric carbon dioxide and water vapor isotopes. *Global Biogeochemical Cycles*, *23*, GB1002.

Liu, N., Bond, G. M., Abel, A., McPherson, B. J., & Stringer, J. (2005). Biomimetic sequestration of CO_2 in carbonate form: Role of produced waters and other brines. *Fuel Processing Technology*, *86*(14-15), 1615-1625.

Michener, R., & Lajtha, K. (2007). *Stable Isotopes in Ecology and Environmental Science* (2. Aufl.). Wiley-Blackwell, Malden, MA, 566 pp.

Miller, J. B., Yakir, D., White, J. W. C., & Tans, P. P. (1999). Measurement of $^{18}O/^{16}O$ in the soil-atmosphere CO_2 flux. *Global Biogeochemical Cycles*, *13*(3), 761-774.

Mills, G. A., & Urey, H. C. (1940). The Kinetics of Isotopic Exchange between Carbon Dioxide, Bicarbonate Ion, Carbonate Ion and Water1. *Journal of the American Chemical Society*, *62*(5), 1019-1026.

Mortazavi, B., Prater, J. L., & Chanton, J. P. (2004). A field-based method for simultaneous measurements of the $\delta^{18}O$ and $\delta^{13}C$ of soil CO_2 efflux. *Biogeosciences*, *1*, 1-9.

Nakazawa, T., Sugawara, S., Inoue, G., Machida, T., Makshyutov, S., & Mukai, H. (1997) Aircraft measurements of the concentrations of CO_2, CH_4, N_2O, and CO and the carbon and oxygen isotopic ratios of CO_2 in the troposphere over Russia. *Journal of Geophysical Research*, *102*(D3), PP. 3843-3859.

Ogée, J., Peylin, P., Cuntz, M., Bariac, T., Brunet, Y., Berbigier, P., Richard, P., u. a. (2004). Partitioning net ecosystem carbon exchange into net assimilation and respiration with canopy-scale isotopic measurements: An error propagation analysis with $^{13}CO_2$ and $CO^{18}O$ data. *Global Biogeochemical Cycles*, *18*, GB2019.

Ometto, J. P. H., Flanagan, L. B., Martinelli, L. A., & Ehleringer, J. R. (2005). Oxygen Isotope Ratios of Waters and Respired CO2 in Amazonian Forest and Pasture Ecosystems. *Ecological Applications*, 15(1), 58-70.

Pearman, G. I., Hyson, P., & Fraser, P. J. (1983). The Global Distribution of Atmospheric Carbon Dioxide: 1. Aspects of Observations and Modeling. *Journal of Geophysical Research*, *88*(C6), 3581-3590.

Penman, H. L. , (1948). Natural evaporation from open water, bare soil and grass. *Proceedings of the Royal Society of London. Series A, Mathematical and PhysicalSciences*, Vol. 193(1032), 120-14.

Peylin, P., Ciais, P., Denning, A. S., Tans, P. P., Berry, J. A., & White, J. W. C. (1999). A 3-dimensional study of delta ^{18}O in atmospheric CO_2: contribution of different land ecosystems. *Tellus B*, *51*(3), 642-667.

Riley, W. J. (2005). A modeling study of the impact of the delta ^{18}O value of near-surface soil water on the delta ^{18}O value of the soil-surface CO_2 flux. *Geochimica et Cosmochimica Acta*, *69*(8), 1939-1946.

Riley, W. J., Still, C. J., Helliker, B. R., Ribas-Carbo, M., & Berry, J. A. (2003). ^{18}O composition of CO_2 and H_2O ecosystem pools and fluxes in a tallgrass prairie: Simulations and comparisons to measurements. *Global Change Biology*, *9*(11), 1567-1581.

Seibt, U., Brand, W. A., Heimann, M., Lloyd, J., Severinghaus, J. P., & Wingate, L. (2004). Observations of O_2:CO_2 exchange ratios during ecosystem gas exchange. *Global Biogeochemical Cycles*, *18*, GB4024.

Seibt, U., Wingate, L., Berry, J. A., & Lloyd, J. (2006). Non-steady state effects in diurnal ^{18}O discrimination by Picea sitchensis branches in the field. *Plant, Cell and Environment*, *29*(5), 928-939.

Seibt, U., Wingate, L., Lloyd, J., & Berry, J. A. (2006). Diurnally variable $\delta^{18}O$ signatures of soil CO_2 fluxes indicate carbonic anhydrase activity in a forest soil. *Journal of Geophysical Research*, *111*, G04005.

Sharp, Z. (2006). *Principles of Stable Isotope Geochemistry*. Prentice Hall, Upper Saddle River, NJ, 344pp.

Stern, L., Baisden, W. T., & Amundson, R. (1999). Processes controlling the oxygen isotope ratio of soil CO_2: analytic and numerical modeling. *Geochimica et Cosmochimica Acta*, *63*(6), 799-814.

Stern, L. A., Amundson, R., & Baisden, W. T. (o. J.). Influence of soils on oxygen isotope ratio of atmospheric CO_2. *Global Biogeochemical Cycles*, *15*(3), 753-759.

Sternberg, L. D. S. L., Moreira, M. Z., Martinelli, L. A., Victoria, R. L., Barbosa, E. M., Bonates, L. C. M., & Nepstad, D. (1998a). The relationship between $^{18}O/^{16}O$ and $^{13}C/^{12}C$ ratios of ambient CO_2 in two Amazonian tropical forests. *Tellus B*, *50*(4), 366-376.

Strong, M., Sharp, Z. D., & Gutzler, D. S. (2007). Diagnosing moisture transport using D/H ratios of water vapor. *Geophysical Research Letters*, *34*(3), L03404.

Tans, P. P. (1998). Oxygen isotopic equilibrium between carbon dioxide and water in soils. *Tellus B*, *50*(2), 163-178.

Tans, P. P., & White, J. W. C. (1998). The Global Carbon Cycle: In Balance, with a Little Help from the Plants. *Science*, *281*(5374), 183-184.

Viktor, A., & Cramer, M. D. (2004). The influence of root assimilated inorganic carbon on nitrogen acquisition/assimilation and carbon partitioning. *New Phytologist*, *165*(1), 157-169.

Wang, Y., McDonald, E., Amundson, R., McFadden, L., & Chadwick, O. (1996). An isotopic study of soils in chronological sequences of alluvial deposits, Providence Mountains, California. *Geological Society of America Bulletin*, *108*(4), 379 -391.

Welp, L. R., Randerson, J. T., & Liu, H. P. (2006). Seasonal exchange of CO_2 and $\delta^{18}O$-CO_2 varies with postfire succession in boreal forest ecosystems. *Journal of Geophysical Research*, *111*, G03007.

Wingate, L., OgéE, J., Burlett, R., & Bosc, A. (2010). Strong seasonal disequilibrium measured between the oxygen isotope signals of leaf and soil CO_2 exchange. *Global Change Biology*,3048-3064.

Wingate, L., Ogée, J., Cuntz, M., Genty, B., Reiter, I., Seibt, U., Yakir, D., u. a. (2009). The impact of soil microorganisms on the global budget of $\delta^{18}O$ in atmospheric CO_2. *Proceedings of the National Academy of Sciences*, *106*(52), 22411 -22415.

Wingate, L., Seibt, U., Maseyk, K., OgéE, J., Almeida, P., Yakir, D., Pereira, J. S., u. a. (2008). Evaporation and carbonic anhydrase activity recorded in oxygen isotope signatures of net CO_2 fluxes from a Mediterranean soil. *Global Change Biology*, *14*(9), 2178-2193.

Yakir, D., & Sternberg, L. D. S. L. (2000). The use of stable isotopes to study ecosystem gas exchange. *Oecologia*, *123*(3), 297-311.

Yakir, D., & Wang, X. (1996). Fluxes of CO_2 and water between terrestrial vegetation and the atmosphere estimated from isotope measurements. *Nature*, *380*(6574), 515-517.

Appendix A: Abbreviations used in the Text:

A	ambient air
ANOVA	Analysis of Variance
α	fractionation factor
α_{A-B}	fractionation factor from scale A to scale B
α_{eq}	equilibrium fractionation factor
α_{XY}	magnitude of fractionation during the transfer of CO_2 from one reservoir to another
B	dimensionless Bunsen coefficient
C	concentration of CO_2 [mol cm^{-3}]
cCO_2	concentration of CO_2 [mol cm^{-3}]
CA	carbonic anhydrase
C^{18}	concentration of $C^{18}O^{16}O$ [mol cm^{-3}]
$[CO_2]_o$	concentration of CO_2 at the cuvette outlet
$[CO_2]_i$	concentration of CO_2 at the cuvette inlet
D	Diffusion coefficient
D_{18}	free air molecular diffusivity of $C^{18}O^{16}O$ [cm^2 s^{-1}]
$D^{18}{}_s$	effective coefficient of $C^{18}O^{16}O$ in the soil [cm^2 s^{-1}]
δ	isotopic composition in δ-notation (‰)
Δ	isotopic discrimination
δD	δ-value of Deuterium
$\delta^{18}O_{V-SMOW}$	δ-value of oxygen composition in CO_2 on V-SMOW scale (‰)
$\delta^{18}O_{V-PDB}$	δ-value of oxygen composition in CO_2 on V-PDB scale (‰)
$\delta^{18}O_{V-PDB-CO2}$	δ-value of oxygen composition in CO_2 on V-PDB-CO_2 scale (‰)
$\delta^{18}O_{resp}$	δ-value of oxygen composition in soil released CO_2 on (‰)
$\delta^{18}O_o$	δ-value of oxygen composition in CO_2 at the cuvette outlet (‰)
$\delta^{18}O_i$	δ-value of oxygen composition in CO_2 at the cuvette inlet (‰)
δ_{S-A}	δ-value of a sample on scale A
δ_{S-B}	δ-value of a sample on scale B
εp	free air porosity
ε	enrichment in heavy isotopologue
ε_a	air-filled pore space
ε_{eq}	equilibrium enrichment
ε_{eq-CO2}	equilibrium oxygen isotope effect between CO_2 and water
ε_k	kinetic enrichment
ε_t	total porosity which equals $\varepsilon_a + B\varepsilon_w$
ε_w	water-filled pore space
E	kinetic Energy
F_{AL}	CO_2 flux from atmosphere into the leaves

F_{AS}	CO_2 flux from atmosphere into the soils
F_{LA}	CO_2 flux from leaves into the atmosphere
F_{SA}	CO_2 flux from soils into the atmosphere
F_{AO}	CO_2 flux from atmosphere into the ocean
F_{OA}	CO_2 flux from ocean into the atmosphere
F_{FA}	CO_2 flux from fossil fuel burning into the atmosphere
F_{XY}	CO_2 flux from reservoir X to reservoir Y
k	rate of CO_2-H_2O isotopic exchange
k_h	rate of isotopic equilibration, which takes place only in the dissolved phase
K_h	hydraulic conductivity of a porous medium [cms^{-1}]
L	liquid water body
m	mass [g]
M_A	moles of gas in the atmosphere
μ	reduced mass
p	water pressure [Pa]
ppm	parts per million
ppmv	parts per million by volume
Φ	production (respiration) of CO_2 per depth increment [moles cm^{-3} s^{-1}]
q_x	volumetric flow rate in the direction x per unit cross sectional area of medium [cms^{-1}]
R_A	ratio of concentration of heavy to light isotopologue in substance A
R_B	ratio of concentration of heavy to light isotopologue in substance B
R_{sample}	ratio of concentration of heavy to light isotopologue in the sample
$R_{standard}$	ratio of concentration of heavy to light isotopologue in the standard
R_S	isotopic ratio of CO_2 which is produced in the soil
R_{eq}	isotopic ratio of CO_2 which is in equilibrium with soil water
R^{18}_p	ratio of $^{18}O/^{16}O$ of CO_2 of the production
R^{18}_{eq}	ratio of $^{18}O/^{16}O$ of CO_2 in equilibrium with soil water
$R^{18}(z)$	ratio of $^{18}O/^{16}O$ of CO_2 of soil CO_2
rH	relative humidity of air (%)
S	rate of CO_2 production [moles cm^{-3} s^{-1}]
SM	soil moisture (%)
Std	standard deviation
t	tortuosity factor
T	absolute temperature (K)
TGA	Trace Gas Analyzer
V	evaporating water vapor
V	velocity [ms^{-1}]
V-SMOW	International Standard Vienna Standard Mean Ocean Water
V-PDB	International Standard Vienna Pee Dee Belemnite

V-PDB-CO_2	International Standard Vienna Pee Dee Belemnite CO_2
WS-CRDS	Wavelength-Scanned Cavity Ring Down Spectroscopy
y_w	weight density of water [$Pacm^{-1}$]
z	depth increment [cm]
z_e	elevation above arbitrary datum [cm]

Appendix B: Measurements of the irrigation water

Table A-1: Measurements of the δ-values of the irrigation water of Experiments IV-VIII.

Nr.	Exp	$\delta^{18}O$ Mean	δD Mean	cH_2O Mean	$\delta^{18}O$ std	δD std	cH_2O std
1	IV	-10.16	-76.49	20292	0.88	2.63	256
2	IV	-10.46	-77.25	22408	0.15	0.74	119
3	IV	-10.47	-78.06	20900	0.18	0.36	135
4	IV	-10.66	-78.24	21372	0.14	0.29	116
5	IV	-10.41	-77.72	21858	0.29	0.46	168
6	IV	-11.36	-80.39	20717	0.09	1.36	32
Mean		**-10.72**	**-78.60**	**21212**	**0.17**	**0.62**	**113**
7	V	58.47	-79.62	21763	0.30	0.63	171
8	V	59.12	-78.06	22229	0.18	0.48	133
9	V	58.07	-80.29	21138	0.18	0.54	148
10	V	59.06	-78.92	21467	0.41	0.60	133
11	V	58.34	-78.38	22850	0.45	0.45	151
12	V	59.10	-81.24	23112	0.32	0.38	140
Mean		**58.64**	**-79.71**	**22142**	**0.34**	**0.49**	**143**
13	VI	53.44	-74.28	20708	0.35	0.41	142
14	VI	56.01	-74.21	18937	0.31	0.94	123
15	VI	58.23	-79.16	20688	0.22	0.52	154
16	VI	57.82	-79.71	20678	0.43	0.59	116
17	VI	57.81	-79.61	18962	0.51	0.52	115
18	VI	58.75	-82.48	19537	0.36	0.28	111
Mean		**58.15**	**-80.24**	**19966**	**0.38**	**0.48**	**124**
19	VII	58.66	-79.13	22557	0.24	0.72	159
20	VII	58.02	-80.06	19833	0.40	0.44	145
21	VII	58.03	-80.07	21165	0.34	0.44	161
22	VII	58.28	-79.74	20003	0.35	0.35	118
23	VII	59.06	-79.05	21555	0.32	0.63	165
24	VII	59.06	-79.76	21081	0.52	0.25	125
Mean		**58.61**	**-79.65**	**20951**	**0.38**	**0.42**	**142**
25	VIII	59.59	-80.50	22293	0.34	0.52	161
26	VIII	59.23	-79.88	22754	0.27	0.11	156
27	VIII	58.84	-77.97	22890	0.26	0.35	165
28	VIII	59.42	-79.68	22433	0.39	0.37	161
29	VIII	59.14	-79.78	22684	0.42	0.42	172
30	VIII	59.24	-79.83	22646	0.41	0.42	145
Mean		**59.16**	**-79.32**	**22663**	**0.37**	**0.39**	**161**

Appendix C: R-Codes

R-Code for TGA data:

```
#DATUM ÄNDERN!!!
#BEIM PLOTTEN EVENTUELL GRENZEN DER Y_ACHSEN VERÄNDERN !!!

setwd("G:/BioAtmo/sperber-c/Exp7 - The effect of a litter layer (beech leaves)")

#Dateien, die eingelesen werden sollen
Datei_TGA          <- "TGA_Sep13-17.csv"
#Überschrift für Plot, d.h. das Datum ändern
Überschrift_Plot_TGA  <- "TGA del values vs. time (Sep13-17)"
#Name der Datei, die ausgegeben werden soll
Plot_TGA           <- "TGA (Sep13-17).wmf"
PT_Datei_auslesen    <- "PT_Sep13-17.csv"

#BEGINN CODE !!!
Messung <- read.table(Datei_TGA, sep=";", dec=",", header=T)

# PT1 und PT2 rausfiltern und als .csv Datei ausgeben
write.table(Messung[,c(1,31,32)],PT_Datei_auslesen,sep = ";", dec = ",", row.names= FALSE)

#Spalten löschen und umbenennen und einfügen
B_TGA <- Messung[,c(1,3,5,6,7,9,10)]
names(B_TGA) <- c("DATE","SITE","MEAN_12C","MEAN_13C","MEAN_18O","D13C_AVG","D18O_AVG")
TIME <- substring(B_TGA[,1],12,16)
C_TGA <- cbind(B_TGA,TIME)
cor_1 <- C_TGA[,c(1,8,2:7)]
cor_1[1:10,]

#Gesamtkonzentration sowie delta13c- und delta18o-Werte des Referenzgases 1 und 2: ANPASSEN!!!
conc_rg1 <- 329
d13c_rg1 <- -46.71435
d18o_rg1 <- -33.64992

conc_rg2 <- 671
d13c_rg2 <- -46.82982
d18o_rg2 <- -33.25852

#Konzentrationsanteil von 12C und 13C im CO2-Referenzgas 1 in Abhängigkeit von delta13C (V-PDB) des Referenzgases
#R(PDB) = 0.0112372 (siehe Lösungsweg im Ordner)
c12c_rg1 <- 1 / (d13c_rg1 / 1000 * 0.0112372 + 1.0112372)
c13c_rg1 <- (d13c_rg1 / 1000 * 0.0112372 + 0.0112372) / (d13c_rg1 / 1000 * 0.0112372 + 1.0112372)
csum_rg1 <- c12c_rg1 + c13c_rg1

#Konzentrationsanteil von 16O und 18O im CO2-Referenzgas 1
#Umrechnung von delta 18O-Werten (VPDB-CO2) über delta 18O-Werte (VPDB) in delta18O-Werte (VSMOW)
d18o_sm1 <- 30.92 + 1.03092 * (d18o_rg1 * 1.01025 + 10.25)
#R(V-SMOW) = 0.0020052
c16o_rg1 <- 0.9976 / (d18o_sm1 / 1000 * 0.0020052+ 1.0020052)
c18o_rg1 <- (d18o_sm1 / 1000 * 0.0020052+ 0.0020052) * 0.9976 / (d18o_sm1 / 1000 * 0.0020052+ 1.0020052)
osum_rg1 <- c16o_rg1 + c18o_rg1

#Konzentrationsanteil von 12C16O2 im CO2-Referenzgas 1 in Abhängigkeit von delta13C (V-PDB) und delta18O (V-PDB) des
Referenzgases
c1216161 <- c12c_rg1 * c16o_rg1 * c16o_rg1 * conc_rg1

#Konzentrationsanteil von 13C16O2 im CO2-Referenzgas 1 in Abhängigkeit von delta13C (V-PDB) und delta18O (V-PDB) des
Referenzgases
c1316161 <- c13c_rg1 * c16o_rg1 * c16o_rg1 * conc_rg1
```

```
#Konzentrationsanteil von 12C16O18O im CO2-Referenzgas 1 in Abhängigkeit von delta13C (V-PDB) und delta18O (V-PDB) des Referenzgases
c1216181 <- c12c_rg1 * c16o_rg1 * c18o_rg1 * 2 * conc_rg1

#Konzentrationsanteil von 12C und 13C im CO2-Referenzgas 2 in Abhängigkeit von delta13C (V-PDB) des Referenzgases
#R(PDB) = 0.0112372
c12c_rg2 <- 1 / (d13c_rg2 / 1000 * 0.0112372 + 1.0112372)
c13c_rg2 <- (d13c_rg2 / 1000 * 0.0112372 + 0.0112372) / (d13c_rg2 / 1000 * 0.0112372 + 1.0112372)
csum_rg2 <- c12c_rg2 + c13c_rg2

#Konzentrationsanteil von 16O und 18O im CO2-Referenzgas 2 in Abhängigkeit von delta18O (V-PDB) des Referenzgases
#Umrechnung von delta18O-Werten (V-PDB) in delta18O-Werte (V-SMOW)
d18o_sm2 <- 30.92 + 1.03092 * (d18o_rg2*1.01025+10.25)

#R(V-SMOW) = 0.0020052
c16o_rg2 <- 0.9976 / (d18o_sm2 / 1000 * 0.0020052+ 1.0020052)
c18o_rg2 <- (d18o_sm2 / 1000 * 0.0020052+ 0.0020052) * 0.9976 / (d18o_sm2 / 1000 * 0.0020052+ 1.0020052)
osum_rg2 <- c16o_rg2 + c18o_rg2

#Konzentrationsanteil von 12C16O2 im CO2-Referenzgas 2 in Abhängigkeit von delta13C (V-PDB) und delta18O (V-PDB) des Referenzgases
c1216162 <- c12c_rg2 * c16o_rg2 * c16o_rg2 * conc_rg2

#Konzentrationsanteil von 13C16O2 im CO2-Referenzgas 2 in Abhängigkeit von delta13C (V-PDB) und delta18O (V-PDB) des Referenzgases
c1316162 <- c13c_rg2 * c16o_rg2 * c16o_rg2 * conc_rg2

#Konzentrationsanteil von 12C16O18O im CO2-Referenzgas 2 in Abhängigkeit von delta13C (V-PDB) und delta18O (V-PDB) des Referenzgases
c1216182 <- c12c_rg2 * c16o_rg2 * c18o_rg2 * 2 * conc_rg2


##########################
###   INTERPOLATION   ###
##########################

#Berechnung des zeitlichen Verlaufs der Gerätedrift für die 12C16O2-Konzentration durch lineare Interpolation zwischen den jeweiligen Referenzgasaufgaben

########################
###   für Refgas1   ###
########################

#Vektor initialisieren
y1_12C <- rep(NA,length(cor_1[,1]))
y1_12C[1:20]

#Wert für Refgas1 in Vektor sonst Lücken mit 0 ausfüllen
for (i in seq(length(cor_1[,1])))
{ if (cor_1[i,3] == 1) {y1_12C[i] <- cor_1[i,4]}
  else y1_12C[i] <- 0 }


#Nullwerte rausfiltern und dadurch Y-Werte für Interpolation erstellen
y1_12C_ohne0 <- y1_12C[y1_12C!= 0]
#X Werte für Interpolation erstellen
x1_12C <- seq(length(y1_12C))
x1_12C_ohne0 <- x1_12C[which(y1_12C!=0)]

#Lineare Interpolation
y1_12C_int <- approx(x1_12C_ohne0,y1_12C_ohne0,x1_12C)
y1_m12c <- y1_12C_int[[2]]
```

```
#####################
##   für Refgas2   ##
#####################

#Vektor initialisieren
y2_12C <- rep(NA,length(cor_1[,1]))

#Wert für Refgas2 in Vektor sonst Lücken mit 0 ausfüllen
for (i in seq(length(cor_1[,1]))) {
  if (cor_1[i,3]==2) {y2_12C[i] <- cor_1[i,4]}
  else (y2_12C[i] <- 0)}

#Nullwerte rausfiltern und dadurch Y-Werte für Interpolation erstellen
y2_12C_ohne0 <- y2_12C[which(y2_12C!=0)]
length(y2_12C_ohne0)
#X Werte für Interpolation erstellen
x2_12C <- seq(length(y2_12C))
x2_12C_ohne0 <- x2_12C[which(y2_12C!=0)]

#Lineare Interpolation
y2_12C_int <- approx(x2_12C_ohne0,y2_12C_ohne0,x2_12C)
y2_m12c <- y2_12C_int[[2]]
length(y2_m12c)

#Berechnung der korrigierten 12C16O2-Konzentration über die Zweipunkteform einer Geraden mit den beiden Punkten
(x1/y1) = Referenzgas 1 und (x2/y2) = Referenzgas 2
#Hierbei steht x für die tatsächliche Konzentration und y für die vom Gerät gemessene und abgespeicherte Konzentration
#Die Berechnung der tatsächlichen Konzentration erfolgt durch Auflösen der Zweipunkteform einer Gerade nach x = (y * (x2
- x1) - x2 * y1 + x1 * y2) / (y2 - y1)
cor_1[1:10,]
m12c_cor <- (cor_1[,4] * (c1216162 - c1216161) - c1216162 * y1_m12c + c1216161* y2_m12c) / (y2_m12c - y1_m12c)
m12c_cor[1:100]

#########################################################################################################
#####################################################
#*Berechnung des zeitlichen Verlaufs der Gerätedrift für die 13C16O2-Konzentration durch lineare Interpolation zwischen
den jeweiligen Referenzgasaufgaben

cor_1[1:5,]
#Vektor initialisieren
y1_13C <- rep(NA,length(cor_1[,1]))
y1_13C[1:20]

#Wert für Refgas1 in Vektor sonst Lücken mit 0 ausfüllen
for (i in seq(length(cor_1[,1])))
{ if (cor_1[i,3] == 1) {y1_13C[i] <- cor_1[i,5]}
  else y1_13C[i] <- 0 }

#Nullwerte rausfiltern und dadurch Y-Werte für Interpolation erstellen
y1_13C_ohne0 <- y1_13C[y1_13C!= 0]
#X Werte für Interpolation erstellen
x1_13C <- seq(length(y1_13C))
x1_13C_ohne0 <- x1_13C[which(y1_13C!=0)]

#Lineare Interpolation
y1_13C_int <- approx(x1_13C_ohne0,y1_13C_ohne0,x1_13C)
y1_m13c <- y1_13C_int[[2]]

#####################
##   für Refgas2   ##
#####################

cor_1[1:5,]
length(cor_1[,1])
```

```
#Vektor initialisieren
y2_13C <- rep(NA,length(cor_1[,1]))

#Wert für Refgas1 in Vektor sonst Lücken mit 0 ausfüllen
for (i in seq(length(cor_1[,1]))) {
  if (cor_1[i,3]==2) {y2_13C[i] <- cor_1[i,5]}
  else (y2_13C[i] <- 0)}

#Nullwerte rausfiltern und dadurch Y-Werte für Interpolation erstellen
y2_13C_ohne0 <- y2_13C[which(y2_13C!=0)]

#X Werte für Interpolation erstellen
x2_13C <- seq(length(y2_13C))
x2_13C_ohne0 <- x2_13C[which(y2_13C!=0)]

#Lineare Interpolation
y2_13C_int <- approx(x2_13C_ohne0,y2_13C_ohne0,x2_13C)
y2_m13c <- y2_13C_int[[2]]
length(y2_m13c)

#*Berechnung der korrigierten 13C16O2-Konzentration über die Zweipunkteform einer Geraden mit den beiden Punkten
(x1/y1) = Referenzgas 1 und (x2/y2) = Referenzgas 2
#*Hierbei steht x für die tatsächliche Konzentration und y für die vom Gerät gemessene und abgespeicherte Konzentration
#*Die Berechnung der tatsächlichen Konzentration erfolgt durch Auflösen der Zweipunkteform einer Gerade nach x = (y *
(x2 - x1) - x2 * y1 + x1 * y2) / (y2 - y1)

m13c_cor <- (cor_1[,5] * (c1316162 - c1316161) - c1316162 * y1_m13c + c1316161 * y2_m13c) / (y2_m13c - y1_m13c)


##########################################################################################################################
##########################################################
#*Berechnung des zeitlichen Verlaufs der Gerätedrift für die 12C16O18O-Konzentration durch lineare Interpolation
zwischen den jeweiligen Referenzgasaufgaben


########################
###   für Refgas1   ###
########################

#Vektor initialisieren
y1_18O <- rep(NA,length(cor_1[,1]))
y1_18O[1:20]

#Wert für Refgas1 in Vektor sonst Lücken mit 0 ausfüllen
for (i in seq(length(cor_1[,1])))
{ if (cor_1[i,3] == 1) {y1_18O[i] <- cor_1[i,6]}
  else y1_18O[i] <- 0 }

#Nullwerte rausfiltern und dadurch Y-Werte für Interpolation erstellen
y1_18O_ohne0 <- y1_18O[y1_18O!= 0]
#X Werte für Interpolation erstellen
x1_18O <- seq(length(y1_18O))
x1_18O_ohne0 <- x1_18O[which(y1_18O!=0)]

#Lineare Interpolation
y1_18O_int <- approx(x1_18O_ohne0,y1_18O_ohne0,x1_18O)
y1_m18o <- y1_18O_int[[2]]


######################
##   für Refgas2   ##
######################
```

```
cor_1[1:15,]
length(cor_1[,1])

#Vektor initialisieren
y2_18O <- rep(NA,length(cor_1[,1]))

#Wert für Refgas1 in Vektor sonst Lücken mit 0 ausfüllen
for (i in seq(length(cor_1[,1]))) {
  if (cor_1[i,3]==2) {y2_18O[i] <- cor_1[i,6]}
  else (y2_18O[i] <- 0)}

#Nullwerte rausfiltern und dadurch Y-Werte für Interpolation erstellen
y2_18O_ohne0 <- y2_18O[which(y2_18O!=0)]
length(y2_18O_ohne0)
#X Werte für Interpolation erstellen
x2_18O <- seq(length(y2_18O))
x2_18O_ohne0 <- x2_18O[which(y2_18O!=0)]

#Lineare Interpolation
y2_18O_int <- approx(x2_18O_ohne0,y2_18O_ohne0,x2_18O)
y2_m18o <- y2_18O_int[[2]]
length(y2_m18o)

#*Berechnung der korrigierten 12C16O18O-Konzentration über die Zweipunkteform einer Geraden mit den beiden Punkten
(x1/y1) = Referenzgas 1 und (x2/y2) = Referenzgas 2
#*Hierbei steht x für die tatsächliche Konzentration und y für die vom Gerät gemessene und abgespeicherte Konzentration
#*Die Berechnung der tatsächlichen Konzentration erfolgt durch Auflösen der Zweipunkteform einer Gerade nach x = (y *
(x2 - x1) - x2 * y1 + x1 * y2) / (y2 - y1)

m18o_cor = (cor_1[,6] * (c1216182 - c1216181) - c1216182 * y1_m18o + c1216181 * y2_m18o) / (y2_m18o - y1_m18o)
m18o_cor[1:100]
#Überprüfen, ob Werte mit SPSS-Datei übereinstimmen
#y1_m12c[1:10]
#y2_m12c[1:10]
#m12c_cor[1:10]
#y1_m13c[1:10]
#y2_m13c[1:10]
#m13c_cor[1:10]
#y1_m18o[1:10]
#y2_m18o[1:10]
#m18o_cor[1:10]




#############################################################################################
#Berechnung der korrigierten delta13C-Werte (V-PDB)
d13c_pdb <-  (m13c_cor / m12c_cor - 0.0112372) / 0.0112372 * 1000

#Berechnung der korrigierten delta18O-Werte (V-SMOW)
d18o_smo <-  (0.5 * m18o_cor / m12c_cor - 0.0020052) / 0.0020052 * 1000

#Berechnung der korrigierten delta18O-Werte (V-PDB)
d18o_pdb <-  (d18o_smo - 30.92) / 1.03092

#Berechnung der korrigierten delta18O-Werte (VPDB-CO2)
d18o_co2 <-  (d18o_pdb - 10.25) / 1.01025


#############################################################################################
#Vektoren der korrigierten Werte erstellen

#############################################################################################
```

```
#### m12c ##############################################################################
##########################################################################################


#IF (site = 3) m12c_inl = m12c_cor .
m12c_inl <- rep(NA,length(cor_1[,1]))
for (i in seq(length(cor_1[,1]))) {
  if(cor_1[i,3]==3){m12c_inl[i] <- m12c_cor[i]}
  else(m12c_inl[i] <- 0) }
m12c_inl[1:15]

#IF (site = 4) m12c_top = m12c_cor .
m12c_top <- rep(NA,length(cor_1[,1]))
for (i in seq(length(cor_1[,1]))) {
  if(cor_1[i,3]==4){m12c_top[i] <- m12c_cor[i]}
  else(m12c_top[i] <- 0) }
m12c_top[1:15]

#IF (site = 5) m12c_bot = m12c_cor .
m12c_bot <- rep(NA,length(cor_1[,1]))
for (i in seq(length(cor_1[,1]))) {
  if(cor_1[i,3]==5){m12c_bot[i] <- m12c_cor[i]}
  else(m12c_bot[i] <- 0) }
m12c_bot[1:15]

#IF (site = 6) m12c_left = m12c_cor .
m12c_left <- rep(NA,length(cor_1[,1]))
for (i in seq(length(cor_1[,1]))) {
  if(cor_1[i,3]==6){m12c_left[i] <- m12c_cor[i]}
  else(m12c_left[i] <- 0) }
m12c_left[1:100]

#IF (site = 7) m12c_right = m12c_cor .
m12c_right <- rep(NA,length(cor_1[,1]))
for (i in seq(length(cor_1[,1]))) {
  if(cor_1[i,3]==7){m12c_right[i] <- m12c_cor[i]}
  else(m12c_right[i] <- 0) }
m12c_right[1:100]

#IF (site = 8) m12c_amb = m12c_cor .
m12c_amb <- rep(NA,length(cor_1[,1]))
for (i in seq(length(cor_1[,1]))) {
  if(cor_1[i,3]==8){m12c_amb[i] <- m12c_cor[i]}
  else(m12c_amb[i] <- 0) }
m12c_amb[1:100]


##########################################################################################
#### m13c ##############################################################################
##########################################################################################

#IF (site = 3) m13c_inl = m13c_cor .
m13c_inl <- rep(NA,length(cor_1[,1]))
for (i in seq(length(cor_1[,1]))) {
  if(cor_1[i,3]==3){m13c_inl[i] <- m13c_cor[i]}
  else(m13c_inl[i] <- 0) }
m13c_inl[1:15]

#IF (site = 4) m13c_top = m13c_cor .
m13c_top <- rep(NA,length(cor_1[,1]))
for (i in seq(length(cor_1[,1]))) {
  if(cor_1[i,3]==4){m13c_top[i] <- m13c_cor[i]}
  else(m13c_top[i] <- 0) }
m13c_top[1:15]
```

```
#IF (site = 5) m13c_bot = m13c_cor .
m13c_bot <- rep(NA,length(cor_1[,1]))
for (i in seq(length(cor_1[,1]))) {
  if(cor_1[i,3]==5){m13c_bot[i] <- m13c_cor[i]}
  else(m13c_bot[i] <- 0) }
m13c_bot[1:15]

#IF (site = 6) m13c_left = m13c_cor .
m13c_left <- rep(NA,length(cor_1[,1]))
for (i in seq(length(cor_1[,1]))) {
  if(cor_1[i,3]==6){m13c_left[i] <- m13c_cor[i]}
  else(m13c_left[i] <- 0) }
m13c_left[1:15]

#IF (site = 7) m13c_right = m13c_cor .
m13c_right <- rep(NA,length(cor_1[,1]))
for (i in seq(length(cor_1[,1]))) {
  if(cor_1[i,3]==7){m13c_right[i] <- m13c_cor[i]}
  else(m13c_right[i] <- 0) }
m13c_right[1:15]

#IF (site = 8) m13c_amb = m13c_cor .
m13c_amb <- rep(NA,length(cor_1[,1]))
for (i in seq(length(cor_1[,1]))) {
  if(cor_1[i,3]==8){m13c_amb[i] <- m13c_cor[i]}
  else(m13c_amb[i] <- 0) }
m13c_amb[1:15]

#############################################################################
#### m18o ###################################################################
#############################################################################

#IF (site = 3) m18o_inl = m18o_cor .
m18o_inl <- rep(NA,length(cor_1[,1]))
for (i in seq(length(cor_1[,1]))) {
  if(cor_1[i,3]==3){m18o_inl[i] <- m18o_cor[i]}
  else(m18o_inl[i] <- 0) }
m18o_inl[1:15]

#IF (site = 4) m18o_top = m18o_cor .
m18o_top <- rep(NA,length(cor_1[,1]))
for (i in seq(length(cor_1[,1]))) {
  if(cor_1[i,3]==4){m18o_top[i] <- m18o_cor[i]}
  else(m18o_top[i] <- 0) }
m18o_top[1:15]

#IF (site = 5) m18o_bot = m18o_cor .
m18o_bot <- rep(NA,length(cor_1[,1]))
for (i in seq(length(cor_1[,1]))) {
  if(cor_1[i,3]==5){m18o_bot[i] <- m18o_cor[i]}
  else(m18o_bot[i] <- 0) }
m18o_bot[1:15]

#IF (site = 6) m18o_left = m18o_cor .
m18o_left <- rep(NA,length(cor_1[,1]))
for (i in seq(length(cor_1[,1]))) {
  if(cor_1[i,3]==6){m18o_left[i] <- m18o_cor[i]}
  else(m18o_left[i] <- 0) }
m18o_left[1:150]

#IF (site = 7) m18o_right = m18o_cor .
m18o_right <- rep(NA,length(cor_1[,1]))
for (i in seq(length(cor_1[,1]))) {
```

```
  if(cor_1[i,3]==7){m18o_right[i] <- m18o_cor[i]}
  else(m18o_right[i] <- 0) }
m18o_right[1:150]

#IF (site = 8) m18o_amb = m18o_cor .
m18o_amb <- rep(NA,length(cor_1[,1]))
for (i in seq(length(cor_1[,1]))) {
  if(cor_1[i,3]==8){m18o_amb[i] <- m18o_cor[i]}
  else(m18o_amb[i] <- 0) }
m18o_amb[1:15]

#############################################################################
#### d13c ###################################################################
#############################################################################
cor_1[1:10,]
#IF (site = 3) d13c_inl = m13c_pdb .
d13c_inl <- rep(NA,length(cor_1[,1]))
for (i in seq(length(cor_1[,1]))) {
  if(cor_1[i,3]==3){d13c_inl[i] <- d13c_pdb[i]}
  else(d13c_inl[i] <- 0) }
d13c_inl[1:15]

#IF (site = 4) d13c_top = d13c_pdb .
d13c_top <- rep(NA,length(cor_1[,1]))
for (i in seq(length(cor_1[,1]))) {
  if(cor_1[i,3]==4){d13c_top[i] <- d13c_pdb[i]}
  else(d13c_top[i] <- 0) }
d13c_top[1:15]

#IF (site = 5) d13c_bot = d13c_pdb .
d13c_bot <- rep(NA,length(cor_1[,1]))
for (i in seq(length(cor_1[,1]))) {
  if(cor_1[i,3]==5){d13c_bot[i] <- d13c_pdb[i]}
  else(d13c_bot[i] <- 0) }
d13c_bot[1:15]

#IF (site = 6) d13c_left = d13c_pdb .
d13c_left <- rep(NA,length(cor_1[,1]))
for (i in seq(length(cor_1[,1]))) {
  if(cor_1[i,3]==6){d13c_left[i] <- d13c_pdb[i]}
  else(d13c_left[i] <- 0) }
d13c_left[1:15]

#IF (site = 7) d13c_right = d13c_pdb .
d13c_right <- rep(NA,length(cor_1[,1]))
for (i in seq(length(cor_1[,1]))) {
  if(cor_1[i,3]==7){d13c_right[i] <- d13c_pdb[i]}
  else(d13c_right[i] <- 0) }
d13c_right[1:15]

#IF (site = 8) d13c_amb = d13c_pdb .
d13c_amb <- rep(NA,length(cor_1[,1]))
for (i in seq(length(cor_1[,1]))) {
  if(cor_1[i,3]==8){d13c_amb[i] <- d13c_pdb[i]}
  else(d13c_amb[i] <- 0) }
d13c_amb[1:15]


#############################################################################
#### d18o CO2 ###############################################################
#############################################################################
#IF (site = 3) d18o_inl = d18o_co2 .
d18o_inl <- rep(NA,length(cor_1[,1]))
for (i in seq(length(cor_1[,1]))) {
```

```
  if(cor_1[i,3]==3){d18o_inl[i] <- d18o_co2[i]}
  else(d18o_inl[i] <- 0) }
d18o_inl[1:15]

#IF (site = 4) d18o_top = d18o_co2 .
d18o_top <- rep(NA,length(cor_1[,1]))
for (i in seq(length(cor_1[,1]))) {
  if(cor_1[i,3]==4){d18o_top[i] <- d18o_co2[i]}
  else(d18o_top[i] <- 0) }
d18o_top[1:15]

#IF (site = 5) d18o_bot = d18o_co2 .
d18o_bot <- rep(NA,length(cor_1[,1]))
for (i in seq(length(cor_1[,1]))) {
  if(cor_1[i,3]==5){d18o_bot[i] <- d18o_co2[i]}
  else(d18o_bot[i] <- 0) }
d18o_bot[1:15]

#IF (site = 6) d18o_left = d18o_co2 .
d18o_left <- rep(NA,length(cor_1[,1]))
for (i in seq(length(cor_1[,1]))) {
  if(cor_1[i,3]==6){d18o_left[i] <- d18o_co2[i]}
  else(d18o_left[i] <- 0) }
d18o_left[1:15]

#IF (site = 7) d18o_right = d18o_co2 .
d18o_right <- rep(NA,length(cor_1[,1]))
for (i in seq(length(cor_1[,1]))) {
  if(cor_1[i,3]==7){d18o_right[i] <- d18o_co2[i]}
  else(d18o_right[i] <- 0) }
d18o_right[1:15]

#IF (site = 8) d18o_amb = d18o_co2 .
d18o_amb <- rep(NA,length(cor_1[,1]))
for (i in seq(length(cor_1[,1]))) {
  if(cor_1[i,3]==8){d18o_amb[i] <- d18o_co2[i]}
  else(d18o_amb[i] <- 0) }
d18o_amb[1:15]

#############################################################################
#### d18o VSMOW ##############################################################
#############################################################################
#IF (site = 3) d18o_inl = d18o_smo .
d18o_inl_smo <- rep(NA,length(cor_1[,1]))
for (i in seq(length(cor_1[,1]))) {
  if(cor_1[i,3]==3){d18o_inl_smo[i] <- d18o_smo[i]}
  else(d18o_inl_smo[i] <- 0) }
d18o_inl_smo[1:100]

#IF (site = 4) d18o_top = d18o_smo .
d18o_top_smo <- rep(NA,length(cor_1[,1]))
for (i in seq(length(cor_1[,1]))) {
  if(cor_1[i,3]==4){d18o_top_smo[i] <- d18o_smo[i]}
  else(d18o_top_smo[i] <- 0) }
d18o_top_smo[1:100]

#IF (site = 5) d18o_bot = d18o_smo .
d18o_bot_smo <- rep(NA,length(cor_1[,1]))
for (i in seq(length(cor_1[,1]))) {
  if(cor_1[i,3]==5){d18o_bot_smo[i] <- d18o_smo[i]}
  else(d18o_bot_smo[i] <- 0) }
d18o_bot_smo[1:100]

#IF (site = 6) d18o_left = d18o_smo .
```

```
d18o_left_smo <- rep(NA,length(cor_1[,1]))
for (i in seq(length(cor_1[,1]))) {
  if(cor_1[i,3]==6){d18o_left_smo[i] <- d18o_smo[i]}
  else(d18o_left_smo[i] <- 0) }
d18o_left_smo[1:15]

#IF (site = 7) d18o_right = d18o_smo .
d18o_right_smo <- rep(NA,length(cor_1[,1]))
for (i in seq(length(cor_1[,1]))) {
  if(cor_1[i,3]==7){d18o_right_smo[i] <- d18o_smo[i]}
  else(d18o_right_smo[i] <- 0) }
d18o_right_smo[1:15]

#IF (site = 8) d18o_amb = d18o_smo .
d18o_amb_smo <- rep(NA,length(cor_1[,1]))
for (i in seq(length(cor_1[,1]))) {
  if(cor_1[i,3]==8){d18o_amb_smo[i] <- d18o_smo[i]}
  else(d18o_amb_smo[i] <- 0) }
d18o_amb_smo[1:15]

# Erstellung der Matrix mit den Vektoren der delta Werte der einzelnen Kanäle
date_time_site <- cor_1[,c(1,2,3)]
neuer <- cbind(date_time_site,m12c_cor,d13c_inl,d13c_top,d13c_bot,d13c_left,d13c_right,d13c_amb,

d18o_inl,d18o_top,d18o_bot,d18o_left,d18o_right,d18o_amb,d18o_inl_smo,d18o_top_smo,d18o_bot_smo,d18o_left_sm
o,d18o_right_smo,d18o_amb_smo)

#Sortieren nach Inl, Top, Bot, left, right, ambient
Sort_neuer <- order(neuer[,3])
neuer_sorted_site <- neuer[Sort_neuer,]
nsort <- neuer_sorted_site[c(which(neuer_sorted_site[,3]== 3),which(neuer_sorted_site[,3]== 4),
                             which(neuer_sorted_site[,3]== 5),which(neuer_sorted_site[,3]== 6),
                             which(neuer_sorted_site[,3]== 7),which(neuer_sorted_site[,3]== 8)),]

nsort_INL   <- neuer_sorted_site[which(neuer_sorted_site[,3]== 3),]
Zeitachse_TGA_INL <- as.POSIXct(strptime(paste(nsort_INL[,1],nsort_INL[,2]),format="%d.%m.%Y %H:%M:%S",tz="CET"))
nsort_left  <- neuer_sorted_site[which(neuer_sorted_site[,3]== 6),]
Zeitachse_TGA_left <- as.POSIXct(strptime(paste(nsort_left[,1],nsort_left[,2]),format="%d.%m.%Y %H:%M:%S",tz="CET"))
nsort_right <- neuer_sorted_site[which(neuer_sorted_site[,3]== 7),]
Zeitachse_TGA_right <- as.POSIXct(strptime(paste(nsort_right[,1],nsort_right[,2]),format="%d.%m.%Y
%H:%M:%S",tz="CET"))

##########################
### PLOTTING !!!#########
##########################

# Korrektur der d18O Werte, des reinen CO2, unter der Annahme, das es zu keiner Invasion von CO2 aus Gasgemisch in die
Bodensäule kommt
# Vektorlängen anpassen
nsort_inl <- nsort_INL[seq(1,length(nsort_INL[,1]),2),]

# maximale Vektorlänge
max_vektorlänge <- min(c(length(nsort_inl[,1]),length(nsort_left[,1]),length(nsort_right[,1])))

nsort_Date <- nsort_inl$DATE[1:max_vektorlänge]
nsort_Time <- nsort_inl$TIME[1:max_vektorlänge]

# unterschiedliche X-Achsen (einmal als Datumsachse, einmal als Stundenachse)
Zeitachse <- as.POSIXct(strptime(paste(substring(nsort_Date,1,10),nsort_Time),format="%d.%m.%Y %H:%M",tz="CET"))
stunden   <-  ((as.numeric(Zeitachse) -  as.numeric(Zeitachse)[1])/3600)

# max Vektoränge auf alle Vektoren übertragen
nsort_d18O_inl    <- nsort_inl$d18o_inl[1:max_vektorlänge]
nsort_d18O_inl_smo <- nsort_inl$d18o_inl_smo[1:max_vektorlänge]
```

```
nsort_d13C_inl    <- nsort_inl$d13c_inl[1:max_vektorlänge]
nsort_cCO2_inl    <- nsort_inl$m12c_cor[1:max_vektorlänge]

nsort_d18O_left    <- nsort_left$d18o_left[1:max_vektorlänge]
nsort_d18O_left_smo <- nsort_left$d18o_left_smo[1:max_vektorlänge]
nsort_d13C_left    <- nsort_left$d13c_left[1:max_vektorlänge]
nsort_cCO2_left    <- nsort_left$m12c_cor[1:max_vektorlänge]

nsort_d18O_right    <- nsort_right$d18o_right[1:max_vektorlänge]
nsort_d18O_right_smo <- nsort_right$d18o_right_smo[1:max_vektorlänge]
nsort_d13C_right    <- nsort_right$d13c_right[1:max_vektorlänge]
nsort_cCO2_right    <- nsort_right$m12c_cor[1:max_vektorlänge]

d18O_CO2rein_left_smo  <- (nsort_d18O_left_smo*nsort_cCO2_left -
nsort_d18O_inl_smo*nsort_cCO2_inl)/(nsort_cCO2_left - nsort_cCO2_inl)
d18O_CO2rein_right_smo <- (nsort_d18O_right_smo*nsort_cCO2_right -
nsort_d18O_inl_smo*nsort_cCO2_inl)/(nsort_cCO2_right - nsort_cCO2_inl)

d18O_CO2rein_left  <- (nsort_d18O_left*nsort_cCO2_left - nsort_d18O_inl*nsort_cCO2_inl)/(nsort_cCO2_left -
nsort_cCO2_inl)[1:100]
d18O_CO2rein_right <- (nsort_d18O_right*nsort_cCO2_right - nsort_d18O_inl*nsort_cCO2_inl)/(nsort_cCO2_right -
nsort_cCO2_inl)



# Grenzen der Y-Achsen der Graphen
# d18O_VSMOW
Ylim1_VSMOW_d18O <- -10
Ylim2_VSMOW_d18O <-  120
# d18O_VPDBCO2
Ylim1_PDBCO2_d18O <- ((Ylim1_VSMOW_d18O-30.92)/1.03092-10.25)/1.01025
Ylim2_PDBCO2_d18O <- ((Ylim2_VSMOW_d18O-30.92)/1.03092-10.25)/1.01025
# d13C
Ylim1_d13C <- -33.4
Ylim2_d13C<-  -31.5
# cCO2
Ylim1_cCO2 <- 350
Ylim2_cCO2 <- 699

#Plotting delta values vs. time (hrs.)
win.metafile(Plot_TGA, width = 8, height = 11)
par(cex = 1,cex.main = 2,cex.axis = 1.5, cex.lab = 1.5, mex = 2, font.main=2, lwd=1,
   mfrow=c(3,1), mar = c(0.2, 5, 1, 5), oma = c(10, 4, 5, 1))

plot(stunden, nsort_d18O_inl_smo,#Einlass
   xaxt="n",ylab = expression(paste(delta^18,"O-C",O[2]," (V-SMOW) [‰]")),
   ylim=c(Ylim1_VSMOW_d18O,Ylim2_VSMOW_d18O),
   pch=19, col = "black", cex=1)
   #title(main= expression(paste("Exp16 TGA ", delta,"-values", "(Carboanhydrase)")),outer=T)
   legend("topleft",bty="n",c("Inlet","Fine Sand","Medium Sand"), cex= 1.5, pch=c(19,4,4), col=c("black","red","blue"),
pt.cex=c(2,2,2),pt.lwd= c(2,2,2))
points(stunden, d18O_CO2rein_right_smo,pch=4, col="blue",cex=1,lwd=2)  # Mittelsand, linke Küvette
points(stunden, d18O_CO2rein_left_smo,pch=4, col="red",cex=1,lwd=2)   # Feinsand, rechte Küvette
pdb_co2 =seq(-50,80, by=10)
vsmow   =1.03091*(((1.01025*pdb_co2)+10.25)+30.91)
axis(4, at = vsmow, labels = as.character(pdb_co2))
mtext(expression(paste(delta^18,"O-C",O[2], paste(" (V-PDB-C",O[2],")"," [‰]"))),side=4,line=3)

plot(stunden, nsort_d13C_inl,
   xaxt="n",
   ylab = expression(paste(delta^13,"C-C",O[2],paste(" (V-PDB-C",O[2],")"," [‰]"))),
   ylim=c(Ylim1_d13C,Ylim2_d13C),
   pch=19, col = "black", cex=1)
```

```
points(stunden,nsort_d13C_right,pch=4, col="blue",cex=1,lwd=2)
points(stunden,nsort_d13C_left,pch=4, col="red",cex=1,lwd=2)

plot(stunden, nsort_cCO2_inl,
   ylab = expression(paste("cC",O[2]," [ppm]")),
   ylim=c(Ylim1_cCO2,Ylim2_cCO2),
   pch=19, col = "black", cex=1)

points(stunden, nsort_cCO2_right,pch=4, col="blue",cex=1,lwd=2)
points(stunden, nsort_cCO2_left,pch=4, col="red",cex=1,lwd=2)
title(xlab = "time (hrs.) ",cex=1,outer=T)

dev.off()
```

R-Code for the Picarro, ECHO-EC5 and RFT-2 data:

```
setwd("G:/BioAtmo/sperber-c/Exp7 - The effect of a litter layer (beech leaves)")

# DATEN UND NAMEN ÄNDERN !!!
##################
### Picarro!!! ###
##################

#Name der Datei, die eingelesen werden soll
Pic_Datei_einlesen   <-  "Pic_Sep13-17.csv"
ECHO5_Datei_einlesen <-  "ECHO5_Sep13-17.csv"

# MESSZEITRAUM:
Messbeginn_Pic   <- "2010-09-13 14:21"
Messende_Pic     <- "2010-09-17 14:21"
Messbeginn_ECHO  <- "2010-09-13 14:21"
Messende_ECHO    <- "2010-09-17 14:21"

#ÜBERSCHRIFTEN PLOT
Pic_Überschrift         <- "Picarro del values vs. time (Sep13-17)"
Überschrift_Bodenfeuchte <- "Bodenfeuchte (Sep13-17)"
Überschrift_RHundTemp    <- "Rel. Luftfeuchte und Lufttemp. (Sep13-17)"

#Name der Dateien, die ausgegeben werden soll
Pic_Dat_Plot     <- "Pic del values (Sep13-17).wmf"
Bodenfeuchte     <- "Bodenfeuchte (Sep13-17).wmf"
RHundTemp        <- "RH,Tair,Bodenf(Sep13-17).wmf"

#Name der PT Datei die eingelesen werden soll
PT_Datei_einlesen <- "PT_Sep13-17.csv"

# ECHO5 Datei einlesen
A_ECHO5 <- read.table(ECHO5_Datei_einlesen, sep = ";", dec = ",", header = T)
Leitfa  <- A_ECHO5[,-c(4,6:8)]

#Sekunden seit 1970 in Datum umwandeln
w <- 1282064700
w
Leitfa[,2] <- ISOdatetime(1970,1,1,1,0,0,tz = "GMT")+ Leitfa[,2] # Zeitzone GMT, da Mitteleuropäische Winterzeit
ECHOa <-  na.omit(Leitfa)

# 10 Minuten Mittel aus den Messwerten rauswerfen
ECHO_ges <- ECHOa[-which(ECHOa[,4]>100),]
names(ECHO_ges) <- c("Nr","Time","Value","Anzahl")

# Erstellung Zeitvektor
ECHO_time_character <- as.character(ECHO_ges[,2])
```

```
ECHO_time_character <- substring(ECHO_time_character,1,16)
ECHO_timech <- cbind(ECHO_ges,ECHO_time_character)
ECHO_timech[,5] <- as.character(ECHO_timech[,5])

# Erstellung Matrix von Messzeitraum
a_ECHO <-which(ECHO_timech[,5]== Messbeginn_ECHO)
b_ECHO <-which(ECHO_timech[,5]== Messende_ECHO)
ECHO <- ECHO_timech[a_ECHO[1]:b_ECHO[1],]

# Einzelne Bodenfeuchtesensoren und RH-Sensoren
A2 <- ECHO[which(ECHO[,1] ==1003),]# Tair Mittelsand
A3 <- ECHO[which(ECHO[,1] ==1004),]# RH Mittelsand
A4 <- ECHO[which(ECHO[,1] ==1005),]# Tair Feinsand
A5 <- ECHO[which(ECHO[,1] ==1006),]# RH Feinsand
B0 <- ECHO[which(ECHO[,1] ==2001),]# unten Mittelsand
B1 <- ECHO[which(ECHO[,1] ==2002),]# mitte Mittelsand
B2 <- ECHO[which(ECHO[,1] ==2003),]# oben Mittelsand
B3 <- ECHO[which(ECHO[,1] ==2004),]# unten Feinsand
B4 <- ECHO[which(ECHO[,1] ==2005),]# nischt
C0 <- ECHO[which(ECHO[,1] ==3001),]# mitte Feinsand
C1 <- ECHO[which(ECHO[,1] ==3002),]# oben Feinsand
C2 <- ECHO[which(ECHO[,1] ==3003),]
C3 <- ECHO[which(ECHO[,1] ==3004),]
C4 <- ECHO[which(ECHO[,1] ==3005),]

# PT Datei einlesen
PT <- read.table(PT_Datei_einlesen, sep = ";", dec = ",", header = T)
PT[1:10,]
length(PT[,1])/3
length(A2[,1])/28
mode(PT[,2])


axa   <- substring(PT[,1],1,13)
axa_l <- as.POSIXct(strptime(axa,format="%d.%m.%Y %H",tz="CET"))
A_PT <- cbind(PT,axa_l)

PT_Mean <- as.vector(tapply(A_PT[,2],A_PT[,4],mean))

length(A4[,2])/119

#nur jeden 120. Wert für die Darstellung der rH
stunden_RH        <- trunc((as.numeric(A5[,2])- as.numeric(A5[,2])[1])/3600)
stunden_RH_alle60 <- stunden_RH[seq(0,length(stunden_RH),60)]
A3_alle60         <- A3[seq(0,length(A3[,3]),60),3]
A5_alle60         <- A5[seq(0,length(A5[,3]),60),3]


#Zeitachse Bodenfeuchte
stunden_bodenfeuchte <- trunc((as.numeric(B0[,2])- as.numeric(B0[,2])[1])/3600)


#Plotting
win.metafile(Bodenfeuchte, width = 8, height = 11)
par(cex = 1,cex.main = 2,cex.axis = 1.5, cex.lab = 1.5, mex = 2, font.main=1, lwd=0.5,
   mfrow=c(3,1), mar = c(0.2, 5, 1, 5), oma = c(10, 4, 5, 1))
plot(A4[,2], A4[,3], #Lufttemp Feinsand (linke Küvette)
   xaxt="n" , ylab = "Temp [°C]",
   ylim=c(20,26),
   lty=1, col = "red",lwd=0.5)
   #title(main= "Exp16 rel. Humdity, Airtemp., Soiltemp. and Soilmoisture",cex= 1,outer=T)
   legend("topleft",bty="n",c("Tair Fine Sand","Tair Medium Sand","Tsoil"), cex= 1.5, lty=c(2,2,2), pch= c(15,15,15),
col=c("red","blue","green"), pt.cex=c(2,2,2),pt.lwd= c(2,2,2))
points(A2[,2], A2[,3],lty=1, col="blue",lwd=0.5)    #Lufttemp Mittelsand (rechte Küvette)
```

```
par(new=TRUE)
plot(stunden_RH_alle60, A5_alle60 , #RH Feinsand (linke Küvette)
   xaxt="n" ,yaxt="n",ylab = " ",ylim=c(0,100),
   pch=2, col = "red", cex=1)
legend("top",bty="n",c("rH Fine Sand", "rH Medium Sand"), cex= 1.5, lty=c(2,2), pch= c(2,2), col=c("red","blue"),
pt.cex=c(2,2),pt.lwd= c(2,2))
points(stunden_RH_alle60, A3_alle60,pch=2, col="blue",cex=1)    # RH Mittelsand (rechte Küvette)
points(stunden_RH_alle60,PT_Mean[1:length(stunden_RH_alle60)], lty=2, col="green",lwd=2)
axis(4)
mtext(" rH [%] ",side=4,line=3) #expression(paste(delta^18,"O-C",O[2], paste(" (PDB-C",O[2],")"," [‰]"))),side=4,line=3)

#par(new=TRUE)
#plot(stunden_RH_alle60, PT_Mean[1:95] ,
#    xaxt="n" ,yaxt="n", ylab = " ",ylim=c(20,50),
#    lty=2, col="green",lwd=2)
axis(3, xaxt="n")
plot(stunden_bodenfeuchte, B0[,3], #Feuchtesensor unten Feinsand
   xaxt="n" ,
   ylab = "VWC [%]",
   ylim=c(0,30),
   lty=2, col = "black", lwd=2)
legend("topleft",bty="n",c("Medium Sand (top)","Medium Sand (middle)","Medium Sand (bottom)"), cex= 1.5,
lty=c(2,2,2),pch= c(15,15,15), col=c("red","blue","black"), pt.cex=c(2,2),pt.lwd= c(2,2))
points(stunden_bodenfeuchte, B1[,3],lty=2, col="blue",lwd=2)    # mitte, Feinsand
points(stunden_bodenfeuchte, B2[,3],lty=2, col="red",lwd=2)  #15 oben, Feinsand

plot(stunden_bodenfeuchte, B3[,3], #Feuchtesensor unten Mittelsand
   ylab = "VWC [%]",
   ylim = c(0,30),
   lty  = 2, col = "black", lwd=2)
legend("topleft",bty="n",c("Fine Sand (top)","Fine Sand (middle)","Fine Sand (bottom)"), cex= 1.5, lty=c(2,2,2),pch=
c(15,15,15), col=c("red","blue","black"), pt.cex=c(2,2),pt.lwd= c(2,2))
points(stunden_bodenfeuchte, C0[,3],lty=2, col="blue",lwd=2)    # mitte, Mittelsand
points(stunden_bodenfeuchte, C1[,3],lty=2, col="red",lwd=2)  #15 oben, Mittelsand
title(xlab = "time (hrs.) ",cex=1,outer=T)
dev.off()


################################
### Weiter mit Picarro !!! ###
################################

#Datei einlesen und vorbereiten
A_Pic <- read.table(Pic_Datei_einlesen, sep=";", dec=",", header=T)
B_Pic <- A_Pic[,-c(3:5)]
TIME <- substring(B_Pic[,2],1,8)
C_Pic <- cbind(B_Pic,TIME)
Pic1 <- C_Pic[,c(1,6,3:5)]

#Eine Spalte nur mit den Minuten erzeugen
Min <-  substring(Pic1[,2],4,5)
Min <- as.numeric(Min)
Pic1a <- cbind(Pic1,Min)
Pic1b <- Pic1a[,c(1,2,6,3,4,5)]

# Datum und Zeit verbinden und ins Zeitformat übertragen
Zeitachse_Pic <- as.POSIXct(strptime(paste(Pic1b[,1],Pic1b[,2]),format= "%d.%m.%Y %H:%M:%S",tz="CET"  ))
Pic2 <- cbind(Pic1b,Zeitachse_Pic)
Pic3 <- Pic2[,-c(1,2)]
Pic4  <- Pic3[,c(5,1:4)]

# Zusätliche Spalte mit Zeit als Datentyp "character"
Pic_time_character <- as.character(Pic4[,1])
```

```
Pic_hrs_min <- substring(Pic_time_character,1,16)
Pic_timech <- cbind(Pic4,Pic_hrs_min)

# Messbeginn und Messende
a_Pic <- which(Pic_timech[,6]== Messbeginn_Pic)
b_Pic <- which(Pic_timech[,6]== Messende_Pic)
c_Pic <- Pic_timech[a_Pic[1]:b_Pic[1],]
c_Pic[,6] <- as.character(c_Pic[,6])
c_Pic[1:10,]
# Mittelwerte der Messungen pro Minute
Pic_means_H2O <- as.data.frame.table(tapply(c_Pic[,3],c_Pic[,6],mean))
names(Pic_means_H2O)<-c("Time","cH2O")

Pic_means_d18O <- as.data.frame.table(tapply(c_Pic[,4],c_Pic[,6],mean))
names(Pic_means_d18O)<-c("Time","d18O")

Pic_means_dD <- as.data.frame.table(tapply(c_Pic[,5],c_Pic[,6],mean))
names(Pic_means_dD)<-c("Time","dD")

Pic_means <- cbind(Pic_means_H2O,Pic_means_d18O[,2],Pic_means_dD[,2])
names(Pic_means )<-c("Time","cH2O","d18O","dD")

Pic_min <- substring(Pic_means[,1],15,16)
Pic_min <- as.numeric(Pic_min)
Pic <- cbind(Pic_means,Pic_min)

# Sortieren in Einlass, linke Küvette, rechte Küvette
Pic_INL   <- Pic[which( (Pic[,5]>=18 & Pic[,5]<=19) | (Pic[,5]>=48 & Pic[,5]<=49)),]
Pic_left  <- Pic[which( (Pic[,5]>=22 & Pic[,5]<=23) | (Pic[,5]>=52 & Pic[,5]<=53)),]
Pic_right <- Pic[which( (Pic[,5]>=27 & Pic[,5]<=28) | (Pic[,5]>=57 & Pic[,5]<=58)),]

names(Pic_INL) <- paste(names(Pic_INL),"INL")
names(Pic_left) <- paste(names(Pic_left),"left")
names(Pic_right) <- paste(names(Pic_right),"right")

# Vorbereitung ECHO Daten für PIC Daten
# linke Küvette mit Luftfeuchtefühler A5
A5_min  <- substring(A5[,5],15,16)
A5_min  <- as.numeric(A5_min)
A5_P    <- cbind(A5,A5_min)
A5_Pleft <- A5_P[which((A5_P[,6]>=23 & A5_P[,6]<=24) | (A5_P[,6]>=53 & A5_P[,6]<=54)),]
length(A5_Pleft[,1])

# rechte Küvette mit Luftfeuchtefühler A3
A3_min  <- substring(A3[,5],15,16)
A3_min  <- as.numeric(A3_min)
A3_P    <- cbind(A3,A3_min)
A3_Pright <- A3_P[which((A3_P[,6]>=28 & A3_P[,6]<=29) | (A3_P[,6]>=58 & A3_P[,6]<=59)),]
length(A3_Pright[,1])

# Berechnung der d18O und dD Werte an der Wasseroberfläche des Bodens über das Craig-Gordon Modell
MilliQ_d18o  <- -58.34
MilliQ_dD    <- -77.89

rH_left  <- (A5_Pleft[,3]/100)
rH_right <- (A3_Pright[,3]/100)

d18O_Bodenw_left  <- Pic_left[,3]*( (1-rH_left) + (( (1-rH_left)*32)/1000))/1.0092 + ( rH_left*Pic_left[,3]+9.2+(1-
rH_left)*32)/1.0092
d18O_Bodenw_right <- Pic_right[,3]*( (1-rH_right) + (( (1-rH_right)*32)/1000))/1.0092 + ( rH_right*Pic_right[,3]+9.2+(1-
rH_right)*32)/1.0092

dD_Bodenw_left <-  Pic_left[,4]*( (1-rH_left) + (( (1-rH_left)*16)/1000))/1.076 + ( rH_left*Pic_left[,4]+76+(1-
rH_left)*16)/1.076
```

```
dD_Bodenw_right <-  Pic_right[,4]*( (1-rH_right) + (( (1-rH_right)*16)/1000))/1.076 + ( rH_right*Pic_right[,4]+76+(1-
rH_right)*16)/1.076


ylim1_bodenw <- min(c(d18O_Bodenw_left,d18O_Bodenw_right))
ylim2_bodenw <- max(c(d18O_Bodenw_left,d18O_Bodenw_right))

#PLOTTING !!!
Zeitachse <- as.POSIXct(strptime(Pic_left[,1],format="%Y-%m-%d %H:%M", tz="GMT"), tz="GMT")
stunden_Pic   <- trunc(as.numeric(Pic_left[,1])/60)

win.metafile(Pic_Dat_Plot, width = 8, height = 11)
par(cex = 2,cex.main = 2,cex.axis = 1.5, cex.lab = 1.5, mex = 2, font.main=2, lwd=1,
   mfrow=c(3,1), mar = c(0.2, 5, 1, 5), oma = c(10, 4, 5, 1))
plot(stunden_Pic, Pic_left[,3],
   xaxt="n" , ylab = expression(paste(delta^18,"O-",H[2],"O (V-SMOW) [‰]")),
   ylim=c(-20,120),
   pch=16, col = "red", cex=1)
#title(main= expression(paste("Exp16 Picarro ", delta,"-values (Carboanhydrase)")),outer=T)
legend("topleft",bty="n",c("Vapor Fine Sand","Vapor Medium Sand", "Liquid Fine Sand", "Liquid Medium Sand"), cex= 1.5,
pch=16, col=c("red","blue","tomato","lightskyblue"), pt.cex=c(1,1,1,1),pt.lwd= c(2,2,2,2))
points(stunden_Pic, Pic_right[,3],pch=16, col="blue",cex=1)
lines(stunden_Pic, d18O_Bodenw_left, lty=3, col="tomato",lwd=3)
lines(stunden_Pic, d18O_Bodenw_right,lty=3, col="lightskyblue",lwd=3)


plot(stunden_Pic, Pic_left[,4],
   xaxt="n" , ylab = expression(paste(delta,"D-",H[2],"O (V-SMOW) [‰]")),
   ylim=c(-180,100),
   pch=16, col = "red", cex=1,tcl=-0.5)
points(stunden_Pic, Pic_right[,4],pch=16, col="blue",cex=1)
lines(stunden_Pic, dD_Bodenw_left, lty=3, col="tomato",lwd=3)
lines(stunden_Pic, d18O_Bodenw_right,lty=3, col="lightskyblue",lwd=3)
plot(stunden_Pic, Pic_left[,2],
   ylab = expression(paste("c",H[2],"O [ppm]")),
   ylim=c(0,34000),
   pch=16, col = "red", cex=1)
points(stunden_Pic, Pic_right[,2],pch=16, col="blue",cex=1)
title(xlab = "time (hrs.)",cex=1,outer=T)
dev.off()
```

Appendix D: Zusammenfassung in deutscher Sprache

Diese Arbeit hat eine neue Methode etabliert, um die Konzentration und die Isotopologe von CO_2 und H_2O über einer Bodensäule unter Laborbedingungensimultan und kontinuierlich zu messen. Dabei wurden zwei unterschiedliche Laser Technologien angewendet, nämlich die Tunable Diode Laser Absorption Spectroscopy (TDLAS) und die Wavelength-Scanned Cavity Ring Down Spectroscopy (WS-CRDS). Zwei Gas-dichte Küvetten wurden hierfür mit zwei unterschiedlichen Sorten von Quartzsänden (Feinsand und Mittelsand) gefüllt. Eine Gasmischung aus trockener Synthetischer Luft und CO_2 wurde in den oberen Teil der Küvette durch geleitet, um die Atmosphäre zu simulieren. Gleichzeit wurde reines CO_2 vom Boden in die Küvette geleitet, um die Boden und Wurzelrespiration zu simulieren. Mehrere Experimente wurden durchgeführt, um den Einfluss der Bodenfeuchte, der organischen Auflage und eines möglichen Vorkommens von Carboanhydrase auf die Isotopenzusammensetzung von bodenbürtigen CO_2 und Wasserdampf über einer Bodensäule zu untersuchen.

Die Resultate der Experimente zeigen, dass die Isotopenzusammensetzung des Wasserdampfs über einer Bodensäule zum einen von der Isotopenzusammensetzung des Bodenwassers und zum anderen von der Evaporationsrate abhängt. Es zeigt sich, dass organische Auflagen hat einen großen Einfluss auf die Evaporationsrate und die Isotopenzusammensetzung haben.

Die Isotopenzusammensetzung von bodenbürtigem CO_2 wird von mehreren Prozessen beeinflusst, die entweder zu einer kinetischen oder thermodynamischen Fraktionierung führen. Während der ersten 24 Stunden der Experimente, bevor die Bodensäule bewässert wurde, kam es zu einer kinetischen Fraktionierung aufgrund von Diffusion. Diese kinetische Fraktionierung war abhängig von der Sandsorte und der Anwesenheit einer organischen Auflage. Nach jeder Bewässerung konnte eine thermodynamische Fraktionierung beobachtet werden, die aufgrund der Gleichgewichtsreaktion zwischen H_2O und CO_2 zustande kam.

Das Vorkommen von Carboanhydrase hatte einen signifikanten Einfluss auf die Sauerstoffisotope des bodenbürtigen CO_2, da dieses Enzym die Gleichgewichtsreaktion zwischen H_2O und CO_2 beschleunigt. Unrealistische hohe δ-Werte des CO_2 ließen darauf schließen, dass bei Anwesenheit von Carboanhydrase ein großer Teil des CO_2, welches von der Atmosphäre in den Boden eindringt, mit dem Bodenwasser reagiert. Daraufhin wurde ein einfaches Modell entwickelt, um den proportionalen Anteil des CO_2, welches in die Bodensäule eindringt und dort mit dem Bodenwasser reagiert, zu ermitteln.

Schlüsselwörter: CO_2, Bodenwasser, Isotope, Evaporation, organische Auflage, Carboanhydrase

Ehrenwörtliche Erklärung

Hiermit erkläre ich, dass die Arbeit selbständig und nur unter Verwendung der angegebenen Hilfsmittel angefertigt wurde.

Ort, Datum Unterschrift